

**Hungarian Academy of Sciences - Dissertation**

**Plastic and creep deformation in terms of the synthetic theory**

**Endre Ruzinkó**

**Budapest 2017**

## **Dedication**

To my father.

## **Abstract**

This dissertation deals with irrecoverable deformation of polycrystalline materials subjected to different types of mechanical and thermal impacts. This study has three major purposes: (1) to describe analytically the peculiarities of plastic and creep deformation due to the stepwise change in acting stresses (2) to model the steady-state creep of metals as a function of the parameters of preliminary mechanical-thermal treatment (3) to investigate and model the effect of ultrasound on the strength properties of metals such as ultrasonic hardening and softening as well as the influence of preliminary ultrasonic treatment upon the steady-state creep of metals.

The implementation of the tasks listed above takes place in terms of the synthetic theory of irrecoverable deformation, which manifests itself as an effective mathematical apparatus to model numerous non-classical problems in the field of plastic and creep deformation.

## Content

Chapter I. Introduction .....	6
1.1 Objectives .....	8
1.2 Scope .....	9
Chapter II. Phenomena studied in the dissertation. State of the art .....	10
2.1 Peculiarities of irrecoverable straining in stress-drop test .....	10
2.2. Ultrasound effects upon the strength properties of metals .....	14
2.2.1 Ultrasonic hardening .....	14
2.2.2 Ultrasonic softening .....	18
2.3 Influence of preliminary treatments upon the steady-state creep of metals .....	22
CHAPTER III. The synthetic theory of irrecoverable deformation .....	28
3.1 The key points of the synthetic theory and state of the art .....	28
3.2 Ilyushin's deviatoric space .....	30
3.3. Two-level approach to calculate inelastic deformations, the Batdorf-Budiansky slip concept .....	30
3.4 Yield surface as an inner envelope of tangent planes. ....	31
3.5 Yield criterion and yield surface in terms of the synthetic theory .....	35
3.6 Yield surface in subspace $\mathcal{S}^3$ . Tangent planes and their traces.....	37
3.7 Evolution of loading surface. Inelastic deformation on the micro- and macro-levels.	38
3.8 Law for inelastic deformation at the microlevel .....	41
3.9 Partial cases.....	46
CHAPTER IV. Generalization of the synthetic theory to the cases pronounced as the objectives of this dissertation .....	48
4.1 Plastic and creep deformation in stress-drop tests .....	48
4.1.1 Generalization of the hardening rule.....	48
4.1.2. Plastic straining .....	50
4.1.3. Creep straining.....	55
4.1.4. Stress drop .....	59
4.1.5. Negative (reverse) creep.....	61
4.1.6. Creep delay .....	65
4.1.7. Inverse creep .....	66
4.1.8. Comparison of the model and experimental results .....	67
CONCLUSION (Thesis 1) .....	70
4.2 Influence of preliminary mechanical-thermal treatment (MTT) upon the secondary creep of metals .....	71

4.2.1 Preconditions.....	71
4.2.2 The generalization of the synthetic theory for the case of secondary creep as a function of the parameters of preliminary MTT .....	74
Case A.....	75
Case B.....	80
Case C.....	83
CONCLUSION (Thesis 2) .....	84
4.3 The generalization of the synthetic theory to the case of ultrasonic effects.....	85
4.3.1 Ultrasound defects.....	85
4.3.2 Acoustic irradiation without static loading: ultrasonic hardening.....	86
4.3.3 Ultrasonic vibrations superimposed on plastic straining: ultrasonic softening ...	88
4.3.4 Influence of preliminary ultrasound treatment upon the steady-state creep of metals of different stacking fault energies .....	89
4.3.5 Results, discussion.....	95
CONCLUSION (Thesis 3) .....	100
Conclusions and suggestions for further work.....	101
References.....	103

## Chapter I. Introduction

Modern industry imposes increasingly severe requirements on the mechanical properties of metals used in its various branches. Plastic and creep deformation of the structural members of mechanisms, machines, etc. holds a special place within this issue.

Considerable, even remarkable, progress has been achieved in the last few decades in the field of Solids Mechanics, both theoretical and experimental. Pleiad of domestic and foreign eminent scientists has formed the basis of Solid Mechanics and given an impetus to its further development. The contribution of the researchers listed below (in chronological order) has formed a conceptual base of this dissertation in terms of Mechanical Engineering taken as a whole and the theory of deformation in particular:

Nádai (1950), Hill (1950), Rabotnov (1969), Kenedy (1962), Ilyushin (1963), Kaliszky, Kurutz, & Nédli (1974), Kurutz-Kovacs (1981), Rusinko, K. (1981), Honeycombe (1984), Rusinko, K. (1986), Bojtár, & Vörös (1986), Béda, & Kozák (1987), Domokos (1988), Stépán (1989), Nédli (1989), Kaliszky (1989), Kaliszky, Kurutzné, & Szilágyi (1990), Gáspár (1993), Scharle (1993), Kollár (1995), Béda, Kozák, & Verhás (1995), Chaboche (1997), Páczelt (1999), Páczelt et al. (1999), Hutchinson (2000), Chakrabarty (2000), Ginzler et al. (2000,2001,2004,2010), Dulácska (2001), Gáspár, & Németh (2002), Zalka (2002), Kollár, & Springer (2003), Tarnai (2003), Farkas, J. (2003), Chen, & Han (2007), Égert (2007), Kaliszky, S., & Lógó, J. (2006), Kiss (2007), Bokor, & Gáspár (2008), Kovács, F., & Tarnai (2009), Páczelt, & Mróz, (2009), Károlyi (2010), Kozák, & Szeidl (2013), Ádány (2013), Kovács, A. (2013), Csébfalvi (2013), Balázs (2015), Farkas, & Jármai (2015), Várkonyi (2016), Bagi (2016), Hegedűs, Farkas, Gy., Dunai, & Kovács (2016), Csizmadia (2016), Bertóti, E. (2016).

At the same time, one of the greatest challenges in Solid Mechanics remains the developing of a complex model to describe the deformation properties of metals subjected to different types of mechanical and thermal impacts and, which is of extreme importance, deriving interplay between them. Indeed, numerous books and papers on various aspects of the strength of metals have been published in the last 20-30 years, but the results focusing upon the relationships between different types of deformations such as time-independent deformation (plastic deformation) and creep as well as plastic/creep deformation and heat treatment remain very limited. This dissertation tries to fill the void noticed above by introducing a novel theory, *THE SYNTHETIC THEORY OF IRRECOVERABLE DEFORMATION*,

which turned out to be an effective apparatus to model numerous non-classical problems in the field of the irrecoverable deformation of solids.

Advantages of the synthetic theory can be listed as below:

- (i) Inelastic deformation at a point of a body is calculated by a two-level approach, macro- and micro-level are considered, i.e. the macrodeformation is strongly connected to the processes occurring on the microscopic level of material.
- (ii) Deformation behavior of material is intimately related to real physical processes governing the development of irrecoverable deformation.
- (iii) Any type of deformation, both plastic and creep deformation, is governing by a sole constitutive equations, which enables to avoid a little artificial classification on plastic and creep deformation. That is why, in terms of the synthetic theory, a single notion, irrecoverable deformation, is used independently of what loading regime induces it.

## 1.1 Objectives

This work is focused on the modelling of small plastic/creep deformation of hardening materials exposed to different modes of mechanical and thermal actions.

Three fundamental objectives are:

- A.** To develop a model dealing with phenomena accompanying the irrecoverable deformation of metals subjected to a step-wise loading at constant temperature such as
  - a) negative creep,
  - b) creep delay,
  - c) inverse creep.
  
- B.** To develop a model relating the steady-state (secondary) creep rate of metals to the parameters of preliminary mechanical thermal treatment (MTT) including two successive operation:
  - a) plastic straining and
  - b) annealing of the work-hardened material.
  
- C.** To develop a model describing the behavior of metals subjected to alternating loading of ultrasonic frequency. The following problems are considered:
  - a) plastic deformation of metals when unidirectional loading is superimposed by ultrasound – ultrasonic softening
  - b) material hardening due to sonication of material, i.e. material is exposed to the action of ultrasound alone, – ultrasonic hardening.
  - c) the steady-state (secondary) creep rate of metals as a function of the parameters of preliminary ultrasonic treatment (UT), which includes the sonication of metal and subsequent annealing.

The implementation of the tasks listed above takes place in terms of a new theory, The Synthetic Theory of Irrecoverable Deformation.

## 1.2 Scope

**Chapter II** highlights the progress, current status, and open challenges of the phenomena studied in this dissertation. The review of both theoretical and experimental results explains the processes occurring in the phenomena of our interests and provides substantiation for analytical manipulations in Chapter IV.

In **Chapter III**, basic concepts, notions, and formulations of the synthetic theory are introduced. First of all, a two-level approach to calculate irrecoverable deformations is proposed. Then the notion of stress vector and strain vector within the framework of five-dimensional stress/strain deviator space is introduced. The next step, which makes up the core of the synthetic theory, is to show the principles of the construction of yield surface (i.e. to define a yield criterion) and the evolution of loading surface (i.e. to define a hardening rule). Further, we write equations for the quantities describing stress-strain state of material on its microscopic level such as strain intensity, defect intensity, and their interrelation. Finally, the procedure of the calculation of macrodeformation is considered.

**Chapter IV** stands out from the rest of this dissertation in that it deals with the generalization of the synthetic theory.

**Sec. 4.1** concentrates upon generalization of the synthetic theory to model the plastic and creep strain under step-wise loading which is accompanied by numerous “non-classical” phenomena. To solve this problem, which is far beyond the scope of the classical theories of plasticity and creep, we introduce into the constitutive equations system a formula governing the strength properties of material in the direction opposite to that of acting stresses. This allows us not only to model the phenomena of our interest, but show interplay between them.

**Sec. 4.2** highlights the generalization of the synthetic theory to the case of creep deformation after preliminary mechanical-thermal treatment. Our goal here is to derive formulas relating the steady-state creep of metals to the parameters of MTT such as the magnitude of plastic deformation as well as the temperature and duration of anneal. Metals with different stacking fault energies are considered. We discuss a thermal stability of the treated material to resist the processes governing steady-state creep.

**Sec. 4.3** develops a model for describing the influence of alternating loading of ultrasonic frequency upon the deformation properties of metals. Ultrasound effect manifests itself in such phenomena as ultrasonic softening and ultrasonic hardening, depending on if the ultrasonic vibrations are superimposed upon plastic straining or act alone, respectively. Further, the influence of preliminary ultrasonic treatment upon the secondary creep of metals with different stacking fault energy is analyzed. For this purpose we introduce into consideration a new function, ultrasound defect intensity, which allows us describe the temporary behavior of the ultrasound defects and their impact upon the deformation characteristics of material.

## Chapter II. Phenomena studied in the dissertation. State of the art

### 2.1 Peculiarities of irrecoverable straining in stress-drop test

Plastic or creep deformation under variable stresses is of great interest due to the rise of such phenomena as negative (reverse) creep, creep delay and inverse creep. These phenomena, which grow out of the competence of the classical theories of plastic/creep deformation, are widely studied in the literature in terms of both theoretical modeling and experimental researches.

As an example, nuclear fuel cladding tubes are subject, in service, to complex multiaxial loading that undergoes sudden change. An accurate description of the strain response due to varying stresses is essential in reliably predicting the accumulated plastic strains in the cladding. Direct extrapolations of the creep behavior under constant load to describe creep due to varying loads would result in strains significantly different from those observed, mainly due to negative creep transients following load drops (Murty, & Yoon, 1979).

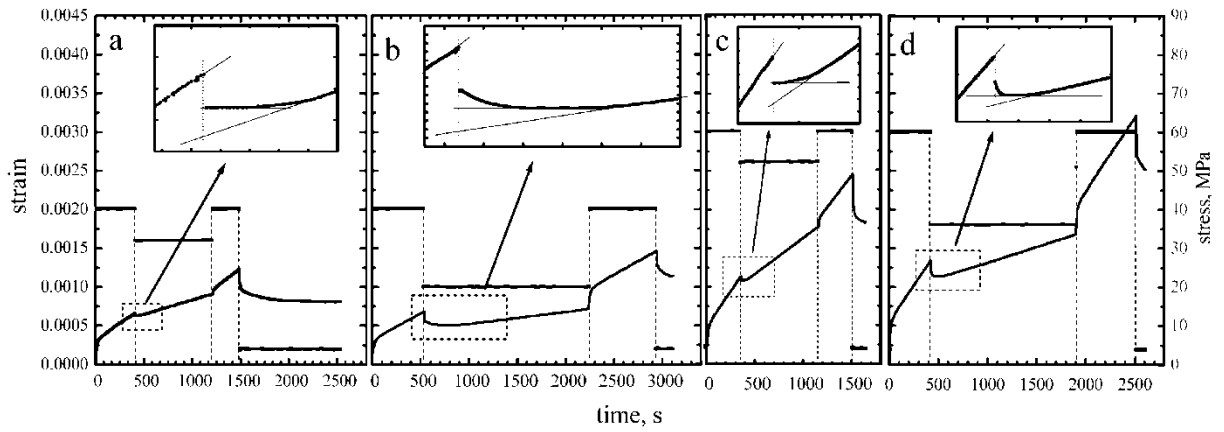
The negative creep is of great importance due to this phenomenon contradicts the hypothesis of creep potential (Rabotnov, 1969), according to which a creep rate is a single-valued function of acting stresses independently of the way these stresses have been reached. In contrast to this, the reverse creep occurs in the direction opposite to what is predicted in terms of the creep potential theory.

A stress-drop test (SDT) has been widely employed as a sensitive experimental technique allowing data on the micromechanisms of creep to be obtained. Fig. 2.1 shows the results of SDT for  $Ti_3SiC_2$  conducted by Radovic and co-workers (2003). Immediately after the stress reduction, the specimen contracts elastically or plastically and subsequently deforms by plastic flow in time (creep). The creep rate is positive after small stress reduction and negative with large stress decreases. At an intermediate stress reduction, the initial creep rate is zero. In contrast to this, many investigators, e. g. Mitra, & McLean, (1966); Davies, & Wilshire (1971), report that even with very small stress reductions an "incubation period" of zero creep rate is observed before the deformation rate accelerates to a new steady value.

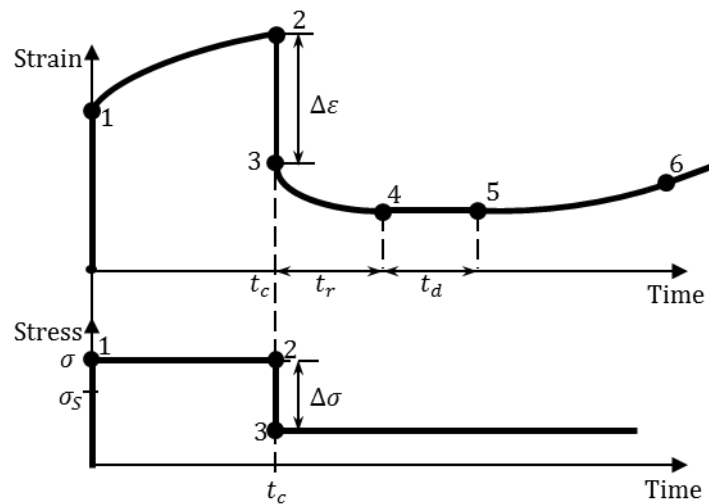
According to some authors (e.g. Cadek, 1987, 1988) the reverse creep can be observed only if there is a plastic contraction due to the stress drop: material needs to obtain some compressive strain energy which then can be released in the form of time-dependent deformation (reverse creep).

Fig. 2.2 demonstrates schematically the results from Fig. 2.1.

Many theories have been developed to explain the behavior patterns observed in stress-drop tests. If to omit minor details in the interpretation of the processes governing creep in SDT, they confirm that: (a) dislocation creep is the dominant mechanism; (b) high plastic anisotropy is a source of the energy inducing processes occurring in material; (c) the



**Fig. 2.1.** SDT tests of  $\text{Ti}_3\text{SiC}_2$  samples at  $1150^\circ\text{C}$ . In all tests initial stress  $\sigma$  was reduced by  $\Delta\sigma$  and then increased again up to  $\sigma$ . (a)  $\sigma = 40$  MPa,  $\Delta\sigma = 8$  MPa; (b)  $\sigma = 40$  MPa,  $\Delta\sigma = 20$  MPa; (c)  $\sigma = 60$  MPa,  $\Delta\sigma = 8$  MPa; (d)  $\sigma = 40$  MPa,  $\Delta\sigma = 24$  MPa. At the end of each test the sample was unloaded down to 4 MPa. (Radovic et al., 2003)



**Fig. 2.2.** Strain-time diagram in the stress-drop test; 1-2: creep portion under  $\sigma$  stress, 2-3: negative contraction  $\Delta\varepsilon$  due to stress-drop  $\Delta\sigma$ , 3-4: negative creep (*applied stress remains positive!*), 4-5: creep delay (incubation period)  $\dot{\varepsilon} = 0$ , 5-6: accelerating (inverse) creep  $\dot{\varepsilon} > 0$ , from point 6: steady state creep  $\dot{\varepsilon} = \text{const}$  corresponding to  $\sigma - \Delta\sigma$  stress. For the case of small stress drop, 3-4 portion is absent and only portions 4-5-6 are observed after the stress drop.

response is dictated by a competition between the rates of recovery and hardening processes.

With instantaneous and time-dependent negative plastic deformation, the following approaches can be distinguished.

*LRIS (Long range internal stress), Composite model* (Kassner et al., 2009,2015). Mughrabi (1983) developed/advanced the concept of relatively high (long-range internal) stresses in association with heterogeneous dislocation substructures (e.g., cell/subgrain walls, dipole bundles, persistent slip bands walls, etc.). He presented the simple case where “hard” (high dislocation density walls, etc.) and “soft” (low dislocation density channels, or cell interiors) elastic-perfectly-plastic regions are compatibly sheared. Each component yields

at different stresses and it is suggested that the “composite” is under a heterogeneous stress-state with the high-dislocation density regions having the higher stress. As soft and hard regions are unloaded in parallel, the hard region eventually places the soft region in compression while the stress in the hard region is still positive. That is, a backstress is created. The plasticity occurs on reversal due to “reverse” plasticity in the soft region. The concept of heterogeneous stresses has also been widely embraced for monotonic deformation (Borbély et al. 1997, 2000) including elevated-temperature creep deformation.

*Non-Backstress explanation.* Sleswyk et al. (1978) proposed a different approach; when analyzing the hardening features in several metals at ambient temperature, he adopted an Orowan-type mechanism (long-range internal stresses or “back-stresses” not especially important) with dislocations easily reversing their motion (across cell). He suggested gliding dislocations, during work-hardening, encounter increasingly effective obstacles and the stress necessary to activate further dislocation motion or plasticity continually increases. On reversal of the direction of straining from a “forward” sense, the dislocations will easily move past those, non-regularly-spaced, obstacles that have already been surmounted. Thus the flow stress on reversal is relatively low. Lloyd and McElroy (1974) shares the same opinion, considering only the unbowing of dislocation segment, immobilized in a bowed out configuration, toward a new configuration at reduced stress. Another observation (Davies, & Wilshire, 1971) says that the instantaneous specimen contraction on decreasing the stress is greater than would be expected from the elastic modulus is a consequence of runback of dislocation pile-ups.

If to return to the notion of internal stress (back-stress), according to Evans (1985), the occurrence of negative creep must mean that the specimen is deforming under a net compressive stress even though the applied stress remain positive at  $\sigma - \Delta\sigma$ . This has led to the view that creep occurs not under the full applied stress  $\sigma$  but under an effective stress  $\sigma_e$ , given as

$$\sigma_e = \sigma - \sigma_i,$$

where  $\sigma_i$  is the internal stress or dislocation back stress. With this approach, a measure of  $\sigma_i$  may be obtained as the stress below which (a) negative creep occurs after the instantaneous specimen contraction or (b) the instantaneous specimen contraction has a plastic component. After a stress change, the value of  $\sigma_i$  established during creep under the applied stress  $\sigma$  will gradually adjust towards the value expected for the new stress imposed. The time-dependent growth in macro-deformation-rate (portion 5-6 in Fig. 2.2) is explained by the increasing number of slip systems getting involved in the production of strain at  $\sigma - \Delta\sigma$  stress.

Depending on the nature of the obstacles to dislocation glide, Poirier (1977,1985) points out the following mechanisms involved in negative creep:

a) Recovery (climb)-controlled creep, where the backward stress of the obstacles is of the nature of a long range internal stress. Creep cannot proceed unless the internal stress is reduced to the level of the applied stress by diffusion-controlled recovery of the substructure.

b) Thermally activated creep, where localized short-range obstacles are superposed to a more or less periodic internal stress field (Jonas, 1970). Thermal agitation directly helps overcoming the obstacles and there is an effective stress defined as the difference between applied stress and internal stress. The obstacles can be very high and far apart and in this case the dislocations have a thermally activated, stress dependent waiting time in front of the obstacle before gliding in a jerky fashion until they are blocked in front of the next obstacle. Such would be the case for cross-slip controlled creep (Friedel, 1964). or creep controlled by the thermal unpinning of attractive junctions [Guyot (1966), Sastry et al. (1974)]. The obstacles may also be less important but present at almost every atomic step of the dislocations, “smeared” so to speak, in this case the thermally activated overcoming of this type of obstacle leads to viscous glide (e.g. solute drag or jog drag). Clearly the two types of obstacles can be present at the same time.

Louchet (1995) proposed the model accounting for a transient creep taking place in some superalloys, opposed to the direction of the applied load, though started by the application of this load. It is based on the reduction of the internal energy of the system during coarsening. The release of internal energy is assumed to be related to stress-induced directional coarsening of precipitates.

Internal stress theory is greatly weakened when one takes account of the results obtained by Davies & Wilshire (1971), according to which, with single crystals, the instantaneous contraction was followed by a period of zero creep rate for all stress reductions. Negative creep was never observed with the single crystal specimens. This casts serious doubts on the technique of measuring internal stresses by this type of stress change experiment, since similar internal stresses should exist in single and polycrystalline specimens.

On the other hand, long range internal stresses were confirmed by Carry, & Strudel (1978) in single crystals of a nickel base superalloy and Kassner (2009, 2015) for monotonically deformed Cu single crystal. Kassner supposes that a combination of LRIS and an Orowan mechanism must be taken into account.

Bayley (2006) advocates the LRIS approach via strain gradient crystal plasticity, which attempts to predict material size effects by taking into account geometrically necessary dislocations that are required to accommodate gradients of crystallographic slip. Since these dislocations have a non-zero net Burgers vector within the material, dislocation induced long range stresses result in a back stress that influences the effective driving force for crystallographic slip.

### ***Summary***

In the last 20 years, remarkable progress has been made in both theory and experiment to model the phenomena intrinsic to stress drop tests. At the same time, the researches considered above make focus mainly on some “knot” in Fig. 2.2 (especially portion 2-3-4), while the preceding and following portions and their roles remain without attention. Thus, it would be of crucial interest to develop a model capable of analytical describing of the whole chain of phenomena in stress-drop test so that to show the interplay between them.

Section 4.1 shows how, in terms of the generalized synthetic theory, this problem can be solved.

## 2.2. Ultrasound effects upon the strength properties of metals

In recent years, the most discussed issues about the influence of ultrasound upon the plastic deformation properties of metals are the phenomena of ultrasonic hardening (UH) and ultrasonic softening (US). The former phenomenon occurs during the sonication of annealed material without a static (unidirectional) loading, while the latter takes place when a high frequency (ultrasonic) variable loading is superimposed upon a static one.

### 2.2.1 Ultrasonic hardening

The ultrasonic hardening manifests itself in the increase of the yield strength of material due to the defects of crystalline structure nucleated and developed by acoustic energy.

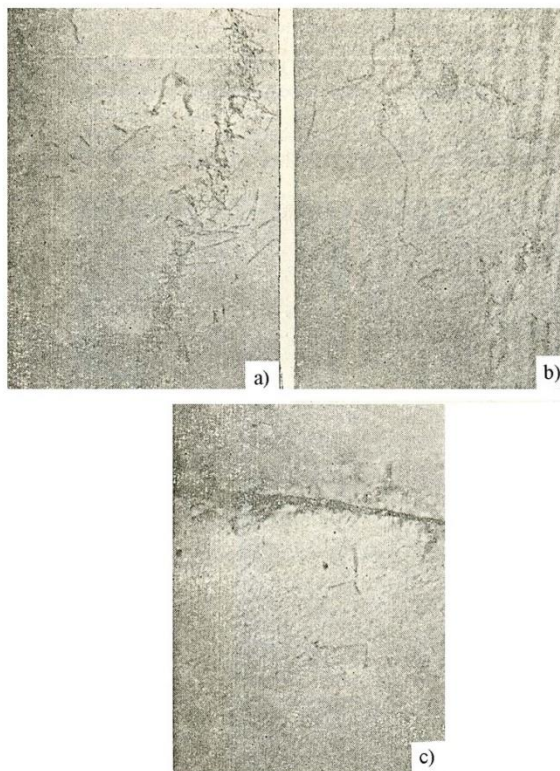
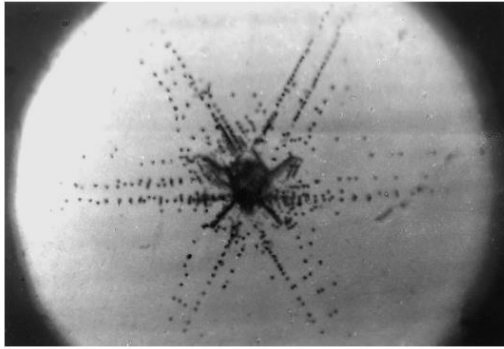


**Fig 2.3.** Dislocation structure of iron subjected to ultrasonic irradiation (x50000):  $t = 20\text{ }^{\circ}\text{C}$ ; stress amplitudes a,b -  $\sigma_m = 200\text{ MPa}$ ; c -  $\sigma_m = 20\text{ MPa}$  after  $2 \cdot 10^6$  cycles, frequency  $f = 20\text{ kHz}$  (Kulemin, 1978).

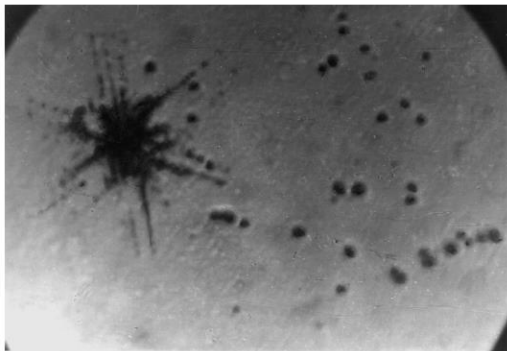
The influence of ultrasound upon metals leads to the change in their initial dislocation structure. First researches on the fine structure of metals have been conducted by Langenecker (1966) on wire specimens of monocrystal aluminum (99.99%). It was found that the ultrasonic irradiation resulted in the increase in dislocation intensity by several orders of magnitude.

Fig. 2.3 demonstrates the transmission electron micrographs of iron-foil (carbon content of 0.003 %) subjected to the action of ultrasound. The dislocations are distributed in a strongly non-homogeneous manner. As a rule, the dislocations are concentrated in tangles and tied into knots, there are a lot of immobile jogs on them. The great number of small dislocation loops formed by the agglomeration of vacancies is observed. Pileups of dislocations near the grain boundaries are also reported in the works of Westmacott

and Langenecker (1965) and it can be assumed that the grain boundaries are the prevailing sources of dislocation under the action of ultrasound. Terentjev et al. (1975) and Mordyuk et al. (2013), dealing with polycrystalline molybdenum and Al-6Mg alloy, report that there are areas with practically initial dislocation structure even under high stress amplitudes. At the same time, the grains (the parts of grains) are observed where the dislocation density is considerably higher than that in the initial state. The distinctive feature of ultrasound induced dislocation structure – extended dislocation pile-ups consisting largely of prismatic dipoles and the great number of dislocation loops and jogs – is reported by Peslo (1984).



**Fig. 2.4.** A dislocation rosette in a control silicon sample without ultrasonic processing (Ostrovskii et al., 2000).



**Fig. 2.5.** A dislocation rosette in a silicon crystal upon 4-h ultrasonic processing. The rosette arm length is about half that in the control sample. The sample surface exhibits traces of vacancy-impurity clusters in the form of dark oval spots (Ostrovskii et al., 2000).

Further, ultrasound leads to a considerable growth of vacancy concentration. In support of this statement consider the results of experiments conducted by Ostrovskii with co-workers (2000). Fig. 2.4 shows the pattern of selective etching for a control silicon sample not subjected to ultrasonic processing (USP). Fig. 2.5 presents the patterns observed upon the selective etching of samples upon USP. As seen from these figures, the rosette arm lengths markedly decrease with increasing USP duration. The arm length of a dislocation rosette is a characteristic of the mobility of dislocations. The USP-induced decrease in the rosette dimensions observed in the experiments is evidence of a reduced mobility of dislocations, that is, of the surface hardening. The surface of the silicon samples etched after USP exhibits characteristic round etch pits (Fig. 2.5), which are conventionally explained by the presence of diffusing impurity coagulants (e.g., vacancy clusters) in the near-surface layer of the crystal.

The quantitative aspect of the change in the dislocation structure, namely, how the dislocation density ( $N_d$ ) depends on a sonication time, temperature, strain amplitude etc., can be elucidated by making use of metallographic method, or etch-pit method.

The micrographs of the surface of germanium and polycrystalline aluminum (99,99%) in initial (annealed) state and after the action of ultrasound ( $f = 20$  kHz) of different sonication time are shown in Fig. 2.6. As seen from this figure, the action of ultrasound leads to the increase in dislocation density. Selective etching reveals rosettes, whose arms spread in six directions, formed by dislocation half-loops (Fig. 2.6c). If the vector of alternating stresses is perpendicular to  $\{111\}$  plane, the rosette arms are oriented along  $\langle 110 \rangle$ . The increase in sonication-time up to  $\sim 7$ -8 min results in the slip bands formation.

The dislocation motions can be traced by the repeated etching of a given area of crystal surface. Fig. 2.6d shows the microstructure of germanium surface after several impulses of ultrasound; every impulse is followed by the etching. It is easy to see that some fracture of etch-pits remains on their spots (immobile dislocations), while others move in appropriate directions (mobile dislocations). Therefore, in ultrasound loading, despite the periodic change in the sign of loading, the dislocations move only in one direction. This peculiarity is explained by the fact that crystal imperfections (point defects) trail behind the moving dislocation.

In the early stages of ultrasonic exposure, a monotone increase in dislocation density is observed (Fig. 2.7). However, beginning from some value of sonication time,  $\tau^*$ , the dislocation density remains unchangeable:  $N_d = \text{const}$  as  $\tau \geq \tau^*$ . This is due to the gradual restraint of Frank-Read sources caused by dislocations nucleated in preceding cycles. In addition, the annihilation of opposite-oriented dislocations, emitted by sources on parallel atomic planes, is observed. Lowering the sonication temperature will considerably increase the value of  $\tau^*$  (30~40 min at  $-50^\circ\text{C}$  and 1 min at  $20^\circ\text{C}$ , see Fig. 2.7a,b).

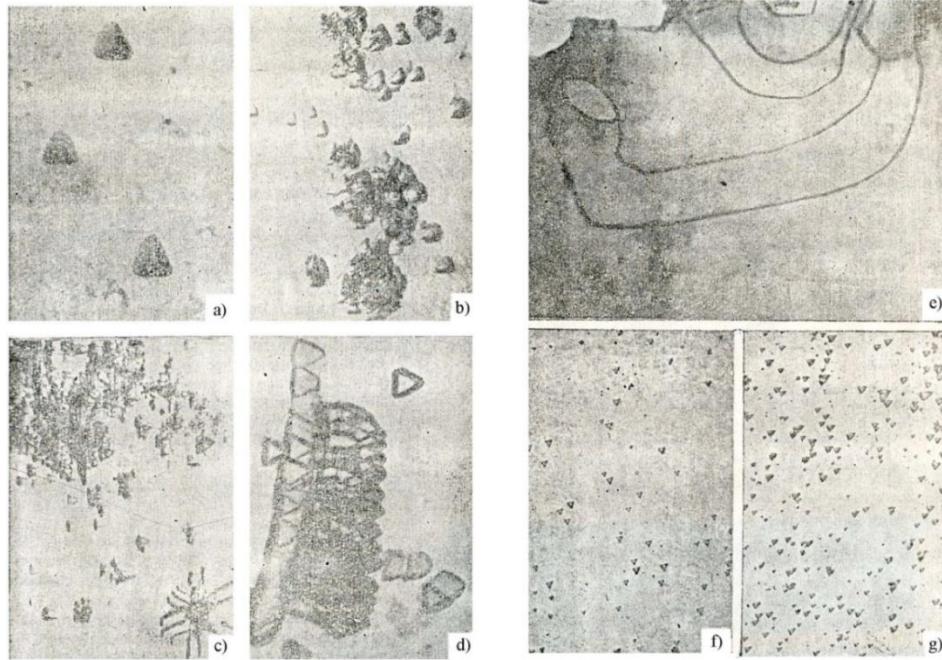


**Fig. 2.6.** Dislocation structure of germanium and aluminum: a) initial surface of germanium ( $\times 450$ ); (b) and (c) after ultrasound of  $\tau = 3$  min and 5 min at  $t = 400^\circ\text{C}$ ,  $\sigma_m = 3$  MPa ( $\times 270$ ); d) layer-by-layer etching after the sonication of  $\tau = 0 - 5$  min,  $\sigma_m = 3$  MPa ( $\times 450$ ); e) electron micrograph of sonicated germanium  $t = 600^\circ\text{C}$ ,  $\sigma_m = 3$  MPa,  $\tau = 10$  min ( $\times 60000$ ); f) and (g) the surface of aluminium in initial and sonicated states:  $t = 20^\circ\text{C}$ ,  $\sigma_m = 3$  MPa,  $\tau = 100$  sec (Kulemin, 1978).

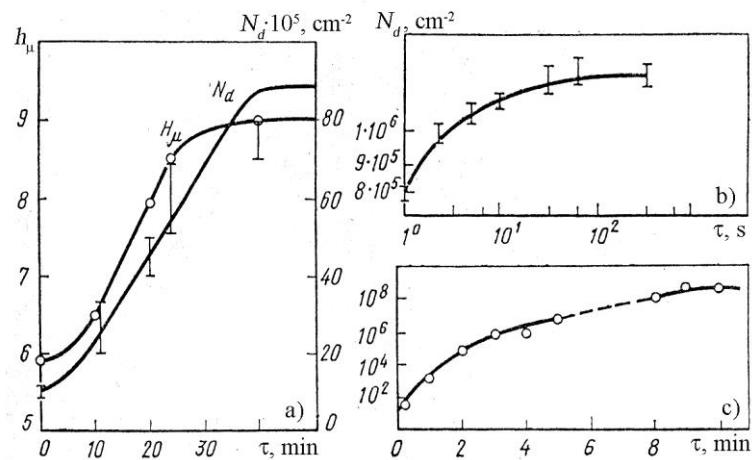


**Fig. 2.7.** Dislocation intensity and microhardness of aluminum (a and b) and germanium (c) as a function of ultrasound-action-time  $\tau$ : a)  $t = -50^\circ\text{C}$ ,  $\sigma_m = 20$  MPa; b)  $t = 20^\circ\text{C}$ ,  $\sigma_m = 18$  MPa; c)  $t = 70^\circ\text{C}$ ,  $\sigma_m = 18$  MPa (Kulemin, 1978).

The increase in stress amplitude at constant temperature leads to the reduction of  $\tau^*$ . Thus, in NaCl, 1 hour is needed for the dislocation density to reach the saturation at the stress amplitude  $\sigma_m$  of 8.5 MPa while  $N_d$  becomes constant already after 5 minutes of vibration for  $\sigma_m = 27$  MPa (Belozerova, 1992.). The time needed for the dislocation density saturation appears to be affected by the plastic properties of metals. Taking into account that dislocation density correlates with other properties of metals, e.g. microhardness or yield limit, one can suggest that the greater the yield limit of annealed material, the longer sonication time is needed to reach the dislocation density saturation.

Fig. 2.8 shows that the number of ultrasound induced dislocations starts to grow only from a certain threshold value of stress amplitude ( $\sigma_{m0}$ ). According to Kulemin (1978), the threshold stress amplitude is related to the yield limit of metal ( $\sigma_S$ ) as  $\sim 0.4 \div 0.5\sigma_S$ . Langenecker and Kralik report that the value of  $\sigma_{m0}$  ranges from  $0.3\sigma_S$  to  $0.85\sigma_S$ . Keith's and Gilman's experiments on LiF single crystals show that if a static stress cannot generate dislocation from a Frank-Read source, the same stress but applied in the opposite direction does induce a dislocation loop. Besides, immobile dislocations (especially long ones, whose lines end on the free surface of crystal) can be unpinned by oscillating stresses, because only a half-stress is needed for this. Furthermore, some amount of dislocation can be nucleated in the zones with great local stresses, e.g., along grain boundaries.

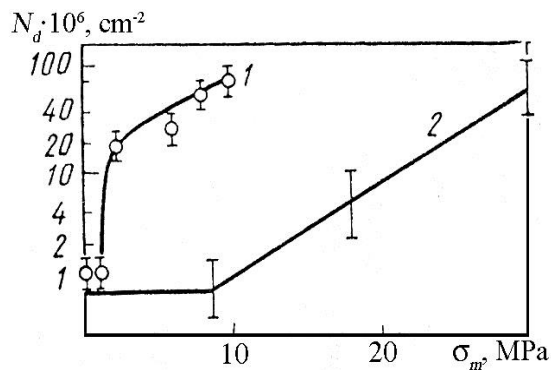


**Fig. 2.8.**  $N_d$  vs  $\sigma_m$  plot for 1) copper at  $t = 450$  °C, and 2) aluminum at  $t = 20$  °C (Kulemin, 1978).

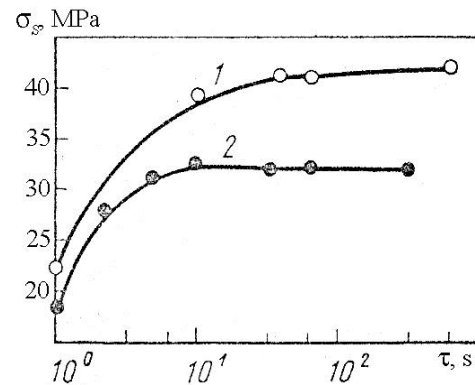


**Fig. 2.9.** Dependence of the yield limit of copper (1 -  $\sigma_m = 67$  MPa) and aluminum (2 -  $\sigma_m = 164$  MPa) on the sonication time  $\tau$  (Kulemin, 1978).

It is of great interest to study how the frequency of loading affects the dislocation distribution through crystals and the value of  $\sigma_{m0}$ . As follows from Gindin et al. (1972), the dislocation structure of nickel due to the cyclic loading of strain amplitude  $\varepsilon_m = 6 \cdot 10^{-4}$  does not change with increasing frequency. The same result is reported by Kromp, & Weiss (1971), where no essential difference in the character of dislocation distribution in copper were observed due to the variable loading ranging from ultrasonic irradiation up to low cycle fatigue. The experiments on the influence of ultrasound upon the crystals of Cu, Ni, NaCl and LiF (Pines, & Omeljanenko, 1969) record no influence of the frequency ranged from 15 to 35 kHz upon the value of  $\sigma_{m0}$ . Similar results are registered for  $f = 20$  kHz and  $f = 44$  kHz. Therefore, we suppose that the dependence of  $\sigma_{m0}$  upon the frequency of loading can be manifested beyond of  $15 \div 45$  kHz frequencies.

Changes in the metal fine structure due to ultrasound considered above affect their mechanical properties. In particular, ultrasonic load leads to the increase in the yield limit of metals ( $\sigma_s$ ) as shown in Fig. 2.9. The monotone growth of  $\sigma_s$  occurs during 10 sec. of sonication for aluminium and 30 sec for copper upon which “saturation stage” comes, i.e.  $\sigma_s(\tau)$  remains constant. The increase in the yield limit is recorded only for the stress amplitudes greater than a threshold magnitude,  $\sigma_{m0}$ . The results from Fig. 2.9 correlate to those from Fig. 2.7.

The fact that the distribution of the ultrasound induced dislocations is of strongly non-homogeneous manner makes ultrasonic processing especially favorable, since sonicated specimens deform in elastic manner on macroscopic scale while the hardening of material develops due to the plastic deformations concentrated in the micro zones (slip bands, etc.) of crystal.

### 2.2.2 Ultrasonic softening

In 1955, Austrian researches F. Blaha and B. Langenecker detected the decrease in the stress needed for the plastic deformation of single crystal zinc to progress when ultrasound (800 kHz) is superimposed. This phenomenon is referred to as ultrasonic (acoustic) softening.

Numerous investigations showed great advantages of the method of plastic deformation used in combination with ultrasonic oscillations in order to decrease forces and consumption of energy, increase the capacity of equipment, and to make it possible to deform materials that fail if processed by conventional methods [wire bonding – Huang et al. (2009), ultrasonic welding – Siddiq, & Ghassemieh (2008), deep drawing – Pasierb, & Wojnar (1992); Astashev and Babitsky (2007), Blagoveshchenskii and Panin (2007), Kirchner et al. (1985), Witthauer et al. (2014) etc.]. In the purest form, the effect of ultrasonic oscillations on the mechanical properties of a metal can be assessed in tension when the contact friction is absent in the process of deformation. Figures 2.10 and 2.11 demonstrate ultrasonic softening for mono- and polycrystalline aluminum, which manifests itself in the decrease in stress to induce plastic straining and the flatter form of  $\sigma \sim \varepsilon$  curve comparing to the case of conventional loading. Experiments carried out on many metals demonstrate that US is proportional to ultrasound intensity ( $I$ ) or stress amplitude, since these are related to each other as  $I = \sigma_m^2 / 2\rho c$ , where  $\rho$  and  $c$  are the density and the sound speed of material. Further, the US phenomenon does not depend on oscillation frequency in the range of 15-80 kHz, the degree of preliminary deformation below 16%, and temperature between 30 and 500°C.

Acoustic softening is explained on the basis of dislocation theory. Ultrasonic waves activate blocked dislocations, hardened under ordinary deformation, and decrease stresses for further plastic deformation. The effect of decrease in static stresses can also be achieved as a result of supply of heat energy; however, to obtain the identical effect, much higher (by several orders) energy must be supplied. This is explained by the fact that the acoustic energy is absorbed mainly in dislocations and other imperfections and is hardly absorbed in the defect-free zones of the crystal, whereas the heat energy is distributed rather uniformly over the entire volume of the metal deformed.

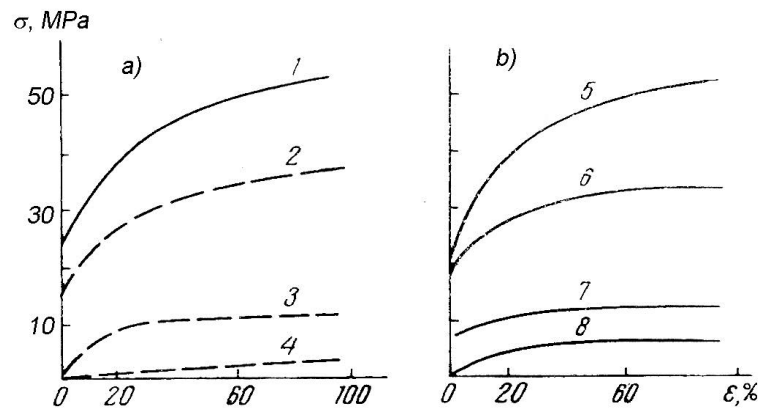


**Fig. 2.10.** Stress-strain diagrams of aluminum with simultaneous ultrasound (a) of different intensity: 1 -  $I = 0$  W/cm<sup>2</sup>, 2 -  $I = 15$  W/cm<sup>2</sup>, 3 -  $I = 35$  W/cm<sup>2</sup>, 4 -  $I = 50$  W/cm<sup>2</sup>; (b) static stress-strain diagrams of aluminum at different temperatures 5 - 18°C, 6 - 200°C, 7 - 400°C, 8 - 600°C (Mordyuk, 1970).

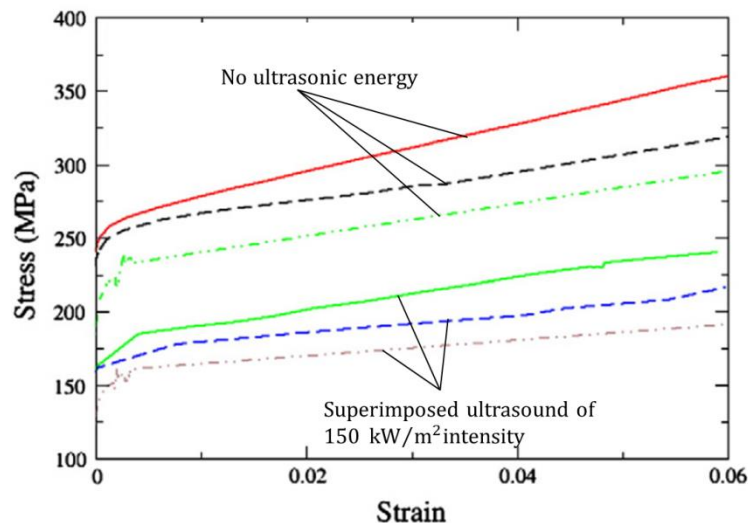


**Fig. 2.11.** Stress-strain response of three different orientations of single crystalline aluminum with no ultrasonic energy and with ultrasound (Siddiq, & Sayed, 2011).

Acoustic softening has been observed for many metals such as copper (Huang et al., 2009), molybdenum (Siu, & Ngan, 2011), gold (Lum et al., 2009), titanium (Singh, & Khamba, 2007), magnesium alloys (Tong et al., 2011).

Creep deformation is also strongly influenced by ultrasonic irradiation. Fig. 2.12 shows the creep diagrams of copper, which demonstrates that vibrating stresses results in a considerable intensification of the primary and secondary creep.

It is of great interest to notice that a simultaneous action of static ( $\sigma$ ) and oscillating stresses with amplitude  $\sigma_m$  cannot be replaced by the action of a static load whose magnitude equals to  $\sigma + \sigma_m$ . Consider the creep diagram of aluminum alloy D16T

(Fig. 2.13) for the case of (i) the simultaneous action of static  $\sigma = 55.6$  MPa and alternating  $\sigma_m = \pm 16.2$  MPa stresses (curve 1) and (ii) static load ( $\sigma_\Sigma$ ) equal to the sum of  $\sigma$  and  $\sigma_m$ ,  $\sigma_\Sigma = 55.6 + 16.2 = 71.8$  MPa (curve 2). As follows from Fig. 2.13, the combined action of static and oscillation stresses give a more intensive development of the creep strain than in the equivalent static load. This fact is of great importance: *one cannot model the simultaneous action of static and alternating load by a simple summation of the static and cyclic stresses*. This conclusion is backed by Daud's researches (2007) who, by measuring the oscillating force response as well as the static force, has shown that the experimentally derived stress-strain data does not satisfy a simple oscillatory stress superposition model.

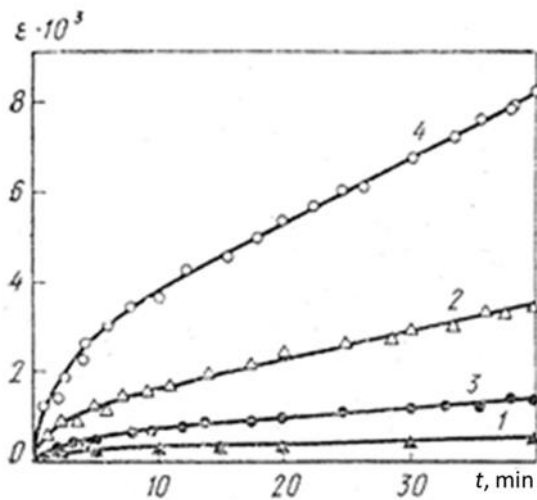


**Fig. 2.12.** Creep diagrams of copper at 30 MPa: 1,2 -  $t = 110^\circ\text{C}$ ; 3, 4 -  $t = 350^\circ\text{C}$ ; 1,2 - without ultrasound; 3, 4 - superimposed ultrasound with  $\sigma_m = 4$  MPa (Kulemin, 1978).

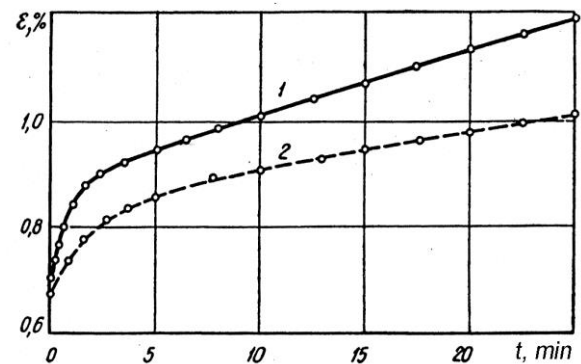


**Fig. 2.13.** Creep diagrams of aluminium alloy D16T ( $t = 300^\circ\text{C}$ ): 1 - simultaneous action of static tension and ultrasound ( $f = 21$  kHz); 2 - static load with the stress equivalent to the combined action of static and ultrasonic loading; (Konovalov, & Remizovskij, 1964).

With the state-of-the-art review of ultrasound effects, the following results can be mentioned.

A substantial body of literature has evolved around experimental investigations of the phenomena of ultrasound hardening: Puga et al. (2015), Eskin, G and Eskin, D (2014), Abramov (1994), Kozlov, & Mordyuk (1986), Severdenko et al. (1979), Kulemin (1978), etc. Peslo (1984) and Biront (1979) classify the stages of UH. Biront proposes an exponential relationship between the number of ultrasonic impulses and the degree of material hardening (via dislocation intensity). Moraru (2007) and Puga (2015) study the strength properties of polycrystalline metals subjected to ultrasound via Hall-Petch equation, i.e. they analyze the change in grain sizes due to sonication.

Statnikov (2004) and Fisher (2001) present technical aspects of ultrasonic impact treatment (UIT), including an experimental and theoretical description of the physics and the means of controlling the ultrasonic impact parameters. UIT provides high-intensity

ultrasonic impacts accompanied by ultrasonic vibrations of indenters. These impacts initiate highly effective plastic deformation and transfer there through high-intensity ultrasonic vibrations and ultrasonic stress waves into the material being treated. The model of UIT is developed through the finite element method where at any instant of time the stressed state is calculated using the global stiffness matrix.

Siddiq and Ghassemieh (2008) give thermomechanical analysis of ultrasonic welding and propose the analytical description of ultrasonic softening in terms of combined nonlinear isotropic/kinematic hardening model. Daud et al. (2007) develop finite element models for ultrasonic assisted tension and compression of aluminum alloy 1050. Siddiq and Sayed (2011) modify a phenomenological crystal plasticity model to account for acoustic (ultrasonic) softening effects based on the level of ultrasonic intensity supplied to single and polycrystalline metals.

### ***Summary***

As one can see, considerable experimental and theoretical results have been attained in the field of ultrasound effects. However, we observe a tendency that ultrasonic softening and ultrasonic hardening are modelled in terms of different approaches.

This fact motivates to develop a model which catches the “dualism” of acoustic energy: ultrasound alone hardens an annealed material, but softens it together with static load. Sections 4.3.1-4.3.3 present a model developed in terms of the synthetic theory, where both ultrasonic hardening and ultrasonic softening are described by means of a unique constitutive equation.

## 2.3 Influence of preliminary treatments upon the steady-state creep of metals

In present-day conditions, new methods of hardening of metals (equally with the traditional means, i.e. alloying, modification, optimization of thermal treatment, coating etc.) assume ever greater importance. These methods are based on the control of the dislocation structure of metal by combined mechanical (unidirectional or variable load of ultrasonic frequency) and heat (annealing) impact. Depending on the sort of the mechanical impact, mechanical-thermal treatment (MTT) and ultrasound treatment (UT) can be distinguished. The application of MTT or UT to materials used in machine building, chemical industry, and other branches of engineering would guarantee a significant increase in the service life and decrease in the weight of workpieces due to the realization of latent reserves of their strength.

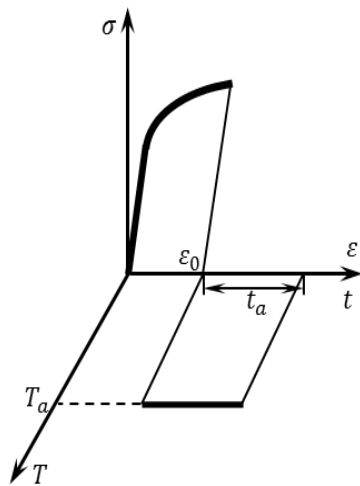


Fig. 2.14. The scheme of MTT.

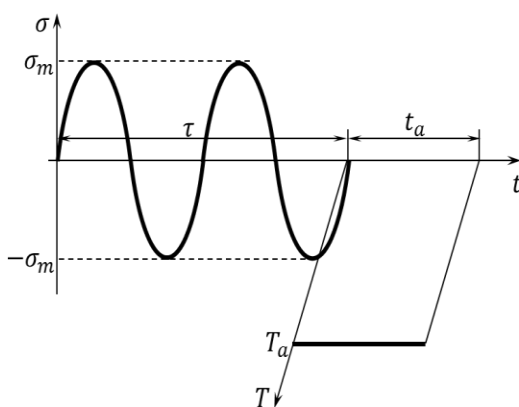


Fig. 2.15. The scheme of UT.

MTT consists of (Fig. 2.14):

- (i) plastic deformation of a batch of specimens in uniaxial tension ( $\varepsilon_0$ ) at room temperature;
- (ii) annealing of the specimens in the unloaded state at a temperature  $T_a$  for a time  $t_a$ .

UT consists of (Fig. 2.15):

- (i) sonication of a batch of specimens in longitudinal vibrations of frequency  $f$  at room temperature for certain time periods,  $\tau$ , at a given stress amplitude and frequency,  $\sigma_m$  and  $f$ , (the values of  $\sigma_m$  and  $f$  are identical for the entire batch);
- (ii) annealing of the specimens in the unloaded state at a temperature  $T_a$  for a time  $t_a$ .

Experimental data show that the preliminary treatments strongly affect the steady-state creep rate of metals. If to load the specimens after MTT under creep condition, let  $\sigma$  and  $T$  denotes the tensile stress and temperature, then their secondary creep rates strongly depend on the magnitude of plastic pre-strain  $\varepsilon_0$ , proviso  $T_a$ ,  $t_a$ ,  $T$  and  $\sigma$ , are hold constant. As

follows from Fig. 2.16, the dependences of the rate of steady-state creep on the magnitude of plastic pre-strain ( $\varepsilon_0$ ) in the course of MTT for aluminium and copper are different and not monotone. Similar situation is observed for the creep after UT. Figs. 2.17 and 2.18 demonstrate the dependence of the secondary creep rate of aluminium and copper on the duration of sonication  $\tau$  (the other parameters –  $\sigma_m, f, T_a, t_a, T$  and  $\sigma$  – are constant).

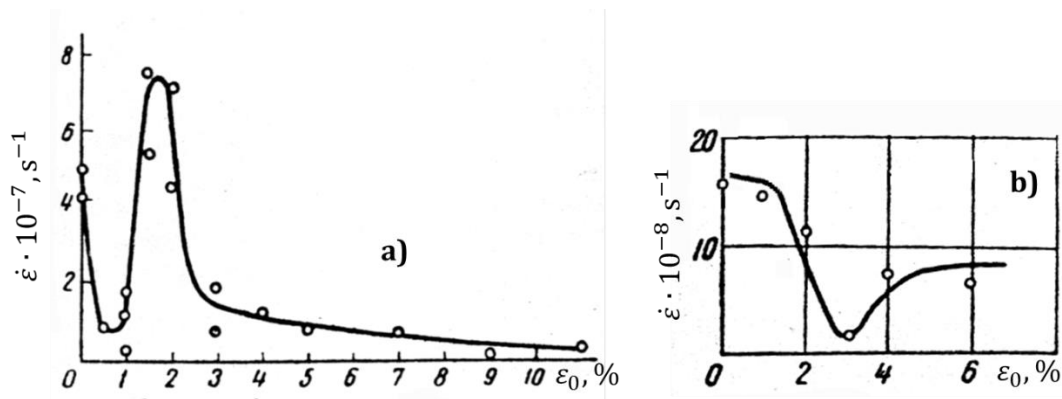


**Fig. 2.16** Dependences of the rate of steady-state creep (uniaxial tension) on the level of plastic prestrain in tension: **a)** aluminum ( $\sigma = 9.6$  MPa,  $T = 260^\circ\text{C}$ ), ( $T_a = 260^\circ\text{C}$ ,  $t_a = 1$  hour); **b)** copper ( $\sigma = 15$  MPa,  $T = 500^\circ\text{C}$ ), ( $T_a = 500^\circ\text{C}$ ,  $t_a = 1$  hour); (Bazelyuk et al., 1970, 1971).

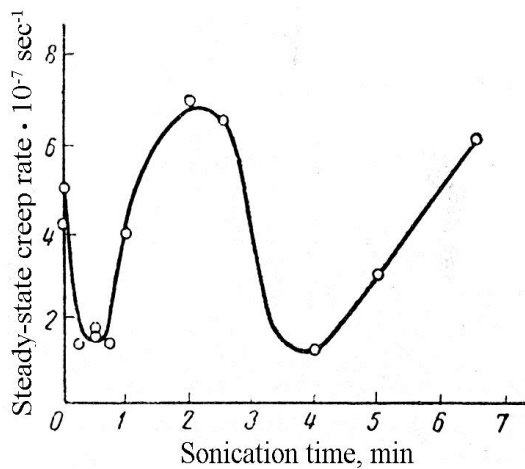


**Fig. 2.17.** Steady-state creep of aluminum in tension ( $T = 260^\circ\text{C}$ ,  $\sigma = 9.6$  MPa) as a function of sonication time in the course of preliminary UT (oscillation frequency and amplitude are  $f = 20$  kHz and  $A = 15 \mu\text{m}$ ;  $T_a = 260^\circ\text{C}$ ,  $t_a = 1$  hour); (Bazelyuk et al., 1970, 1971).

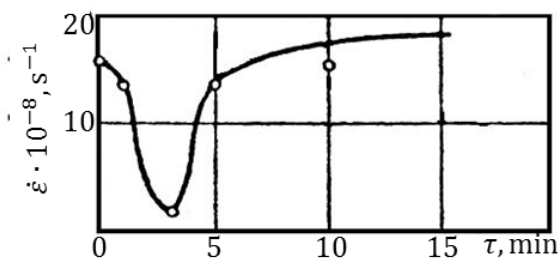


**Fig. 2.18.** Steady-state creep rate of copper in tension ( $T = 500^\circ\text{C}$ ,  $\sigma = 15$  MPa) as a function of sonication time in the course of preliminary UT (oscillation frequency and amplitude are  $f = 20$  kHz and  $A = 25 \mu\text{m}$ ;  $T_a = 500^\circ\text{C}$ ,  $t_a = 1$  hour); (Bazelyuk et al., 1970, 1971).

The changes in the rate of steady-state creep after MTT or UT were observed also for nickel and its alloys (Mordyuk, 1970), molybdenum (Mordyuk, & Demchenko, 1978), and stainless steel (Bazelyuk et al., 1980).

The hardening caused by the preliminary treatments can be attributed to the changes in the crystal structure of the specimens subjected to plastic straining or ultrasonic irradiation and stabilizing annealing. Although the dynamic of dislocation structure evolution during MTT and UT is different, the following common tendencies can be pointed out.

In the process of both plastic flow and sonication, the number of defects such as dislocations, dislocation loops and dipoles as well as point defects grows dramatically, which results in that original relatively perfect crystals split into fragments whose sizes and orientations depend on the level of pre-strain or sonication time [Siu, & Ngan (2011), Peslo (1984), Kulemin (1978), Biront (1979), Bazelyuk et al. (1980)]. The boundaries of the fragments form a three-dimensional network of subboundaries and play the role of sites of dislocation pileups.

Using transmission electron microscopy and X-ray investigations, Bazelyuk et al. (1970, 1971), Demchenko et al. (1976), and Novikov (1974) report the formation of thermally stable dislocation substructure during the anneal of a cold-hardened or sonicated metal. Some defects annihilate, reducing the internal stresses, and the remaining dislocations are redistributed into energy-favorable configurations (subboundaries) (McLean, D. 1957); point-defect atmospheres pin the subboundary networks.

The dislocation substructure formed in the course of the preliminary treatments impedes the development of creep by restricting the free path of dislocations (i.e. both coarse and fine sliding decreases), and by blocking the dislocation sources (Bazelyuk et al. 1970, 1971, 1980; Kulemin, 1978). As a result, the steady-state creep of the material subjected to preliminary MTT or UT decreases. However, this hardening phenomenon has a non-monotone character. As seen from Figs. 2.16-18, the  $\dot{\epsilon} = \dot{\epsilon}(\epsilon_0)$  and  $\dot{\epsilon} = \dot{\epsilon}(\tau)$  function decreases only for a certain range,  $\epsilon_0 \in [0, \epsilon_{0opt}]$  and  $\tau \in [0, \tau_{opt}]$ , where  $\epsilon_{0opt}$  and  $\tau_{opt}$  is an optimal plastic pre-strain and sonication time, respectively ( $\epsilon_{0opt} \approx 1.0\%$  and  $\epsilon_{0opt} \approx 3.2\%$ ,  $\tau_{opt} \approx 0.5$  min and  $\tau_{opt} \approx 3$  min for aluminum and copper, respectively) For  $\epsilon_0 > \epsilon_{0opt}$  and  $\tau > \tau_{opt}$  the creep rate tends to its initial value. Bazelyuk et al. (1970, 1971), Kulemin (1978), and Bazelyuk et al. (1980) explain this by the defect-substructure formed in the course of treatments loses its thermomechanical stability. This means that the defect-energy stored in material during the treatments, which is above the optimal value, induces softening processes (an active recrystallization starts, subgrain walls fall apart, etc.) dominating over the hardening ones, which results in the increasing portion of  $\dot{\epsilon} = \dot{\epsilon}(\epsilon_0)$  and  $\dot{\epsilon} = \dot{\epsilon}(\tau)$  curves (from 1.0 to 2.0 % for aluminum and above 3.2% for copper; from 0.5 to 2 min for aluminum and above 3 min for copper).

On passing the minimum,  $\dot{\epsilon} = \dot{\epsilon}(\epsilon_0)$  and  $\dot{\epsilon} = \dot{\epsilon}(\tau)$  curves for copper and aluminum from Figs. 2.16-18 exhibit different types of behavior. The major two reasons for this phenomenon can be explained by the interplay between (i) the number of the point defects nucleated in preliminary plastic deformation or sonication and (ii) different mechanisms of the recovery in the course of secondary creep for materials with different stacking-fault energies,  $\gamma$ , ( $\gamma_{Al} = 0.2$  J/m<sup>2</sup>,  $\gamma_{Cu} = 0.04$  J/m<sup>2</sup>, i.e.,  $\gamma_{Al}/\gamma_{Cu} \approx 5$ ). As well-known, steady-

state creep develops through a thermally activated recovery (softening), which can be of two types: polygonization and recrystallization. The recovery mechanism depends on the level of the stacking fault energy of metal (SFE): polygonization dominates in the metals with a high SFE while recrystallization does for a low SFE [Cadek (1988), Rabotnov (1966)].

As stated above, the number of point defects grows with an increase in  $\varepsilon_0$  or  $\tau$  and beginning from a certain magnitude they start to play a considerable role in the common hardening of material. According to Bazelyuk et al. (1970, 1971), the plastic deformation and the sonication time needed to induce the sufficient number of point defects for a considerable pinning of subgrain boundaries in aluminum is about 2% and 2 min, respectively. That is why the  $\dot{\varepsilon} = \dot{\varepsilon}(\varepsilon_0)$  and  $\dot{\varepsilon} = \dot{\varepsilon}(\tau)$  curves for aluminum show the second decreasing portion as  $\varepsilon_0 > 2\%$  and  $\tau > 2$  min. At the same time, in copper, the creep rate for  $\varepsilon_0 > 6\%$  and  $\tau > 5$  min tends to the level corresponding to the absence of preliminary treatment (while the number of plastic flow and ultrasound induced point defects monotonically grows).

Bazelyuk et al. (1970, 1971, 1980) and Kulemin (1978) explain this by the difference in the recovery processes, which are in equilibrium with hardening ones and determine the secondary creep rate. Copper, as a metal with low stacking-fault energy, softens mainly as a result of recrystallization, which nucleates preferentially in the regions with the highest defect densities (Price, 1990; Poirier, 1985). Therefore, if the number of defects from preliminary MTT or UT exceeds a critical value, the subgrains boundaries containing them become centers of recrystallization. In the course of recrystallization (Buerger, 1979; Novikov, 1974), the resistance of the metal to plastic deformation significantly decreases since rapid migration of the boundaries intensely "cleans" the deformed matrix, which facilitates the motion of dislocations under conditions of creep and increases the rate of steady-state creep as compared with its value at the optimal pre-sonication time. Thus, the optimal value of  $\varepsilon_0$  or  $\tau$  should be chosen to avoid intense recrystallization during the subsequent creep. Another conclusion to be drawn is once the MTT- or UT-substructure loses its thermal stability, which is manifested via recrystallization leading to the formation of a defect-free structure, the point defects cannot serve as an additional factor enhancing the hardening effect from the preliminary treatments. Therefore, the dependence  $\dot{\varepsilon} = \dot{\varepsilon}(\varepsilon_0)$  and  $\dot{\varepsilon} = \dot{\varepsilon}(\tau)$  for copper possesses a single minimum, at which the optimal compromise between the number of dislocations constituting the MTT- or UT-substructure and the thermal stability of the substructure is achieved.

In materials with high stacking fault energy such as aluminum, the most important microstructural evolution during creep consists in the rearranging of free dislocations into subgrains surrounded by low-angle grain boundaries, i.e. aluminum undergoes recovery by polygonization [Price (1990), Poirier (1985)]. If  $\varepsilon_0$  or  $\tau$  is such that the energy stored in MTT- or UT-substructure exceeds a critical value, the preliminary formed subgrain boundaries fall apart under the action of creep-stress and high temperature and terminate to be effective hindrances to the development of the creep. However, the MTT- or UT-substructure can regain its thermal stability if to pin the subgrain boundaries by point defects, which is possible if their number achieves a sufficient value (Bazelyuk et al., 1970, 1971). This situation is observed in Figs. 2.17 and 2.18 for the pre-sonication time-period between 2 and 4 min and for the pre-strain above 2%. Therefore, the dislocation

substructure pinned by point defects again disturbs a balance between the recovery and hardening during creep in favor of latter (the second decreasing portion of  $\dot{\epsilon} = \dot{\epsilon}(\epsilon_0)$  and  $\dot{\epsilon} = \dot{\epsilon}(\tau)$  curves in Figs. 2.17 and 2.18). It is worth noting that  $\dot{\epsilon} = \dot{\epsilon}(\tau)$  curve again increases due to an intensive nucleation and development of microcracks in the course of preliminary ultrasonic irradiation for  $\tau > 4$  min (Fig. 2.17).

The main advantage of UT over MTT is that the dimensions of sonicated specimen remain unchangeable (see Sec. 2.2.1). It is of interest to compare subgrain-boundary angles formed in plastic deformation and sonication giving the same values of microhardness (Ni+1,8Al alloy; Demchenko et al., 1976). The action of ultrasound with  $18 \div 20 \mu\text{m}$  amplitude for several minutes gives an increase in the subgrain-boundary angles of  $\approx 5$  mrad while plastic deformation of  $\approx 5\%$  results in the increase of  $25 \div 30$  mrad. It is the dislocation prismatic loops and dipoles vastly observed during the sonication that contribute to the dislocation density without considerable increasing in width of X-ray reflections. Therefore, the grain boundary energy accumulated in the course of UT is lower than that in mechanical-thermal treatment, i.e. UT leads to the formation of a more stable dislocation structures compared to those obtained in MTT.

If to hold plastic prestrain  $\epsilon_0$  and annealing time  $t_a$  constant, experiments give  $\dot{\epsilon} = \dot{\epsilon}(T_a)$  dependence as shown in Fig. 2.19. It must be noted that there is exist a minimum temperature of annealing ( $T_{min}$ ) starting from which MTT gives the decrease in the steady state creep. As  $T_a \leq T_{min}$ , thermal energy is insufficient to induce processes leading to the formation of stable defect-configurations. For example, polygonization does not occur and the plastic strain induced defects are abundant within the material matrix but they are not arranged in thermal stable configurations and incapable of offering resistance to high temperature creep.

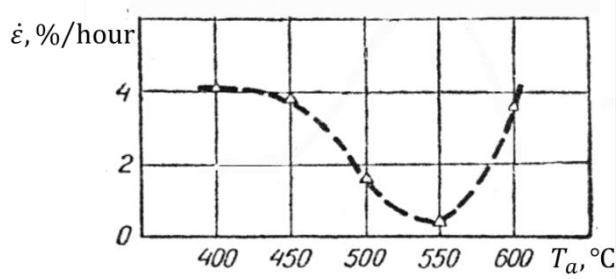


**Fig. 2.19.** Influence of annealing temperature  $T_a$  in the course of preliminary MTT upon the steady-state creep rate of Armco iron in uniaxial tension ( $\sigma = 20$  MPa,  $T = 400$  °C) for the plastic prestrain of 5 % and the anneal duration of 25 hours (Ivanova et al., 1967).

These defects are not effective barriers against the development of irrecoverable strain in the course of steady-state creep due to the high temperature contributes greatly to the disintegration of the pre-existing dislocation grid. As  $T_a > T_{min}$ , subgrain boundaries are being formed in the course of annealing, putting bounds upon the free path of dislocations during the creep, i.e. decreasing the rate of creep strain. The greater value of  $T_1$  (to some extent), the greater impetus for forming subgrain structures. Above a certain annealing-temperature, the

dislocation structure, formed in plastic deformation, cease to be an effective restriction to the following creep strain due to the intensification of recrystallization. As a result, the resistance of the metal to irrecoverable deformation significantly decreases since the rapid migration of dislocation boundaries intensely "cleans" the deformed matrix, which facilitates the motion of dislocations under conditions of creep and increases the rate of

stationary creep as compared with its optimal value. Beginning from a certain value of temperature ( $T_a = T_{max}$ ) the positive effect from MTT completely vanishes, i.e. the steady-state creep rate increases again and comes back to initial values according to the absence of preliminary MTT. Thus, the optimal degree of temperature,  $T_{opt}$ , should be chosen to avoid the possibility of intensive recrystallization.

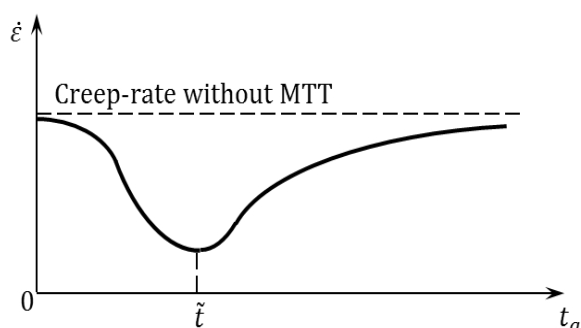


**Fig. 2.20.** Dependence of the rate of steady-state creep under the conditions of uniaxial tension on the duration of annealing  $t_a$  in the course of MTT (Ivanova, & Gordienko, 1964).

Similar, non-monotone, dependence is observed for  $\dot{\epsilon} = \dot{\epsilon}(t_a)$  function as both  $\epsilon_0$  and  $T_a$  are constant. To explain the  $\dot{\epsilon} = \dot{\epsilon}(t_a)$  dependence one needs to use once more the dislocation theory. As stated above, in the course of stabilizing annealing of a material, a part of dislocations generated by cold hardening annihilates and the remaining dislocations rearrange into a more favorable energy configuration (the temperature of annealing must exceed a certain minimum value required to realize nonconservative motion of dislocations but, at the same

time, must be lower than the temperature of recrystallization). The greater the duration of annealing, the larger the number of dislocations entering the boundaries of polygonal subgrains. At the same time, the boundary of a subgrain with large number of dislocations can turn into a center of recrystallization. Moreover, recrystallization can be absent in the process of annealing but occur in the course of creep tests under the favorable influence of high temperatures and force loading (Novikov, 1974). The structure formed after recrystallization is flawless. Clearly, it cannot inhibit the motion of dislocations. The presence of recrystallization shows that the substructure formed in the course of thermomechanical treatment is thermally unstable and its influence on the rate of steady-state creep vanishes. Thus, there exists a duration of annealing  $\tilde{t}$  (Fig. 2.20) corresponding to the optimal combination of the resistance of the substructure with its thermal stability. The family of dislocations generated solely by plastic strains without stabilization in the process of annealing does not affect creep because the dislocations do not form thermally stable structures.

### Summary

It is clear that the classical theories of creep (the theory of hardening and aging as well as the hypothesis of equation of state), see, e.g., Rabotnov (1966), Bethen (2005), are incapable of modeling the dependence of steady state creep rate on the parameters of preliminary treatments, because they study the rate of creep as a function of the acting stress only and neglect the prehistory of loading.

Therefore, together with a huge amount of publications separately discussing the behavior of metals subjected to different steps of MTT or UT, a new theory, solving the problem as a whole, is strongly needed (see Sections 4.2 and 4.3.4).

## CHAPTER III. The synthetic theory of irrecoverable deformation

The synthetic theory of irrecoverable deformation incorporates the Budiansky slip concept and the plastic flow theory developed by Sanders. This theory, which is concerned only with small plastic/creep strains of polycrystalline materials, falls within the category of work-hardening theories of inelastic deformation (Rusinko, A., & Rusinko, K., 2009,2011).

### 3.1 The key points of the synthetic theory and state of the art

**I.** It is of both mathematical and physical nature. As a mathematical (formal) model, the synthetic theory is in full agreement with basic laws and principles of plastic deforming such as Drucker's postulate, the law of deviator proportionality, isotropy postulate, etc.

On the other hand, the synthetic theory is a physical one which includes the characteristics of the microstructure of metal (the nucleation and evolution of crystal lattice defects) and their interplay with microscopic and macroscopic plastic flow. This is motivated by that classical theories of plasticity (e.g. the theory of isotropic or kinematic hardening) suffer from a formal approach in modeling deformation, leaving unaddressed interplay between an inelastic deformation and the evolution of material microstructure in the course of straining.

Being of two-level nature, the synthetic theory is akin to the crystal plasticity theories [Asaro (1983), Hutchinson (2000), Nemat-Nasser, & Okinaka (1996)]. The key question is: which mechanisms of plastic/creep deformation should be taken into account and in what manner plastic microstrains should be related to their carriers, the crystal lattice defects? For the basic mechanism of permanent (irrecoverable) strain we take a slip of the parts of crystal grains relative to each other. To construct a relationship between microstrains and defects, we focus only on incontrovertible facts about in what interplay the defects of crystal lattice and plastic/creep straining are, while those of secondary importance are omitted from consideration. This makes possible to introduce relatively simple relations on the micro-level of material which, at the same time, adequately reflect the real behavior of material in irrecoverable deforming. An excessive concretization of the mechanisms, which accompany/induce the deformation, leads inevitably to extremely cumbersome expressions in which the role of dominating processes can be unjustifiably veiled.

Summarizing, the synthetic theory is aimed to strike a compromise between a physical adequacy and simplicity in calculations to be more readily applied to engineering design.

**II.** Independently on the type of deformation – plastic deformation or high-temperature creep – to be modeled, a single notion, irrecoverable (permanent) deformation, is introduced, i.e. the deformation is not splitted into plastic (“instantaneous”) and creep (viscous) parts (Rusinko, A. 2008, 2009). The manifestation of plastic or creep component and their interrelations depend on concrete loading/temperature-regimes. The correctness to use the notion of irrecoverable deformation follows from the similarity of the mechanism of time-dependent and plastic deformation. Indeed, their dominant mechanism is a slip of the parts of crystal grains relative to each other. These slips are induced mainly

by the motions of dislocations which, in turn, are induced/accompanied by other microstructural imperfections (defects) of crystalline lattice (vacancies, interstitial atoms, etc.). Undoubtedly, the driving forces and configurations of defects are different under different conditions. Nevertheless, despite of the variety of processes occurring in a body subjected to different loading regimes, numerous experiments systematically record the arising of dislocation gliding. Other facts justifying the similarity of the nature of plastic and time-dependent deformation are **(i)** a hydrostatic stress does not affect creep deformation; **(ii)** the axes of principal stress and creep strain rate coincide; **(iii)** no volume change occurs during creep (Betten, 2005). These results are the same as those for plastic deformation [Chen, & Han (2007), Chakrabarty (2000)].

**III.** Following the tendency of unified approaches to model permanent deformation (see e.g. Chaboche et al., 1996 and 1997), the system of constitutive equations that governs the whole spectrum of inelastic deformation has been worked out. In terms of the synthetic theory, the universality of this system is based on:

**(i)** a single equation provides the relation between a) microdeformation, b) crystalline structure defects induced by this deformation, and c) time. Further, the procedure of the transition between micro- and macro-level is also uniformed: the sum of irrecoverable micro-strains determines the magnitude of macro-strain.

**ii)** the hardening rule is set in such a way that the evolution of loading surface obeys an unique rule. In addition, the kinetics of the loading surface transformation is not set a priori but is fully determined by a given loading path.

In contrast to plastic flow theories with smooth loading surfaces, the synthetic theory, being the “successor” of slip concept (Rusinko, K., 1981, 1986), predicts the appearance of a corner point on the loading surface and thus is capable of describing the peculiarities of plastic deformation in the vicinity of an orthogonal additional loading. On the other hand, the slip concept has one serious shortcoming, namely a contradiction with the deviator proportionality law. It results in that the calculation of a strain in uniaxial tension, for the constants that are determined to best fit the experimentally obtained curve in torsion, shows a large deviation from experimental data (Joshimure, 1958). Therefore, neither flow plasticity theories nor the Batdorf-Budiansky slip concept satisfy, to a full extent, the main requirements imposed on the theories of plasticity. Therefore, it is necessary to use a more effective mathematical model.

Summarizing, the synthetic theory is capable of embracing both plastic and creep deformation. In addition, numerous non-classical problems such as negative and inverse creep, creep as a function of preliminary mechanical-thermal and ultrasound processing, etc. has been successfully solved. These problems refute the erroneous conjecture that plastic and creep deformations do not affect each other and thus must be described by separate models. In addition, they contradict the hypothesis of creep potential (Betten, 2005; Rabotnov, 1969) that defines the creep strain as a single-valued function of acting stress and temperature independently on the loading prehistory.

### 3.2 Ilyushin's deviatoric space

Consider the five-dimensional Ilyushin deviatoric stress and strain spaces,  $\mathcal{S}^5$  and  $\mathcal{E}^5$ , [Ilyushin (1963), Béda et al. (1995)]. The components of stress- and strain-vector,  $\vec{\mathcal{S}} = S_i \vec{g}_i$  and  $\vec{\mathcal{E}} = e_i \vec{f}_i$  (the vectors  $\vec{g}_i$  and  $\vec{f}_i$  are unit base vectors in  $\mathcal{S}^5$  and  $\mathcal{E}^5$ ; they are coaxial, but have different scales), are defined as follows

$$S_1 = \sqrt{3/2} S_{xx}, \quad S_2 = S_{xx}/\sqrt{2} + \sqrt{2} S_{yy}, \quad S_3 = \sqrt{2} S_{xz}, \quad S_4 = \sqrt{2} S_{xy}, \quad S_5 = \sqrt{2} S_{yz}, \quad (3.2.1)$$

$$e_1 = \sqrt{3/2} e_{xx}, \quad e_2 = e_{xx}/\sqrt{2} + \sqrt{2} e_{yy}, \quad e_3 = \sqrt{2} e_{xz}, \quad e_4 = \sqrt{2} e_{xy}, \quad e_5 = \sqrt{2} e_{yz}, \quad (3.2.2)$$

where  $S_{ij}$  and  $e_{ij}$  ( $i, j = x, y, z$ ) denote the deviatoric components of stress and strain tensor, respectively:  $S_{ij} = \sigma_{ij} - \sigma \delta_{ij}$ ,  $e_{ij} = \varepsilon_{ij} - \varepsilon \delta_{ij}$ ;  $\delta_{ij}$  is the Kronecker's delta,  $\sigma = \frac{1}{3} \sum_{k=1}^3 \sigma_{kk}$ ,  $\varepsilon = \frac{1}{3} \sum_{k=1}^3 \varepsilon_{kk}$ .

The length of the vector  $\vec{\mathcal{S}}$  is related to the second invariant of stress deviator tensor,  $J_2$ , as  $|\vec{\mathcal{S}}| = 2\sqrt{3}J_2$ . Besides, the  $|\vec{\mathcal{S}}|$  can be related to the so-called shear stress intensity,  $\tau_0$ , as  $|\vec{\mathcal{S}}| = \sqrt{2/3} \tau_0$ .

In terms of the synthetic theory, the establishment of strain-stress and strain-time relationships takes place in the three-dimensional subspace ( $\mathcal{S}^3$ ) of  $\mathcal{S}^5$ .

### 3.3. Two-level approach to calculate inelastic deformations, the Batdorf-Budiansky slip concept

The main statements of Batdorf-Budiansky slip concept are (Batdorf, & Budiansky, 1949):

**(i)** Plastic strain is determined on micro- and a macro-level. For the macro-level we take as the elementary volume of a body,  $\mathbb{V}$ , which is considered as point in the mathematical sense. This volume consists of a large quantity of volumes,  $\mathbb{V}_0$  (the micro-level), each being continuum, capable of deforming under the applied stresses. The micro-volume is suggested to be a crystalline grain. Lichatchev (1993) substantiates the sizes of volumes  $\mathbb{V}$  and  $\mathbb{V}_0$ .

**(ii)** The stress condition distribution over the volumes  $\mathbb{V}_0$  is assumed to be homogeneous, i.e. if a point of body experiences, e.g., two-axial tension, every volume  $\mathbb{V}_0$  is subjected to the two-axial tension as well.

**(iii)** Plastic deformation within the microvolume  $\mathbb{V}_0$  is assumed as slip of one part of  $\mathbb{V}_0$  in relation to another. Therefore, in contrast to the even distribution of the stress over microvolumes or slip systems  $\mathbb{V}_0$ , the plastic strain (or plastic slip) strongly depends on the orientation of the slip system relative to the direction of the acting forces. It is assumed that the quantity of  $\mathbb{V}_0$  is so great (theoretically it tends to infinity) that every possible orientation of slip systems exists in volume  $\mathbb{V}$ .

**(iv)** The total plastic strain in  $\mathbb{V}$ , i.e. the strain at a point in a body, is determined as the sum of the strain components generated in volumes  $\mathbb{V}_0$ .

### 3.4 Yield surface as an inner envelope of tangent planes.

Consider, as a starting point, the Tresca yield criterion. Following Sanders (1954), we propose to construct planes tangential to the yield surface instead of the yield surface itself. As a result, the yield surface can be treated as the inner envelope of the tangent planes.

Shear stress  $\tau_{nl}$  at a point in a body (the resolved shear stress), in terms of stress vector components  $S_i$ , can be expressed as

$$\tau_{nl} = \frac{1}{\sqrt{2}} [\sqrt{3}l_x n_x S_1 + (l_y n_y - l_z n_z) S_2 + (l_x n_z + l_z n_x) S_3 + (l_x n_y + l_y n_x) S_4 + (l_y n_z + l_z n_y) S_5], \quad (3.4.1)$$

where  $n_i$  and  $l_i$  ( $i = x, y, z$ ) are the direction cosines of orthonormal vectors  $\vec{n}$  and  $\vec{l}$ , respectively in Descartes coordinate system at a point of body (see Fig. 3.1). The vector  $\vec{n}$  defines the plane on which stress  $\tau_{nl}$  acts and the vector  $\vec{l}$ , lying in this plane, defines the direction of the acting stress. The specified vectors  $\vec{n}$  and  $\vec{l}$  constitute a slip system. The cosines  $n_i$  and  $l_i$  may be expressed via spherical angles,  $\tilde{\alpha}$ ,  $\tilde{\beta}$ , and  $\omega$  (Rusinko, K., 1981). It is clear from Eq. (3.4.1) that each fixed value of  $\tilde{\alpha}$ ,  $\tilde{\beta}$ , and  $\omega$  corresponds to a plane in  $\mathcal{S}^5$  space, thereby expressing the physical sense of the planes: every plane from (3.4.1) represents a slip system at the point of body.

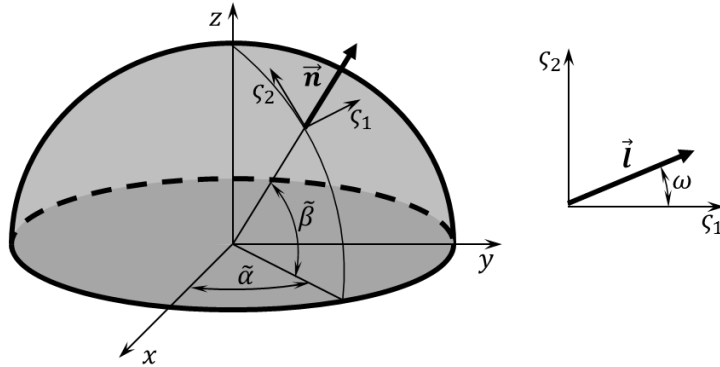


**Fig. 3.1.** Spherical coordinates ( $\tilde{\alpha}$  and  $\tilde{\beta}$ ) of slip plane on a hemisphere of unit radius; slip direction on the slip plane is given by angle  $\omega$  within  $\zeta_1 - \zeta_2$  coordinate system.

The Tresca yield criterion, which states that the first plastic shearing occurs in that slip system where the maximum shearing stress reaches the value of the yield stress,  $\tau_s$ , may be expressed analytically as:

$$\frac{\partial \tau_{nl}}{\partial \tilde{\alpha}} = \frac{\partial \tau_{nl}}{\partial \tilde{\beta}} = \frac{\partial \tau_{nl}}{\partial \omega} = 0, \quad (3.4.2)$$

$$\tau_{nl} = \tau_s. \quad (3.4.3)$$

On the other hand, Eqs. (3.4.2) and (3.4.3) constitute the system of equations from which, by the elimination of  $\tilde{\alpha}$ ,  $\tilde{\beta}$  and  $\omega$ , the envelope of planes (3.4.3) may be constructed.

Therefore, we conclude that the Tresca yield surface is the envelope of the following family of planes:

$$\sqrt{3}l_x n_x S_1 + (l_y n_y - l_z n_z)S_2 + (l_x n_z + l_z n_x)S_3 + (l_x n_y + l_y n_x)S_4 + (l_y n_z + l_z n_y)S_5 - \sqrt{2}\tau_S = 0. \quad (3.4.4)$$

The following question may arise, whether the family of planes from Eq. (3.4.4) gives all tangent planes to the Tresca yield surface, since, as follows from Eq. (3.4.4), the orientation of a plane in five-dimensional space is determined by only three parameters, angles  $\tilde{\alpha}$ ,  $\tilde{\beta}$  and  $\omega$ .

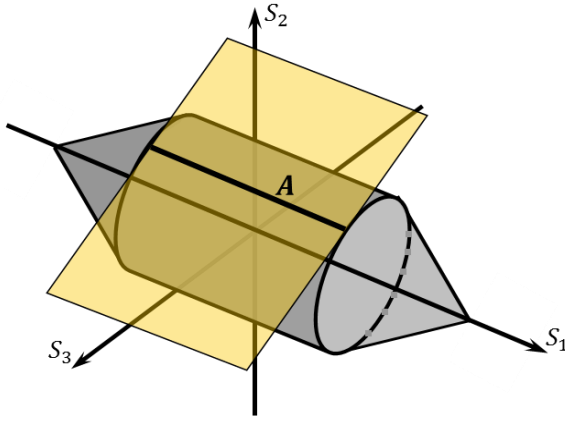


**Fig. 3.2.** Locus of contact (line A) between the Tresca yield surface and tangent plane for the case of plane stress state in  $\mathcal{S}^3$ .

The answer is positive because from the system of equations (3.4.2)-(3.4.3) (four equations for five variables) it follows that contact between the Tresca yield surface and its tangent planes occurs, in general case, along some curve which play the role of the fifth variable. To provide a simple illustration of this, consider the Tresca yield surface for the case of the plane stress state in three-dimensional subspace  $\mathcal{S}^3$ . It can be seen from Fig. 3.2 that locus of contacts between the Tresca yield surface and the tangent plane is line A.

Components of vector  $\vec{N}(N_1, \dots, N_5)$  normal to plane (3.4.4) can be calculated as

$$\begin{aligned} N_1 &= \sqrt{3}l_x n_x, & N_2 &= l_y n_y - l_z n_z, & N_3 &= l_x n_z + l_z n_x, \\ N_4 &= l_x n_y + l_y n_x, & N_5 &= l_y n_z + l_z n_y, \end{aligned} \quad (3.4.5)$$

and it is easy to verify that the vector  $\vec{N}$  is unit. Therefore, Eq. (3.4.4) gives the planes equidistant from the origin of coordinates,  $H_N = \sqrt{2}\tau_S$  (an index 'N' indicates on the normal vector  $\vec{N}$ ). It must be underlined that this result in no way means that the inner envelope of the planes from (3.4.4) gives, for example, a sphere in  $\mathcal{S}^3$ . By way of example, Fig. 3.2 demonstrates the Tresca yield surface for the case of plane stress state, which consists of a cylinder and two cones.

In three-dimensional subspace  $\mathcal{S}^3$  ( $S_4 = 0, S_5 = 0$ ), Eq. (3.4.4) becomes

$$\sqrt{3}l_x n_x S_1 + (l_y n_y - l_z n_z)S_2 + (l_x n_z + l_z n_x)S_3 - \sqrt{2}\tau_S = 0. \quad (3.4.6)$$

Eq. (3.4.6) gives the trace of five-dimensional plane (3.4.4) in three-dimensional subspace  $\mathcal{S}^3$ . The normalization factor,  $d$ , for the plane (3.4.6) has the form

$$d = \sqrt{1 - l_y^2 - n_y^2 + 4l_y^2 n_y^2}. \quad (3.4.7)$$

Let us write down the equation of the plane from Eq. (3.4.6) via a distance from the origin of coordinates in  $\mathcal{S}^3$  ( $h_m$ ) and a plane normal vector,  $\vec{m}(m_1, m_2, m_3)$ , as

$$m_1 S_1 + m_2 S_2 + m_3 S_3 = h_m, \quad (3.4.8)$$

where  $m_i$  ( $i = 1, 2, 3$ ) are (Fig. 3.3)

$$m_1 = \cos \alpha \cos \beta, \quad m_2 = \sin \alpha \cos \beta, \quad m_3 = \sin \beta. \quad (3.4.9)$$

Let us introduce angle  $\lambda$  between normals  $\vec{N}$  and  $\vec{m}$  as

$$\cos \lambda = \vec{N} \cdot \vec{m}. \quad (3.4.10)$$

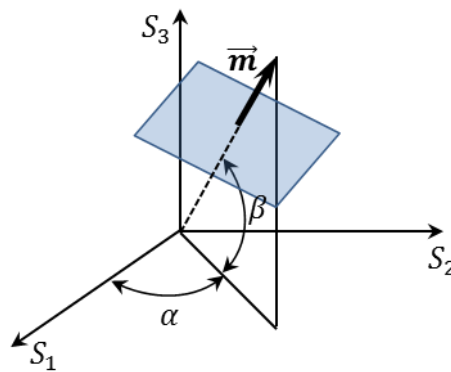


**Fig. 3.3.** Orientation of  $\vec{m}$  in  $\mathcal{S}^3$ .

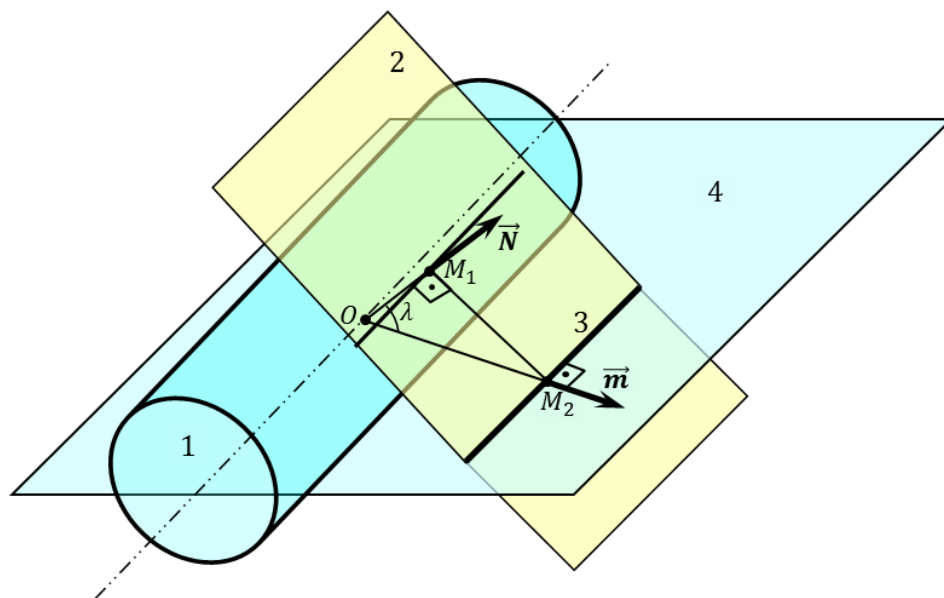


**Fig. 3.4.** Illustration of the relation between the distance to a plane and its trace.

Distance  $h_m$  is related to  $H_N$ , via angle  $\lambda$ , as (Rusinko, K., & Andrusik, 1993)

$$H_N = h_m \cos \lambda. \quad (3.4.11)$$

The above formula is illustrated by Fig. 3.4 where, for simplicity, the yield surface, marked by 1, plays the part of that in  $\mathcal{S}^5$ ; the tangent plane to this surface and its trace (line) on plane 4 are marked by 2 and 3, respectively.  $OM_1 = H_N = \sqrt{2}\tau_S$  is the distance to the plane 2, and  $OM_2 = h_m = H_N/\cos \lambda$  is that to its trace 3. As Eqs. (3.4.6) and (3.4.8) represent one and the same plane, then

$$\begin{aligned} m_1 &= \sqrt{3}l_x n_x / d, & m_2 &= (l_y n_y - l_z n_z) / d, & m_3 &= (l_x n_z + l_z n_x) / d, \\ h_m &= \sqrt{2}\tau_S / d. \end{aligned} \quad (3.4.12)$$

From Eqs. (3.4.6), (3.4.8) and (3.4.11) it follows that  $d = \cos \lambda$ , and from Eq. (3.4.12) we have

$$\sqrt{3}l_x n_x = m_1 \cos \lambda, \quad l_y n_y - l_z n_z = m_2 \cos \lambda, \quad l_x n_z + l_z n_x = m_3 \cos \lambda. \quad (3.4.13)$$

Eqs. (3.4.5) and (3.4.13) give

$$N_k = m_k \cos \lambda \quad \text{for } k = 1, 2, 3. \quad (3.4.14)$$

In addition, due to the orthonormality of vectors  $\vec{l}$  and  $\vec{n}$ , we have

$$l_x^2 + l_y^2 + l_z^2 = 1, \quad n_x^2 + n_y^2 + n_z^2 = 1, \quad l_x n_x + l_y n_y + l_z n_z = 0. \quad (3.4.15)$$

Eqs. (3.4.13) and (3.4.15) constitute the system of six equation over six variables  $l_x, \dots, n_z$ . In solving this system we obtain:

$$l_x n_y + l_y n_x = \pm \sqrt{\frac{\sin^2 \lambda}{2} + \chi}, \quad l_z n_y + l_y n_z = \pm \sqrt{\frac{\sin^2 \lambda}{2} - \chi}, \quad (3.4.16)$$

where

$$\chi = \frac{(\bar{m}_1 - m_2)(3\bar{m}_1 + m_2)\{1 - [3 - 2(\bar{m}_1 - m_2)^2 \cos^2 \lambda]\} - 4m_3 \sqrt{1 - (\bar{m}_1 - m_2)^2 D}}{2[4 - 3(\bar{m}_1 - m_2)^2]}, \quad (3.4.17)$$

$$D = 1 - [2 - (\bar{m}_1 - m_2)^2] \cos^2 \lambda + [1 - (\bar{m}_1 - m_2)^2]^2, \quad \bar{m}_1 = m_1 / \sqrt{3}.$$

The substitution of Eq. (3.4.16) into Eq. (3.4.4) leads to the following equation for tangent plane

$$S_1 m_1 \cos \lambda + S_2 m_2 \cos \lambda + S_3 m_3 \cos \lambda + S_4 \left( \pm \sqrt{\frac{\sin^2 \lambda}{2} + \chi} \right) + S_5 \left( \pm \sqrt{\frac{\sin^2 \lambda}{2} - \chi} \right) \quad (3.4.18)$$

$$= \sqrt{2} \tau_S.$$

Eqs. (3.4.4) and (3.4.18) represent one and the same plane tangential to the Tresca yield surface. The only difference between these two equations is that the coefficients at  $S_i$  in Eq. (3.4.4) are expressed in terms of the Budiansky slip concept, angles  $\tilde{\alpha}$ ,  $\tilde{\beta}$ , and  $\omega$ , while Eq. (3.4.18) utilizes the terms of the Ilyushin deviatoric stress space, angles  $\alpha$ ,  $\beta$ , and  $\lambda$ . In other words, similarly to the slip concept, the orientation of the plane tangential to the Tresca yield surface in  $\mathcal{S}^5$  is fully determined by three parameters, angles  $\alpha$ ,  $\beta$ , and  $\lambda$ .

From Eq. (3.4.17), it is evident that the quantity  $D$  can take a negative value for some values of  $m_i$  and  $\lambda$  (for example for  $m_1 = m_3 = 1$ ,  $m_2 = 0$ ,  $\lambda = 0$ ). Therefore, the function  $\chi$  can take a complex value. This means that there are such planes (directions) for which their envelope is undefined.

### 3.5 Yield criterion and yield surface in terms of the synthetic theory

The main proposition is that the Tresca yield surface, which is the inner-envelope of planes (3.4.18), is replaced by a new one which is the inner-envelope of the following family of planes (Rusinko, A., & Rusinko, K., 2009):

$$S_1 m_1 \cos \lambda + S_2 m_2 \cos \lambda + S_3 m_3 \cos \lambda +$$

$$S_4 \left( \pm \sqrt{\frac{\sin^2 \lambda}{2} + \chi_0(\lambda)} \right) + S_5 \left( \pm \sqrt{\frac{\sin^2 \lambda}{2} - \chi_0(\lambda)} \right) = \sqrt{2} \tau_S. \quad (3.5.1)$$

Eq. (3.5.1) differs from Eq. (3.4.18) in replacing of the function  $\chi(\alpha, \beta, \lambda)$  by  $\chi_0(\lambda)$  which depends only upon one variable,  $\lambda$ . In this case, the normal vector  $\vec{N} = N_i \vec{g}_i$  ( $\vec{g}_i$  are unit base vectors in space  $\mathcal{S}^5$ ) has the following components:

$$N_1 = m_1 \cos \lambda, \quad N_2 = m_2 \cos \lambda, \quad N_3 = m_3 \cos \lambda,$$

$$N_4 = \pm \sqrt{\frac{\sin^2 \lambda}{2} + \chi_0(\lambda)}, \quad N_5 = \pm \sqrt{\frac{\sin^2 \lambda}{2} - \chi_0(\lambda)} \quad (3.5.2)$$

Together with the vector  $\vec{N}$ , consider its increments due to increments in  $\alpha$ ,  $\beta$  and  $\lambda$ :

$$d\vec{N}_\alpha = \frac{\partial N_i}{\partial \alpha} \vec{g}_i d\alpha, \quad d\vec{N}_\beta = \frac{\partial N_i}{\partial \beta} \vec{g}_i d\beta, \quad d\vec{N}_\lambda = \frac{\partial N_i}{\partial \lambda} \vec{g}_i d\lambda. \quad (3.5.3)$$

The volume of the parallelepiped,  $V$ , constructed on vectors  $d\vec{N}_\alpha$ ,  $d\vec{N}_\beta$ , and  $d\vec{N}_\lambda$  is calculated by the Gram determinant:

$$(dV)^2 = \begin{vmatrix} d\vec{N}_\lambda \cdot d\vec{N}_\lambda & d\vec{N}_\lambda \cdot d\vec{N}_\alpha & d\vec{N}_\lambda \cdot d\vec{N}_\beta \\ d\vec{N}_\alpha \cdot d\vec{N}_\lambda & d\vec{N}_\alpha \cdot d\vec{N}_\alpha & d\vec{N}_\alpha \cdot d\vec{N}_\beta \\ d\vec{N}_\beta \cdot d\vec{N}_\lambda & d\vec{N}_\beta \cdot d\vec{N}_\alpha & d\vec{N}_\beta \cdot d\vec{N}_\beta \end{vmatrix}, \quad (3.5.4)$$

which is reduced, for the case of normal vector components from Eq. (3.5.2), to the view

$$(dV)^2 = \begin{vmatrix} \frac{\partial \vec{N}}{\partial \lambda} \cdot \frac{\partial \vec{N}}{\partial \lambda} & 0 & 0 \\ 0 & \cos^2 \beta \cos^2 \lambda & 0 \\ 0 & 0 & \cos^2 \lambda \end{vmatrix} (dad\beta d\lambda)^2 = \frac{\partial \vec{N}}{\partial \lambda} \cdot \frac{\partial \vec{N}}{\partial \lambda} \cos^2 \beta \cos^4 \lambda (dad\beta d\lambda)^2. \quad (3.5.5)$$

If to require that the volume  $dV$  be

$$dV = \cos \beta dad\beta d\lambda \quad (3.5.6)$$

and that the function  $\chi_0$  be dependent upon only one variable,  $\lambda$ , we ensure the regularity of the yield surface with tangential planes from Eq. (3.5.1). As follows from Eqs. (3.5.5) and (3.5.6),

$$\frac{\partial \vec{N}}{\partial \lambda} \cdot \frac{\partial \vec{N}}{\partial \lambda} = \frac{1}{\cos^4 \lambda}. \quad (3.5.7)$$

On the base of Eq. (3.5.2), the above formula takes the form of Ricatti differential equation:

$$\left(\frac{d\chi_0}{d\lambda}\right)^2 - 4\cot\lambda \cdot \chi_0 \cdot \frac{d\chi_0}{d\lambda} + 4\left(\frac{1}{\cos^4 \lambda \sin^2 \lambda} - 1\right)\chi_0^2 - \tan^2 \lambda (\tan^2 \lambda + \sin^2 \lambda) = 0 \quad (3.5.8)$$

whose solution is

$$\chi_0(\lambda) = \frac{1}{2} \sin^2 \lambda \sin y_0, \quad (3.5.9)$$

$$y_0 = 2\sqrt{2} \left[ F_0\left(\lambda, \frac{1}{\sqrt{2}}\right) - E_0\left(\lambda, \frac{1}{\sqrt{2}}\right) + \sqrt{\lambda - \frac{1}{2} \sin^2 \lambda \tan \lambda} \right],$$

where  $F_0$  and  $E_0$  are incomplete elliptic integrals of the first and of the second kind:

$$F_0\left(\lambda, \frac{1}{\sqrt{2}}\right) = \int_0^\lambda \frac{d\lambda}{\sqrt{1 - \frac{1}{2} \sin^2 \lambda}}, \quad E_0\left(\lambda, \frac{1}{\sqrt{2}}\right) = \int_0^\lambda \sqrt{1 - \frac{1}{2} \sin^2 \lambda} d\lambda. \quad (3.5.10)$$

In contrast to the function  $\chi(\alpha, \beta, \lambda)$ , the function  $\chi_0(\lambda)$  does not take a complex value at any angle  $\lambda$ . Since the complex values of the function  $\chi(\alpha, \beta, \lambda)$  expresses the existence of corner points on the Tresca yield surface (where a derivative does not exist). Then, the real values of  $\chi_0(\lambda)$  at any angle  $\lambda$  are viewed as a sufficient condition of the regularity of the

surface with tangent planes from (3.5.1). Therefore, now it possible to apply the standard mathematical procedure to determine the envelope of planes (3.5.1).

### 3.6 Yield surface in subspace $\mathcal{S}^3$ . Tangent planes and their traces

Let us restrict ourselves further to three-dimensional subspace  $\mathcal{S}^3$ , where the trace of plane (3.5.1) can be written as

$$S_1 m_1 \cos \lambda + S_2 m_2 \cos \lambda + S_3 m_3 \cos \lambda = \sqrt{2} \tau_S. \quad (3.6.1)$$

The equation of the inner envelope of planes (3.6.1) can be obtained from the equation system consisting of Eq. (3.6.1) and the following expressions

$$\frac{d\tau}{d\alpha} = \frac{d\tau}{d\beta} = \frac{d\tau}{d\lambda} = 0, \quad (3.6.2)$$

where  $\tau$  is the left-hand side in Eq. (3.6.1). From Eqs. (3.6.1) and (3.6.2), it follows that

$$\tan \alpha = \frac{S_2}{S_1}, \quad \tan \beta = \frac{S_3}{S_1 \cos \alpha + S_2 \sin \alpha}, \quad \lambda = 0. \quad (3.6.3)$$

If to substitute the values of  $\alpha$ ,  $\beta$ , and  $\lambda$  from the formula above into Eq. (3.6.1), we will obtain the equation of yield surface as

$$S_1^2 + S_2^2 + S_3^2 = 2\tau_S^2. \quad (3.6.4)$$

Therefore, the yield surface in  $\mathcal{S}^3$  is a sphere that corresponds to the von Mises yield criterion. According to Sanders, in a virgin state, the sphere (3.6.4) can be thought of the inner envelope of equidistant planes,  $H_N(\lambda = 0) = h_m = \sqrt{2}\tau_S$  for all directions. However, it is very important to note that this sphere is the trace of that five-dimensional yield surface which is neither the Tresca (because of changes made in Eq. (3.5.1)) nor von Mises yield surface.

One of the key points of the synthetic theory is that the position of the tangent plane in  $\mathcal{S}^5$  can be determined via its trace in  $\mathcal{S}^3$ . As seen from Eq. (3.4.11), the quantity  $h_m$  varies within the following range:

$$\sqrt{2}\tau_S < h_m < \infty. \quad (3.6.5)$$

Therefore, the traces of the tangent planes, given by Eq. (3.6.1), fill up the whole space beyond the sphere (3.6.4) in  $\mathcal{S}^3$ . In other words, any plane located beyond the sphere (3.6.4) is the trace of some plane tangential to the yield surface in  $\mathcal{S}^5$ .

Fig. 3.5 illustrates the case when tangent planes in  $\mathcal{S}^5$ , marked by **0**, **1** and **2**, with different normal vectors  $\vec{N}_0$ ,  $\vec{N}_1$  and  $\vec{N}_2$ , have their traces with identically oriented normal vectors  $\vec{m}$  in  $\mathcal{S}^3$ . As is seen from Fig. 3.5 and Eq. (3.4.11), the angle  $\lambda$  gives the possibility to distinguish identically oriented planes in  $\mathcal{S}^3$  as the traces of different planes in  $\mathcal{S}^5$ . Namely,

two planes in  $\mathcal{S}^3$  with identical orientation, i.e. for a fixed value of  $\alpha$  and  $\beta$ , but with different values of  $\lambda$ , are parallel to each other, but have different distances  $h_m$ . Furthermore, Eq. (3.4.11) gives  $H_N = h_m$  as  $\lambda = 0$ ; therefore, the plane tangential to the yield surface in  $\mathcal{S}^5$  is at the same time tangential to its trace in  $\mathcal{S}^3$ , sphere (3.6.4), (the plane is marked by  $\mathbf{0}$  in Fig. 3.5).

In general, any plane in  $\mathcal{S}^3$  is the trace of an infinite set of planes from  $\mathcal{S}^5$ , of which one is tangent to the yield surface in  $\mathcal{S}^5$ . Those planes which are not tangential to the yield surface in  $\mathcal{S}^5$  are not taken into consideration.

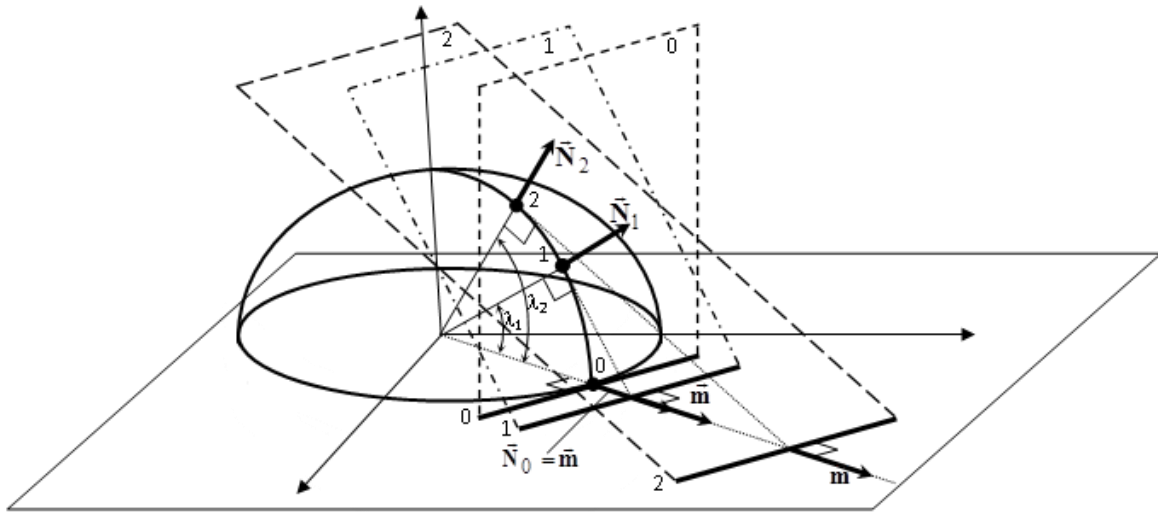


**Fig. 3.5.** Tangent planes and their traces (for simplicity, the hemisphere plays the role of yield surface in  $\mathcal{S}^5$ , and the circle does that of subsurface in  $\mathcal{S}^3$ ).

### 3.7 Evolution of loading surface. Inelastic deformation on the micro- and macro-levels.

Sanders (1954) extended the provision that a yield surface can be constructed as an inner envelope of planes to the case of loading as well. In the course of loading, vector  $\vec{S}$  moves (shifts) at its endpoint (load point) a set of planes from their initial position. The movements of the planes located at the endpoint of vector  $\vec{S}$  are translational, i.e. the plane orientations remain unchangeable. Those planes which are not at the endpoint of vector  $\vec{S}$  remain unmovable. The displacement of plane at the endpoint of stress vector symbolizes the development of plastic microdeformation within corresponding slip system.

The condition that a plane is reached/shifted by stress vector is

$$H_N = \vec{S} \cdot \vec{N}. \quad (3.7.1)$$

As a result, the loading surface, which is constructed as an inner-envelope of tangent planes, takes the shape fully determined by loading trajectory, i.e. by the current positions of planes.

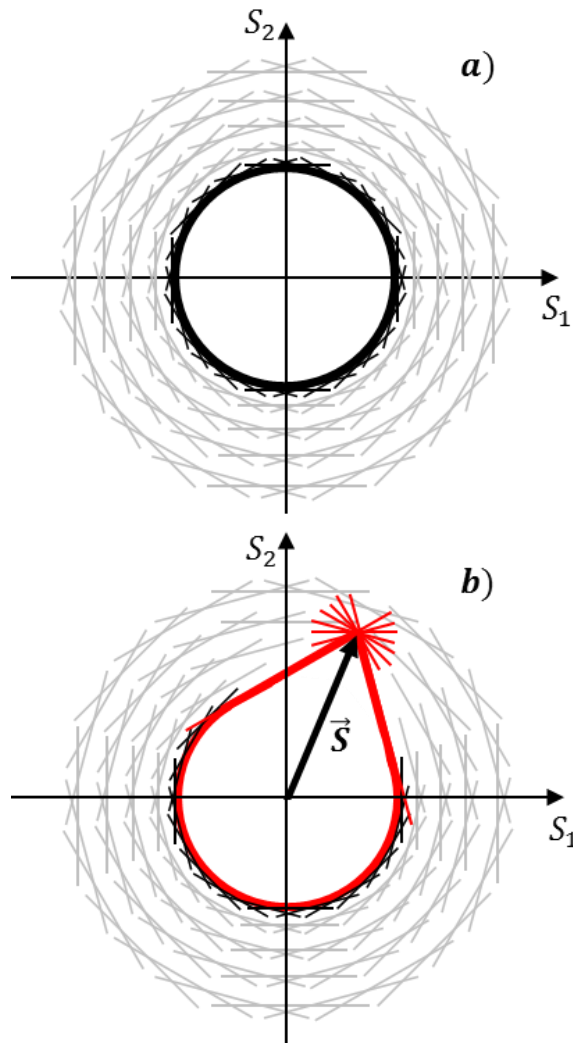


**Fig. 3.6.** Yield and loading surfaces according to Sanders.

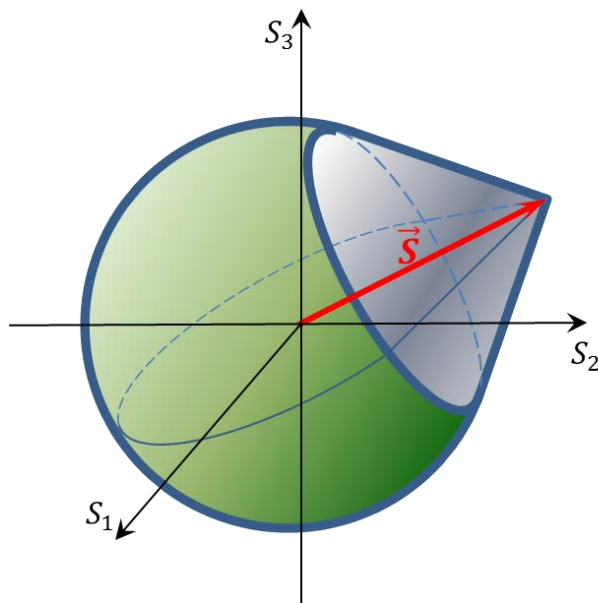


**Fig. 3.7.** Loading surface in  $S^3$  (planes are not shown).

Fig. 3.6a shows the locations of planes at a virgin state and their inner envelope, sphere (3.6.4), while Figs. 3.6b and 3.7 demonstrate the loading surface when some set of planes is displaced by the vector  $\vec{S}$ . The loading surface consists of two parts: a) sphere (3.6.4) constructed as the envelope of motionless planes ( $H_N = \sqrt{2}\tau_S$ ), and b) a cone whose generators are formed by the boundary planes shifted by the vector  $\vec{S}$ . On the top of this cone there are planes shifted by the vector  $\vec{S}$  during loading. It is easy to see that a corner point arises on the loading surface at the load point. This fact is of great importance especially when one calculates inelastic deformation for the case of curvilinear loading paths [Rusinko, & Fenyvesi (2014), Rusinko (2014)].

Therefore, in contrast to many theories, e.g. the theory of isotropic or kinematic hardening, the evolution of a loading surface, in terms of synthetic theory, is not prescribed a priori but is fully determined by the hodograph of stress vector.

Figures 3.6 and 3.7 show that a material is supposed to be isotropic at its virgin state, but demonstrates a strong anisotropy in the course of plastic deformation.

Since every tangent plane corresponds to a certain slip system, we can assume that the displacement of each plane shifted by vector  $\vec{S}$  represents an elementary process of irrecoverable deformation within the slip system thereby connecting the tangent planes displacements with real physical processes accompanying plastic straining. An incremental plastic strain-vector,  $d\vec{e}$ , is assumed to be in the direction of the outer normal to the plane and proportional to the volume  $dV$  from Eq. (3.5.6) (Fig. 3.8). It is

defined as

$$d\vec{e} = \varphi_N \vec{N} dV, \quad (3.7.2)$$

where  $\varphi_N$  is a new term called the irrecoverable deformation intensity; an index 'N' indicates on the normal vector  $\vec{N}$ . The irrecoverable deformation intensity is a scalar magnitude that expresses an average continuous measurement of plastic slip within one slip system. The way how  $\varphi_N$  relates to other quantities will be discussed in Section 3.8.

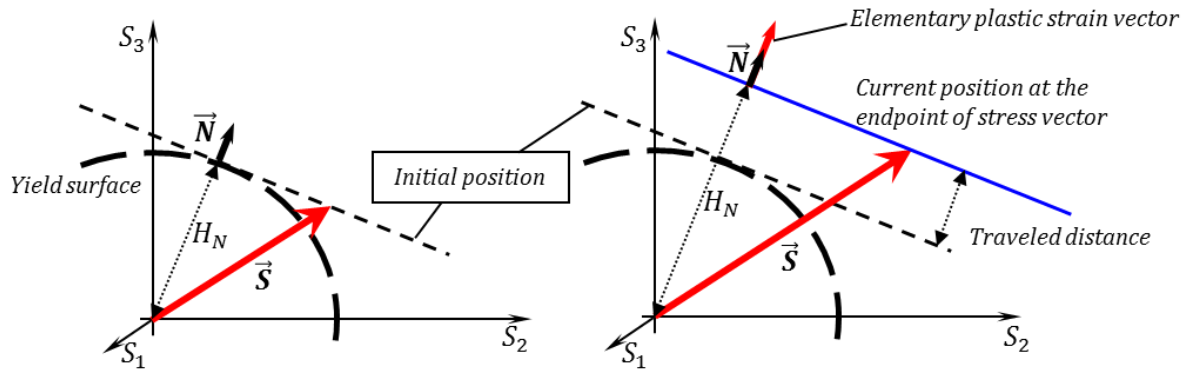


**Fig. 3.8.** Displacement of tangent plane at the endpoint of stress vector.

A total plastic strain-vector ( $\vec{e}$ ) is defined as the sum (three-folded integral) of microdeformations “generated” on movable planes:

$$\vec{e} = \iiint_V \varphi_N \vec{N} dV, \quad (3.7.3)$$

$$e_k = \int_{\alpha} \int_{\beta} \int_{\lambda} \varphi_N m_k \cos \lambda \cos \beta \, d\alpha d\beta d\lambda \quad k = 1, 2, 3. \quad (3.7.4)$$

The volume  $dV$  includes an elementary set of the planes located on the surface  $\cos \beta \, d\alpha d\beta$  (shown by hatching in Fig. 3.9) whose distances vary within  $dh$  which is proportional to  $d\lambda$ . It must be noted that Eq. (3.7.3) may be used only if  $\vec{S} \in \mathcal{S}^3$  ( $S_i \neq 0$  for  $i = 1, 2, 3$ ;  $S_4 = S_5 = 0$ ), i.e. the synthetic theory is inapplicable for modeling plastic straining when  $\vec{S} \in \mathcal{S}^5$  ( $S_i \neq 0$  for  $i = 1, \dots, 5$ ).

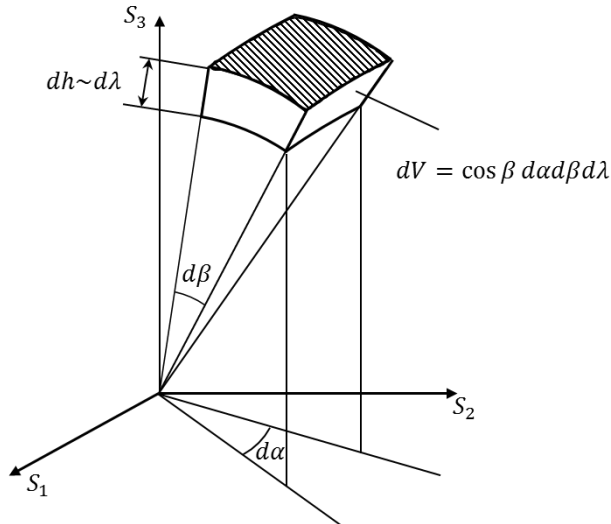


**Fig. 3.9.** Elementary volume of planes expressed in terms of angles  $\alpha$ ,  $\beta$  and  $\lambda$ .

It is very important to note that, according to any flow plasticity theory, strain is associated to five-dimensional loading surface independently of the quantity of nonzero stress deviator vector components. Therefore, despite the fact that  $\vec{S} \in \mathcal{S}^3$ , the movements of all planes symbolize the development of plastic deformation, and not only those tangential to sphere (3.6.4). That is why we must study the displacements of all planes located beyond the sphere (3.6.4) in  $\mathcal{S}^3$ . At the same time, since the loading surface follows tangent planes as their inner envelope, the evolution of loading surface in  $\mathcal{S}^3$  is determined by the planes for which  $\lambda = 0$ .

### **Discussion.**

1. Koiter (1953) showed that the application of the Sanders hardening rule in terms of Budiansky's angles  $\tilde{\alpha}$ ,  $\tilde{\beta}$  and  $\omega$  leads to the stress-strain relations identical with those obtained in the framework of the slip concept. It is a very interesting result that two entirely different approaches, the slip concept and the Sanders flow theory result in the same relations. However, in this case, the result obtained by Koiter "inherits" all shortcomings of the slip concept. It is this fact that prompts modifying the Tresca yield surface, by means of changes made in the equation of tangent planes, Eq. (3.5.1).

2. The following question may arise that perhaps it is possible to take sphere (3.6.4) as the projection of five-dimensional hypersphere. The answer is negative, because, in terms of any flow theory, the plastic strain is accumulated due to the evolution of loading surface in five-dimensional deviatoric space independently of the quantity of nonzero stress components at a given loading. On the other hand, the von Mises yield criterion, a hypersphere in  $\mathcal{S}^5$ , is not suitable due to the following reason (Popov, 1987). The orientation of tangent plane in  $\mathcal{S}^5$  is defined by four angles (therefore, it is very difficult to trace the movements of the planes), whereas, in terms of the synthetic theory, tangent planes from  $\mathcal{S}^5$  are determined by three parameters, angles  $\alpha$ ,  $\beta$ , and  $\lambda$ . This result agrees with the statement of the Budiansky concept that any slip system can be determined by three angles.

### **3.8 Law for inelastic deformation at the microlevel**

In order to calculate the plastic vector components via Eq. (3.7.4), we need to establish a relationship for  $\varphi_N$  which governs the development of inelastic deformation within one slip system.

For this purpose, we

- (i) introduce a **yield criterion** and define a **hardening rule** via relating the plane distances  $H_N$  to new quantities, **defect intensity** ( $\psi_N$ ) and **rate integral** ( $I_N$ ),
- (ii) establish a **constitutive equation** giving relationship between strain intensity  $\varphi_N$ , defect intensity  $\psi_N$ , and time.

(i) First of all, the fact that the magnitude of  $H_N$  expresses the degree of material hardening is undoubted. Indeed, the greater distance to a plane, the greater stress vector must be applied to reach the plane and displace it, i.e. to give an increment in plastic deformation. The  $H_N = H_N(\psi_N, I_N)$  relationship can be defined in a linear fashion,

$$H_N = S_p + \psi_N + I_N, \quad (3.8.1a)$$

or as a quadratic function:

$$H_N = \sqrt{S_p^2 + \psi_N + I_N^2}. \quad (3.8.1b)$$

In the above formulae,  $S_p = \sqrt{2/3} \sigma_p = \sqrt{2} \tau_p$ , where  $\sigma_p$  and  $\tau_p$  are the creep limit of metal in uniaxial tension and pure shear, respectively. The  $S_p$  is defined as a stress vector needed to induce permanent strain at the loading rate tending to zero.

Further throughout, we use a sphere of radius  $S_p$  – **von Mises yield criterion** – as an initial yield surface<sup>1</sup>:

$$S_1^2 + S_2^2 + S_3^2 = S_p^2. \quad (3.8.2)$$

This sphere can be obtained from Eq. (3.8.1) by letting  $\psi_N = 0$  and  $I_N = 0$  that corresponds to a virgin state of material. Indeed, formula  $H_N = S_p$  gives a set of equidistant planes whose inner envelope is sphere (3.8.2),

The difference between  $S_s$  (yield limit) and  $S_p$  (creep limit) is governed by the rate integral and will be discussed in Chapter IV. Therefore, it is the creep limit of material at a given temperature that is interpreted as its initial strength.

Defect intensity represents an average scalar continuous measure of crystallographic defects inherent in real bodies (dislocations, vacancies, interstitial defects, etc.), which nucleate and multiply in the course of inelastic straining within a slip system. The presence of  $\psi_N$  in (3.8.1) reflects the well-known phenomenon of strain hardening of a material during its inelastic deforming. Therefore, the object, whose plastic/creep deformation to be modelled, is a **continuous medium** possessing a continuous function,  $\psi_N$ , reflecting the strain hardening. At a virgin state the defect intensity is assumed to be equal to zero.

We deliberately have disregarded an actually type of defects – we will call the defects any crystal lattice imperfections caused by non-elastic deformations that obstruct its further development –, the  $\psi_N$  reflects the only fact, whose correctness has been proved by numerous experiments, that a permanent deformation leads to the nucleation and multiplication of crystal defects.

Due to the fact that  $H_N = H_N(\alpha, \beta, \lambda)$ , Eq. (3.8.1) shows that  $\psi_N$  is a function angles  $\alpha$ ,  $\beta$ , and  $\lambda$  as well. In other words,  $\psi_N$  symbolizes the number of defects generated in one slip

---

<sup>1</sup> Sphere (3.6.4) of radius  $\sqrt{2}\tau_s$  can be used for plastic strains only.

system. Furthermore,  $\psi_N$  is a time-dependent quantity because of  $I_N = I_N(\alpha, \beta, \lambda, t)$  (see below, Eq. (3.8.4)). So, finally,  $\psi_N = \psi_N(\alpha, \beta, \lambda, t)$ .

Since, in terms of the synthetic theory, the development of inelastic deformation is modelled by the displacement of planes at the endpoint of stress vector, formulae (3.8.1) can be written as

$$\psi_N = \begin{cases} H_N - I_N - S_p & \text{for the planes which are riched by } \vec{S}, \text{ i. e. } H_N = \vec{S} \cdot \vec{N} \\ 0 & \text{for the planes which are not riched by } \vec{S}, \text{ i. e. } H_N > \vec{S} \cdot \vec{N} \end{cases} \quad (3.8.3a)$$

or

$$\psi_N = \begin{cases} H_N^2 - I_N^2 - S_p^2 & \text{for the planes wich are riched by } \vec{S}, \text{ i. e. } H_N = \vec{S} \cdot \vec{N} \\ 0 & \text{for the planes wich are not riched by } \vec{S}, \text{ i. e. } H_N > \vec{S} \cdot \vec{N} \end{cases} \quad (3.8.3b)$$

The formulae above as well as Fig. 3.8 evidently demonstrate that the greater distance is traveled by a plane, the greater number of defects and, consequently, the deformation is cumulated on it.

The issue about the value of power coefficient in (3.8.3), 1 or 2, was discussed in terms of the slip concept (Rusinko, K. 1981,1986). As a result, it has been established that the maximum value of power coefficient in the relationship governing the hardening of material on microlevel is 2, which is substantiated from the point of view of the deviator proportionality law. Therefore, a researcher has room for “maneuver” to choose the relation which gives the best agreement with experiments. On the other hand, there are problems that can be solved only with concrete version of Eq. (3.8.3). For example, the problem of the development of plastic deformation due to a finite additional loading (Rusinko, A. and Rusinko, K., 2011) can be solved only by utilizing Eq. (3.8.3b), while the phenomena of negative creep can be modelled only via Eq. (3.8.3a).

The formula for the rate integral,

$$I_N(t) = B \int_0^t \frac{d\vec{S}}{ds} \cdot \vec{N} \exp(-p(t-s)) ds, \quad (3.8.4)$$

( $0 < B < 1$  and  $p$  are model constants), has been obtained from the statistical analysis of the stress/strain distribution over a grain [Rusinko, A., & Rusinko, K. (2009), Rusinko, A. (2010)]. It is has been shown that an increase in loading rate makes this distribution more non-uniform (Kuksa et al., 1986). So,  $I_N$  provides an average measure of *local peak stresses*, which can be substantiated by the following chain of thoughts.

As said earlier, an inelastic strain leads to the formation of dislocation pile-ups, dislocation tangles, unmovable jogs, etc., where the strain energy is mainly stored. These structures, being of strongly local character, cause an uneven stress/strain distribution through the crystal lattice that, in turn, leads to crystal lattice distortion. Kuksa’s experiments performed on specimens of pure copper, iron and titanium for elastic and plastic deformations report that micro-stresses of the second and third kind considerably deviate from their mean values, and the local peak stresses can take significant values. It must be noted that the crystal lattice distortion is observed at elastic deformation as well.

The non-uniform stress distribution makes a metal more unstable compared with its annealed state. Once favorable conditions arise, e.g. constant stresses (as in creep tests), the recovery/relaxation of crystal lattice distortions occurs. It is the difference between the local and average stresses provides a driving force for the process of recovery. In other word, the energy stored during plastic loading starts to release giving rise to temporary deformation (e.g. primary creep). This process manifests itself in spontaneous slips in grains induced by thermally activated movements of dislocation due to locked and tangled dislocations and the obstructions in their way themselves become progressively movable thereby causing the development of deformation.

Asaro, & Rice (1977) and Peirce et al. (1983) indicate the following properties of the stresses arising around lattice distortions (local peak microstresses):

- 1) they, being directly correlated with the dislocation density, make a material harder,
- 2) the higher the loading rate, the larger local stresses act,
- 3) they are unstable, i.e. they decrease with time as soon as favorable conditions arise.

Therefore, on the one hand, the local microstresses cause the “rate-hardening” of material during active loading but, on the other hand, they can relax that leads to the recovery of material. A time-dependent macrodeformation of material is the result of the competitive processes of the rate-hardening and recovery.

By integrating in (3.8.4), we obtain  $I_N \sim t$  plot for the case when loading consists of two parts,  $\dot{\vec{S}} \geq 0$  for  $t \in [0, t_M]$  and  $\dot{\vec{S}} = 0$  for  $t > t_M$  (Fig. 3.10):

$$I_N = \frac{B}{p} (\dot{\vec{S}} \cdot \vec{N}) [1 - \exp(-pt)], \quad t \in [0, t_M] \quad (3.8.5)$$

$$I_N = \frac{B}{p} (\dot{\vec{S}} \cdot \vec{N}) [\exp(pt_M) - 1] \exp(-pt), \quad t \geq t_M \quad (3.8.6)$$

Formulae above show that the integral  $I_N$  behaves in the same manner as the local peak stresses, namely:

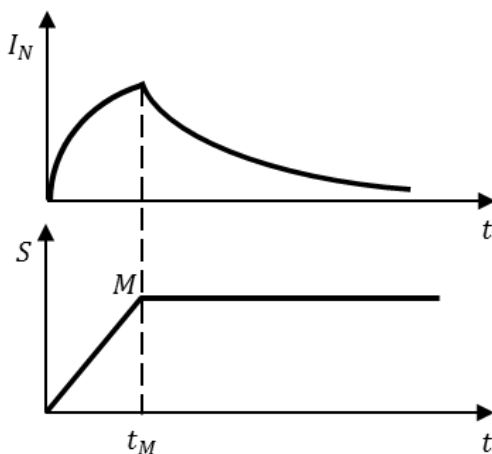


**Fig. 3.10.**  $I_N$  vs  $t$  plot ( $S$  denotes the length of stress vector).

a)  $I_N$  grows under a fast (“active”) loading, which symbolizes the rate-hardening of material (the number of tangled and locked dislocations monotonically increases; this process is more intensive, the greater is the loading rate),

b)  $I_N$  decreases under constant stresses (favorable conditions arise to unlock the dislocations from their obstruction, etc., i.e. the recovery of material takes place). The condition  $I_N \rightarrow 0$  means that  $H_N(t) = \text{const}$  in Eqs. (3.8.3) for  $t > t_M$ , which symbolizes that recovery balances hardening. Such a situation is typical for steady-state creep and, therefore,  $I_N \rightarrow 0$  can be interpreted as the transition between the primary and secondary creep.

Summarizing, the degree of material hardening, plane distance  $H_N$  in formulae (3.8.1), depends on two quantities: the defect intensity ( $\psi_N$ ) and the rate integral ( $I_N$ ).

To complete the formulation of the strain state of material on the micro-level, one needs to relate the strain intensity  $\varphi_N$  to the defect intensity  $\psi_N$  and time.

**(ii)** Let us designate through  $d\psi_N$  and  $d\varphi_N$  an increment of  $\psi_N$  and  $\varphi_N$  in time  $dt$  for a fixed plane, i.e.  $d\alpha = d\beta = d\lambda = 0$ . Similarly to the slip concept, we relate the strain intensity to the defect intensity and time by the following equation

$$d\psi_N = rd\varphi_N - K\psi_N dt. \quad (3.8.7)$$

Eq.(3.8.7) says that the development of defects is governed by the following two simultaneous processes:

- $\psi_N$  grows due to the increment of irrecoverable deformation ( $d\varphi_N > 0$ ) and
- $\psi_N$  decreases in the course of deformation, as a function of time, due to the term ( $-K\psi_N dt$ ) which models defect recovery (relaxation).

In (3.8.7),  $r$  is the material constant and  $K$  is a function of the shear stress intensity ( $\tau_0$ ) and homologous temperature,  $\Theta$  (see below, Eq.(3.9.3)).

**Summarizing, the formulae presented below constitute the family of the basic equations of the synthetic theory:**

$S_1 = \sqrt{3/2} S_{xx}, S_2 = S_{xx}/\sqrt{2} + \sqrt{2}S_{yy}, S_3 = \sqrt{2}S_{xz}, S_4 = \sqrt{2}S_{xy}, S_5 = \sqrt{2}S_{yz}.$	(3.2.1)
$H_N = \vec{S} \cdot \vec{N}$	(3.7.1)
$I_N(t) = B \int_0^t \frac{d\vec{S}}{ds} \cdot \vec{N} \exp(-p(t-s)) ds$	(3.8.4)
$\psi_N = H_N - I_N - S_P$ or $\psi_N = H_N^2 - I_N^2 - S_P^2$	(3.8.3)
$d\psi_N = rd\varphi_N - K\psi_N dt$	(3.8.7)
$\vec{e} = \iiint_V \varphi_N \vec{N} dV$	(3.7.3)
$e_1 = \sqrt{3/2} e_{xx}, e_2 = e_{xx}/\sqrt{2} + \sqrt{2}e_{yy}, e_3 = \sqrt{2}e_{xz}, e_4 = \sqrt{2}e_{xy}, e_5 = \sqrt{2}e_{yz}.$	(3.2.2)

Let us specify the units of quantities considered (see the table below)

**Table 3.1** Units in terms of the synthetic theory

Quantity	Unit	Quantity	Unit
$H_N$	MPa	$r$	MPa <sup>2</sup> for the case of Eq. (3.8.3b)
$\psi_N$	MPa for the case of Eq. (3.8.3a)	$K$	s <sup>-1</sup>
$\psi_N$	MPa <sup>2</sup> for the case of Eq. (3.8.3b)	$p$	s <sup>-1</sup>
$\varphi_N$	1	$B$	1
$r$	MPa for the case of Eq. (3.8.3a)		

### 3.9 Partial cases

Inspect partial forms of Eq. (3.8.7).

**(A)** Consider the case of steady-state creep, for which it is characteristic to exhibit a balance between the processes of work hardening and recovery. This fact implies that  $\psi_N(t)$  remains unchangeable in the course of steady-state creep. Indeed, since  $\vec{S}(t) = \text{const}$  and  $I_N \rightarrow 0$ , Eqs. (3.7.1) and (3.8.1) give that  $H_N(t) = \text{const}$  and  $\psi_N(t) = \text{const}$ . Consequently, we have  $d\psi_N = 0$  and Eq. (3.8.7) becomes

$$r\dot{\varphi}_N = K\psi_N = \text{const}, \quad (3.9.1)$$

or

$$r\varphi_N = r\varphi_N^0 + K\psi_N t, \quad (3.9.2)$$

where  $\varphi_N^0$  is the permanent strain intensity accumulated prior to the steady-state creep. The obtained intensity  $\varphi_N$  relates linearly to time  $t$  and, via Eq. (3.7.3), describes the stationary stage of creep. As it is seen from (3.9.1), function  $K$  regulates the steady-state creep rate, which, as well known from experiments, takes extremely small values. Therefore, we can conclude that the term  $K\psi_N t$  in Eq. (3.9.2) exerts essential influence upon  $\varphi_N$  only for a long-termed loading, or very high temperatures. The function  $K$  is defined as follows (Rusinko, A. and Rusinko, K., 2011)

$$K = K_1(T)K_2(\tau_0), \quad K_1 = \exp\left(-\frac{Q}{RT}\right), \quad (3.9.3)$$

$$K_2 = \frac{9cr}{\pi^2} \tau_0^{k-1} \text{ for (3.8.3a) and } K_2 = \frac{9\sqrt{3}cr}{2\sqrt{2}\pi} \tau_0^{k-2} \text{ for (3.8.3b), } c \text{ and } k = \text{const},$$

where  $Q$  is the creep activation energy,  $T$  is temperature. Constant  $k$  regulates the slope of  $\log \dot{\epsilon} \sim \log \sigma$  lines.

**(B)** The integration in (3.8.7) gives

$$r\varphi_N = \psi_N + K \int_0^t \psi_N dt. \quad (3.9.4)$$

This is the most general formula of the synthetic formula which can be used for any type of deformation – from instantaneous plastic strain up to primary and secondary creep. Temporal dependence of deformation is ensured by the second term in (3.9.4) and the rate integral  $I_N$  involved into  $\psi_N$ .

Taking into account that the  $K$  takes small values, a tangible contribution of the second term on the right-hand side in (3.9.4) can be obtained only for a long termed loading or high homology temperatures. Thus, the second term can be neglected for the case of plastic strain (as  $t \rightarrow 0$ ). If so, we get

$$r\varphi_N = \psi_N. \quad (3.9.5)$$

This equation shows that the increment in defects is observed only in those slip systems, where irrecoverable deformation takes place. This is fully coordinated with experiments: if slip systems of a crystal grain are oriented relative acting stresses so that there are no plastic shears in them, no structural changes are observed in these slip systems. As is seen from (3.9.5), the constant  $r$  characterizes the hardening of material in the course of inelastic deformation.

At the same time, Rusinko (2015) shows that the plastic deformation of materials with low melting point, e.g. tin, at room temperature must be modeled by taking into account both the terms in (3.9.4).

**(C)** After a complete or partial unloading, when the increment in permanent deformation is terminated,  $d\varphi_N = 0$ , Eq. (3.8.7) becomes

$$d\psi_N = -K\psi_N dt. \quad (3.9.6)$$

This formula describes the defect relaxations such as the annihilation of dislocations of opposite signs, collapses of grain boundary, the reduction of the efficiency of obstacles to impede dislocation motion, etc.

Therefore, the unique constitutive equation (3.8.7) governs on the microlevel of material

- a) plastic straining,
- b) primary and secondary creep,
- c) defect relaxation at free-load state.

It must be stressed again that the notion of deformation is treated in a uniform way, we make no difference between “instant” and time-dependent deformation. The only notion used is irrecoverable deformation, whose development depends on the concrete loading regime and is governed by the processes occurring on the microlevel of material structure.

The approach to model irrecoverable strains presented above makes the synthetic theory effective “instrument” for modelling various non-classical problems. Besides the problems considered in details in the following chapter, numerous other interesting problems and phenomena have been modelled. They are Haazen-Kelly effect, phase transformation, Feigin phenomenon, the effect of direct current on creep (Rusinko, A., 2011,2014-2016).

## CHAPTER IV. Generalization of the synthetic theory to the cases pronounced as the objectives of this dissertation

### 4.1 Plastic and creep deformation in stress-drop tests

This chapter proposes the generalization of the synthetic theory to describe the phenomena recorded in stress-drop tests (see Fig. 2.2) such as

- negative!!! increment in plastic and creep deformation under the action of positive net stress (portion 2-3 and 3-4),
- creep delay (4-5), and
- inverse creep (5-6).

#### 4.1.1 Generalization of the hardening rule

To model the phenomena listed above we need to establish a law that governs how plastic/creep strain in one direction affects the material hardening in the opposite direction. This approach attunes the synthetic theory with the thoughts considered in Sec. 2.1.

In terms of the synthetic theory, this question sounds like “How does a plastic straining, which is modeled by the movements of planes with normals  $\vec{N}$  at the endpoint of stress vector  $\vec{S}$ , affect the plane distances with opposite normals  $-\vec{N}$ ,  $H_{-N}$ ? The planes with positive and negative normals as well as angles  $\alpha$  and  $\beta$  defining their orientation are shown in Fig. 4.1.

According to Eq. (3.8.3a),  $H_{-N}$  for normals  $-\vec{N}$  is

$$H_{-N} = S_p + \psi_{-N} + I_{-N}. \quad (4.1.1)$$

Therefore, the question posed above can be rephrased as: “How to set the relation between  $\psi_{-N}$  and  $\psi_N$  as well as between  $I_{-N}$  and  $I_N$ ?”

Eq. (3.8.4) gives the rate integral  $I_{-N}$  for normals  $-\vec{N}$  as

$$I_{-N} = B \int_0^t \frac{d\vec{S}}{ds} \cdot (-\vec{N}) \exp[-p(t-s)] ds = -B \int_0^t \frac{d\vec{S}}{ds} \cdot \vec{N} \exp[-p(t-s)] ds = -I_N. \quad (4.1.2)$$

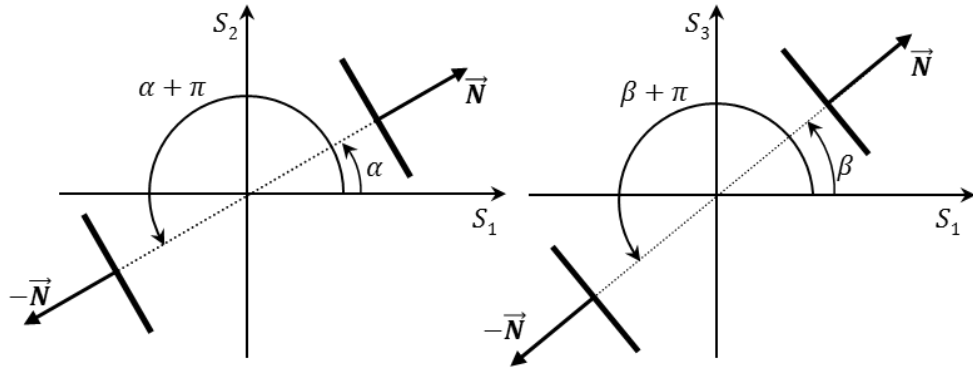


**Fig. 4.1.** The orientation of  $\vec{N}$  and  $-\vec{N}$ .

Since the rate hardening of material in initial loading does not exert any influence upon that in the subsequent loading of opposite sign, we say that if  $I_N$  is positive, then  $I_{-N}$  is set to be zero and vice versa [Rusinko, A., & Rusinko, K. (2011), Rusinko, A. (2012)]:

$$\text{If } I_N > 0, I_{-N} = 0 \text{ or} \quad (4.1.3)$$

$$\text{if } I_{-N} > 0, I_N = 0.$$

To reflect the influence of  $\psi_N$  upon  $H_{-N}$ , the following formula is proposed (Rusinko, 2012)

$$\psi_{-N} = -\psi_N. \quad (4.1.4)$$

Summarizing, Eq. (4.1.1) becomes

$$H_{-N} = S_P - \psi_N - I_N \quad (4.1.5)$$

**Discussion** The non-zero value of  $\psi_{-N}$  from (4.1.4) by no means represents any defects generated in the course of inelastic deformation because the planes with normals  $-\vec{N}$  are not at the endpoint of vector  $\vec{S}$ , while the magnitude of  $\psi_N$  is directly related to the value of irrecoverable strain. Therefore, the main postulate of the synthetic theory that irrecoverable deformation is modeled by the planes shifted by stress vector remains intact. The only aim of Eq. (4.1.4) is to establish, by means of Eq. (4.1.5), the relationship between the plastic deformation induced by loading in one direction and the degree of hardening relative to the opposite-sign-loading. Indeed, the growth of defect intensity  $\psi_N$  leads to the decrease in the distance  $H_{-N}$  in Eq. (4.1.5) that symbolizes the softening of material with respect to the loading of opposite sign.

The softening of material expressed by Eq. (4.1.5) is in full harmony with Sleswyk's (1978), Lloyd's and McElroy's (1974) opinion (see Sec. 2.1) that dislocations easily reverse their motion in the direction opposite to the initial plastic flows. In other words, less stresses are needed to induce irrecoverable deformation in the opposite direction.

In addition, formula (4.1.5) correlates with the notions of effective and backward stresses and their interplay with the dislocation behavior (Kassner et al., 2009), Mughrabi (1983), Evans (1985). Really, internal stresses defining the effective stresses and eventually the degree of material softening in reversal loading directly depend on the number of defects and stress field around them raised in the direct loading. The same situation is observed in Eq. (4.1.5) where terms  $\psi_N$  and  $I_N$  stand for the number of defects and the lattice distortion caused by their presence.

Summarizing, the generalization proposed here makes it possible to model

- a) Bauschinger effect,
- b) negative increment in plastic or creep strain due to the stress-drops even if the net stress remain positive. Really, if the initial loading is of such a magnitude that  $\psi_N + I_N > S_p$ , then  $H_{-N}$  from Eq. (4.1.5) becomes negative meaning that the planes with normals  $-\vec{N}$  have got over the origin of coordinate. This means that planes whose motion models the increment in compressive strain can be reached by the stress vector with positive coordinates. The notion of “Bauschinger super effect” can be encountered in the literature (Osipiuk , 1990, 1991, 1996).

The following calculations correspond to the portions/points in Fig. 2.2 which is repeated in Figs. 4.5 and 4.8.

#### 4.1.2. Plastic straining

**Portion 0-1.** Consider the case of uniaxial tension. If to designate through  $\sigma$  the only non-zero stress tensor component acting along the axis of specimen, then the stress vector components, according to Eq. (3.2.1), are

$$S_1 = \sqrt{2/3} \sigma, \quad S_2 = S_3 = 0, \quad (4.1.6)$$

i.e. the vector  $\vec{S}(S_1, 0, 0)$  is co-directed with  $S_1$ -axis and  $|\vec{S}| = S_1$ .

Scalar product  $\vec{S} \cdot \vec{N}$ , according to Eqs. (3.4.9) and (3.4.14), is

$$\vec{S} \cdot \vec{N} = S_1 N_1 = S_1 m_1 \cos \lambda = S_1 \Omega, \quad \Omega = \cos \alpha \cos \beta \cos \lambda. \quad (4.1.7)$$

Let us consider first angle ranges  $-\pi/2 \leq \alpha \leq \pi/2$  and  $-\pi/2 \leq \beta \leq \pi/2$ .

At the beginning of loading – point **0**,  $t = 0$  (virgin state of material) – we have

- a) no defects induced by plastic deformation:  $\psi_N = 0$ ,
- b) Eq. (3.8.4) at  $t = 0$  gives that  $I_N = 0$ ,
- c) as a result, Eq. (3.8.3a) gives that  $H_N = S_p$ , i.e. we have the set of equidistant planes whose inner envelope is sphere (3.8.2) (see Fig. 4.2a).

Recall the main principle of the synthetic theory: there is no inelastic deformation and, consequently, no defect ( $\psi_N = 0$ ) until the stress vector does not reach a plane. Therefore, prior to the onset of plastic deformation, Eq. (3.8.3a) is

$$H_N = S_p + I_N, \quad (4.1.8)$$

where the rate integral is calculated by Eq. (3.8.6) as (proviso that the loading rate ( $\vec{v}$ ) is assumed to be constant)

$$I_N = \frac{B(\vec{v} \cdot \vec{N})}{p} [1 - \exp(-pt)] = \frac{BS_1\Omega}{pt} [1 - \exp(-pt)]. \quad (4.1.9)$$

Formulae (4.1.8) and (4.1.9) describe the motion of planes outward the origin of coordinates, which does not imply the onset of plastic deformations due to these planes are not reached by the stress vector.

If we take the duration of plastic loading to be infinitely small,  $t \rightarrow 0$ , we can approximate the exponential function in (4.1.9) by the first-order Taylor series, which results in the following relation:

$$I_N = BS_1\Omega. \quad (4.1.10)$$

Consider the instant when the stress vector reaches the first plane, i.e. Eq. (3.7.1) holds true for this plane. This situation symbolizes the onset of plastic deformation and the stress vector length is treated as the yield strength of material. Since the first planes achieved by the stress vector is obviously perpendicular to  $S_1$ -axis, we conclude that for this plane  $\alpha = \beta = \lambda = 0$ , i.e.  $\Omega = 1$ . If to designate the length of the stress vector at the onset of plastic deformation through  $S_S$ , Eqs (3.7.1) and (4.1.7) give that  $H_N = S_S$  as  $\Omega = 1$ . Now, the interplay between the yield- and creep-limit of material can be obtained from Eq. (4.1.8) as

$$S_S = S_p + I_N = S_p + BS_S \Rightarrow S_S = \frac{S_p}{1 - B}. \quad (4.1.11)$$

Therefore, in terms of the synthetic theory, the yield point of material is not treated as a material constant at a given temperature, but strongly depends on a loading rate which is characterized by  $I_N$  (Rusinko, 2010).

The inner envelope of the planes whose distances are determined via Eqs. (4.1.8) at the instant when  $|\vec{S}| = S_S$  is shown in Fig. 4.2b.

The further increase in the  $|\vec{S}|$  leads to the formation of two sets of planes:

$$H_N = \begin{cases} S_1\Omega, & \text{for the planes translated by } \vec{S}, \text{ Eqs (3.7.1) and (4.1.7)} \\ I_N + S_p, & \text{for the rest of planes, Eq. (4.1.8)} \end{cases} \quad (4.1.12)$$

and

$$\psi_N = \begin{cases} S_1\Omega - I_N - S_p, & \text{for the planes translated by } \vec{S}, \text{ Eqs. (3.8.3a) and (4.1.7)} \\ 0, & \text{for the rest of planes} \end{cases}. \quad (4.1.13)$$

The inner envelope of the planes (loading surface) whose distances are given by (4.1.12) is shown in Fig. 4.2c.

Since the scalar product  $\vec{S} \cdot \vec{N} = S_1\Omega$  is treated as a resolved shear stress acting within the corresponding slip system, formula (4.1.13) takes the following physical sense: only those slip systems take part in the development of plastic deformation, where the resolved shear stress is greater than the resistance to plastic shifts (in our case  $I_N + S_p$ ).

Due to the symmetry over the  $S_1$ -axis, the range of angles giving the orientations of planes displaced by the stress vector ( $\Omega_0$ ) is  $-\alpha_0 \leq \alpha \leq \alpha_0$ ,  $-\beta_0 \leq \beta \leq \beta_0$  (Fig. 4.2c). For every direction, there is the set of planes shifted by  $\vec{S}$  which can be defined via angle  $\lambda$ . Its boundary value we designate through  $\lambda_0$  and its range is  $0 \leq \lambda \leq \lambda_0$ .

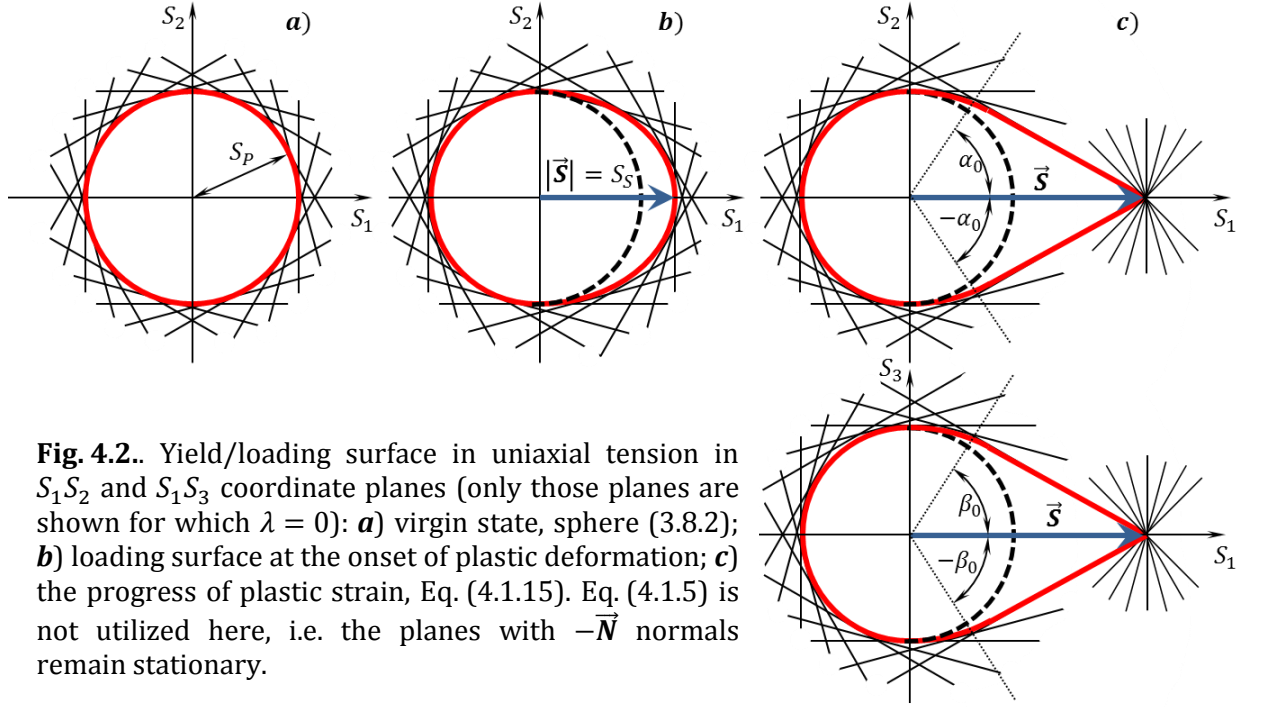


**Fig. 4.2.** Yield/loading surface in uniaxial tension in  $S_1S_2$  and  $S_1S_3$  coordinate planes (only those planes are shown for which  $\lambda = 0$ ): **a)** virgin state, sphere (3.8.2); **b)** loading surface at the onset of plastic deformation; **c)** the progress of plastic strain, Eq. (4.1.15). Eq. (4.1.5) is not utilized here, i.e. the planes with  $-\vec{N}$  normals remain stationary.

Boundary angles  $\lambda_0$ ,  $\alpha_0$ , and  $\beta_0$  are calculated by letting successively  $\psi_N = 0$ ,  $\lambda = 0$ , and  $\beta = 0$  as

$$\Omega_0: \quad -\alpha_0 \leq \alpha \leq \alpha_0, \quad -\beta_0 \leq \beta \leq \beta_0, \quad 0 \leq \lambda \leq \lambda_0,$$

$$\cos \lambda_0 = \frac{S_P}{S_1(1-B) \cos \alpha \cos \beta}, \quad \cos \beta_0 = \frac{S_P}{S_1(1-B) \cos \alpha}, \quad (4.1.14)$$

$$\cos \alpha_0 = \frac{S_P}{S_1(1-B)}.$$

Finally, we rewrite Eqs. (4.1.12) and (4.1.13) as

$$H_N = \begin{cases} S_1 \Omega, & \text{for } \Omega_0 \\ BS_1 \Omega + S_P, & \text{for } \Omega_0^* \end{cases} \quad (4.1.15)$$

and

$$\psi_N = \begin{cases} S_1(1-B)\Omega - S_P, & \text{for } \Omega_0 \\ 0, & \text{for } \Omega_0^* \end{cases} \quad (4.1.16)$$

where  $\Omega_0^*$  stands for  $\alpha_0, \beta_0 \leq |\alpha|, |\beta| \leq \pi/2$ .

Eq. (3.7.4) gives the plastic strain vector components as

$$e_1 = \iiint_{\Omega_0} \varphi_N N_1 dV, \quad (4.1.17)$$

$$e_2 = \iiint_{\Omega_0} \varphi_N N_2 dV, \quad e_3 = \iiint_{\Omega_0} \varphi_N N_3 dV, \quad (4.1.18)$$

where  $\varphi_N$  is related to  $\psi_N$  via Eq. (3.9.5).

It is easy to show that, for the case of uniaxial tension,  $e_2 = e_3 = 0$ , which can be, in particular, geometrically provable. Indeed, the location of tangent planes moved by  $\vec{S}$  is symmetric above  $S_1$ -axis (see Fig. 4.3), i.e. the increments of plastic strain components  $d\vec{e}_3$  on the opposite sides of  $S_1$ -axis are equal in magnitude and opposite in direction, and their summation (integration) leads to mutual elimination (this is valid for components  $d\vec{e}_2$  as well). Consequently, we have only one nonzero strain component,  $e_1$ , i.e. the total strain vector  $\vec{e}$  is directed along  $S_1$ -axis.

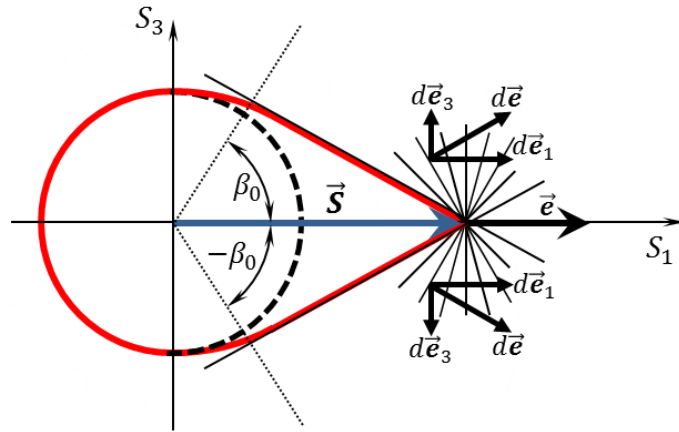


**Fig. 4.3.** Loading surface for uniaxial tension and elementary strain vectors on a plane locating at the endpoint of the stress vector

Formula (4.1.17), together with (3.9.5) and (4.1.16), takes the following form (further throughout, for the case of uniaxial tension, we will omit index "1" in  $e_1$ )

$$e = \frac{\sqrt{2}}{\sqrt{3}r} \int_{-\alpha_0}^{\alpha_0} \int_{-\beta_0}^{\beta_0} \int_0^{\lambda_0} [\sigma(1 - B) \cos \alpha \cos \beta \cos \lambda - \sigma_p] \cos \alpha \cos^2 \beta \cos \lambda \, d\alpha d\beta d\lambda. \quad (4.1.19)$$

Integrating in the formula above gives

$$e = a_0 \Phi(a), \quad (4.1.20)$$

$$a_0 = \frac{\sqrt{2}\pi\sigma_P}{3\sqrt{3}r}, \quad (4.1.21)$$

$$a = \frac{\sigma_P}{\sigma(1-B)}, \quad 0 < a \leq 1 \quad (4.1.22)$$

$$\Phi(a) = \frac{\arccos a}{a} - 2\sqrt{1-a^2} + a^2 \ln \frac{1+\sqrt{1-a^2}}{a}, \quad \Phi(1) = 0. \quad (4.1.23)$$

Axial plastic strain tensor component,  $\varepsilon$ , is calculated by Eq. (3.2.2) as

$$\varepsilon = \sqrt{\frac{2}{3}} e. \quad (4.1.24)$$

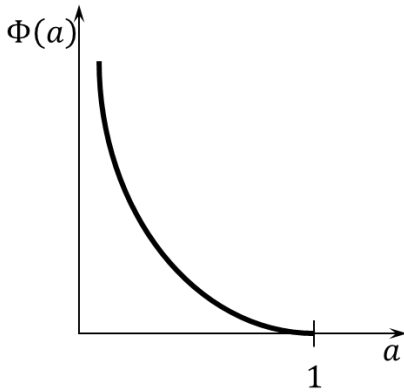


**Fig. 4.4.**  $\Phi(a)$  plot.

Fig. 4.4 shows the plot of  $\Phi(a)$ , a monotone decreasing function of  $a$ . Therefore, the increase in  $\sigma$  implies the decrease in the  $a$  which, in turn, means the growth of  $\Phi$  and, consequently, deformation.

Now, consider angle range  $\pi/2 \leq |\alpha|, |\beta| \leq \pi$ , where the normal vector component  $N_1$  is negative.

According to Eqs. (4.1.1) and (4.1.3), the distance to the planes with normals  $-\vec{N}$  is

$$H_{-N} = S_P + \psi_{-N}. \quad (4.1.25)$$

Because of Eq. (4.1.4),  $\psi_{-N}$  takes non-zero values for  $\pi - \alpha_0 \leq |\alpha| \leq \pi$  and  $\pi - \beta_0 \leq |\alpha| \leq \pi$ . Within this domain  $H_{-N}$  is

$$H_{-N} = S_P - \psi_N = 2S_P - S_1(1-B)\Omega. \quad (4.1.26)$$

For  $\pi/2 \leq |\alpha| \leq \pi - \alpha_0$  and  $\pi/2 \leq |\beta| \leq \pi - \beta_0$ ,  $\psi_{-N} = -\psi_N = 0$ , and Eq. (4.1.26) gives

$$H_{-N} = S_p, \quad (4.1.27)$$

i.e. the planes remain on sphere (3.8.2).

Dependently on the values of  $S_p$ ,  $S_1$  and  $B$ , the distance  $H_{-N}$  form (4.1.26) can take both positive and negative values. The negative value of  $H_{-N}$  means that the plane with normal  $-\vec{N}$  has gone over the origin of coordinates.

Having at hand the plane distances (4.1.15) and (4.1.26), the inner envelope of the planes constitutes the loading surface shown in Fig. 4.5b. Planes in Figs. 4.5 and 4.8 are colored in the following way, the planes located at the endpoint of  $\vec{S}$  are shown in red and all other planes are depicted in black. The surface in Fig. 4.5b is obtained on the assumption that  $H_{-N} < 0$  for some set of planes.

The difference between Figs. 4.2c and 4.5b shows vividly the effect attained by introducing Eq. (4.1.1).

**Remark** It is clear that the quadratic relationship (3.8.3b) cannot be applicable here because, in this case, Eq. (4.1.25) becomes  $H_{-N} = \sqrt{2S_p^2 - S_1^2(1 - B^2)\Omega^2}$  and can lead to complex values for negative radicands.

### 4.1.3. Creep straining

**Portion 1-2.** Eq. (3.8.6) gives the rate-integral as

$$I_N = \frac{B(\vec{v} \cdot \vec{N})}{p} [\exp(pt_1) - 1] \exp(-pt) = \frac{BS_1\Omega}{pt_1} [\exp(pt_1) - 1] \exp(-pt), \quad t \geq t_1 \quad (4.1.28)$$

If to assume, again, that  $t_1 \rightarrow 0$  and apply Taylor series, Eq. (4.1.28) becomes

$$I_N = BS_1\Omega \exp(-pt). \quad (4.1.29)$$

For angle range (4.1.14), the distances to planes remain unchangeable due to they continue to be at the endpoint of stress deviator vector. At the same time, the planes in those directions where  $\psi_N = 0$  at  $t = 0$  start to move toward the origin of coordinates, which is caused by the decrease in  $I_N$  from (4.1.29). Then Eq. (3.8.3a) yields the following form:

$$H_N = S_p + I_N = S_p + BS_1\Omega \exp(-pt). \quad (4.1.30)$$

Once a plane is at the endpoint of  $\vec{S}$ , it becomes to be involved in the producing of creep deformation. Due to the decrease in  $I_N$ , the defect intensity from (3.8.3a) grows in time as

$$\psi_N = S_1(1 - B \exp(-pt))\Omega - S_p. \quad (4.1.31)$$

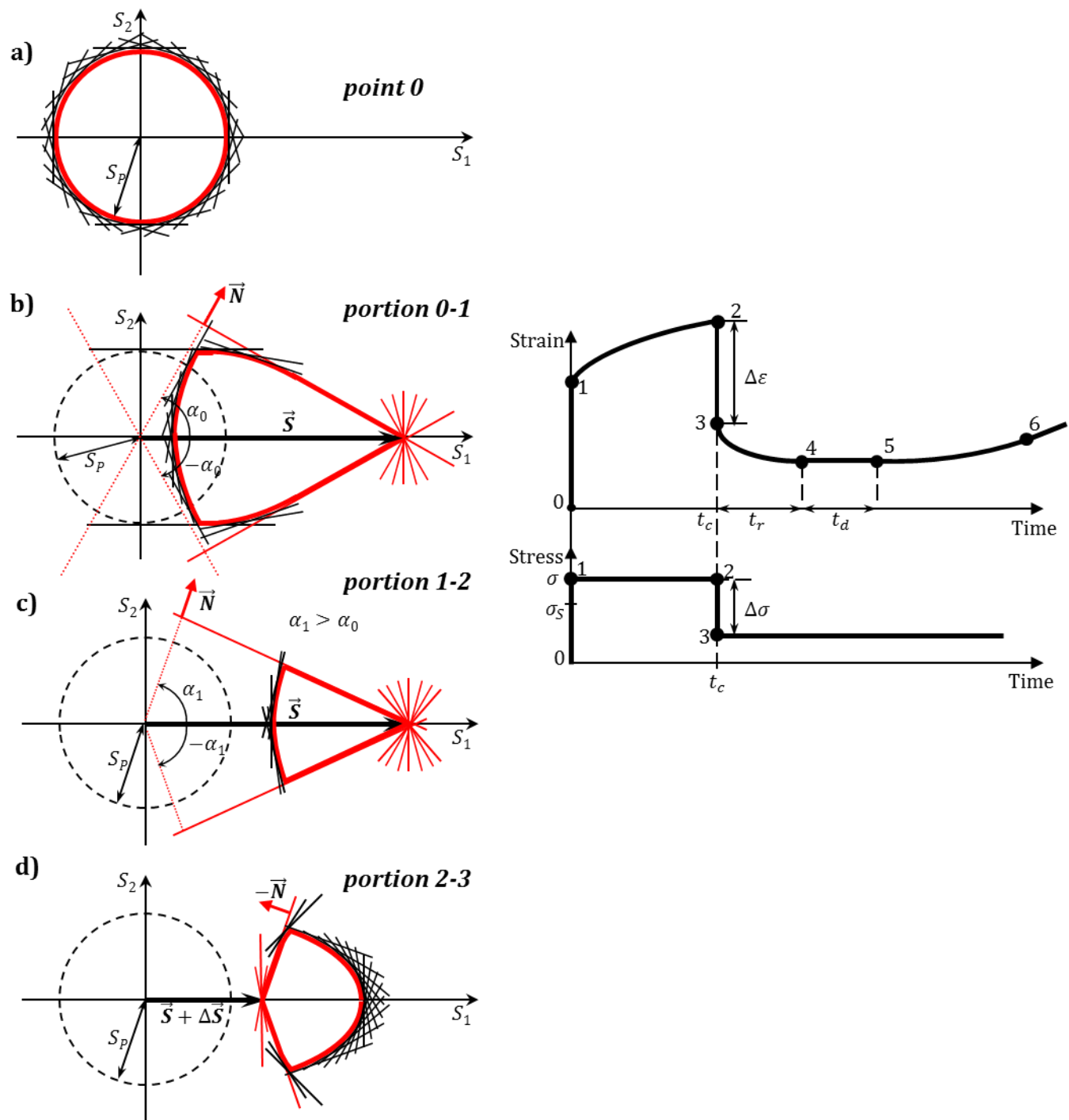


**Fig. 4.5.** Yield surface (a) and loading surfaces (b-d) in  $S_1S_2$  coordinate plane corresponding to the portions 0-1-2-3. The planes with  $\lambda = 0$  are shown only.

The domain of angles with positive  $\psi_N$  ( $\Omega_1$ ) grows in time as well:

$$\Omega_1: \quad -\alpha_1 \leq \alpha \leq \alpha_1, \quad -\beta_1 \leq \beta \leq \beta_1, \quad 0 \leq \lambda \leq \lambda_1, \quad (4.1.32)$$

$$\cos \lambda_1 = \frac{S_p}{S_1(1 - B \exp(-pt)) \cos \alpha \cos \beta}, \quad \cos \beta_1 = \frac{S_p}{S_1(1 - B \exp(-pt)) \cos \alpha}, \quad (4.1.33)$$

$$\cos \alpha_1 = \frac{S_p}{S_1(1 - B \exp(-pt))}.$$

Beyond (4.1.32) -  $\Omega_1^*$ :  $\alpha_1, \beta_1 \leq |\alpha|, |\beta| \leq \pi/2 - \psi_N = 0$ . Summarizing,

$$H_N = \begin{cases} S_1 \Omega, & \text{for } \Omega_1 \\ S_p + B S_1 \Omega \exp(-pt), & \text{for } \Omega_1^* \end{cases} \quad (4.1.34)$$

The strain intensity is calculated by Eqs. (3.8.7) and (4.1.31) as

$$r \dot{\varphi}_N = B p S_1 \exp(-pt) \Omega + K [S_1(1 - B \exp(-pt)) \Omega - S_p]. \quad (4.1.35)$$

By utilizing Eq. (3.7.3), i.e. by integrating  $\dot{\varphi}_N$  form the formula above within the limits (4.1.32), the creep-strain-rate-vector-component ( $\dot{\epsilon}$ ) is obtained as

$$\dot{\epsilon} = \int_{-\alpha_1}^{\alpha_1} \cos \alpha \, d\alpha \int_{-\beta_1}^{\beta_1} \cos^2 \beta \, d\beta \int_0^{\lambda_1} \dot{\varphi}_N \cos \lambda \, d\lambda = a_0 K \Psi(a, b), \quad (4.1.36)$$

$$\Psi(a, b) = \frac{\arccos b}{a} - \left(3 - \frac{b}{a}\right) \sqrt{1 - b^2} + \left(3 - \frac{2b}{a}\right) b^2 \ln \frac{1 + \sqrt{1 - b^2}}{b}, \quad (4.1.37)$$

$$a = \frac{K \sigma_p}{\sigma [B p \exp(-pt) + K(1 - B \exp(-pt))]}, \quad b = \frac{\sigma_p}{\sigma(1 - B \exp(-pt))}.$$

The analysis of these formulae shows that  $\dot{\epsilon}$  is a decreasing function of time. This is due to the decrease in  $I_N$  as  $\sigma(t) = \text{const}$ . As  $\exp(-pt) \rightarrow 0$  with the growth of time,  $b \rightarrow a$  implying that  $\Psi(a, b)$  tends to  $\Phi(\sigma_p/\sigma)$  from (4.1.23). Since the ratio  $\sigma_p/\sigma$  remains unchangeable in time, formula  $\dot{\epsilon} = a_0 K \Phi(\sigma_p/\sigma)$  is the relationship to calculate the steady state creep rate. In terms of the loading surface, the condition  $I_N \rightarrow 0$  means the termination of the movements of planes, and the steady state creep rate is modelled by the set of stationary planes located at the endpoint of stress vector (compare surfaces from Fig. 4.6).

Consider the domain that is the mirror reflection of that from (4.1.32):

$$\tilde{\Omega}_1: \quad \pi - \alpha_1 \leq |\alpha| \leq \pi, \quad \pi - \beta_1 \leq |\beta| \leq \pi. \quad (4.1.38)$$

The defect intensity  $\psi_{-N}$  and plane distance  $H_{-N}$ , according to Eqs. (4.1.1), (4.1.3), (4.1.4) and (4.1.31), are

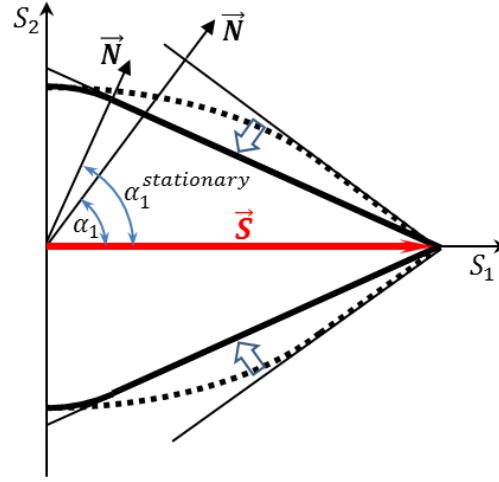


**Fig. 4.6.** Loading surfaces for primary (-----) and secondary creep (solid line) in  $S_1S_2$ -plane (boundary planes at the endpoint of stress vector are shown only; arrows show the direction of the loading surface evolution)

$$\psi_{-N} = \begin{cases} S_P - S_1(1 - B\exp(-pt))\Omega & \text{for } \tilde{\Omega}_1 \\ 0 & \text{for } \tilde{\Omega}_1^* \end{cases} \quad (4.1.39)$$

$$H_{-N} = \begin{cases} 2S_P - S_1(1 - B\exp(-pt))\Omega & \text{for } \tilde{\Omega}_1 \\ S_P & \text{for } \tilde{\Omega}_1^* \end{cases} \quad (4.1.40)$$

where  $\tilde{\Omega}_1^*$  stands for  $\pi/2 \leq |\alpha| \leq \pi - \alpha_1$ ,  $\pi/2 \leq |\beta| \leq \pi - \beta_1$ . The loading surface in Fig. 4.5c is constructed as the inner envelop of planes whose distances are governed by Eqs. (4.1.34), and (4.1.40) at  $t = t_c$ .

**Intermediate remarks.** To model portions **2-3** and **3-4** from Fig. 4.5, we need to give the following preliminary reasoning. Since both of them are of compressive nature, they can be modeled only by means of planes with normal vectors  $-\vec{N}$ . The occurrence of negative plastic strain increment (**2-3**) is possible only if the stress increment vector  $\Delta\vec{S}$  reaches and moves a set of planes with negative normals  $-\vec{N}$ . The description of reverse(negative) creep under the constant stress  $\vec{S} + \Delta\vec{S}$  (**3-4**) also can be modelled only by the manipulations with planes with normals  $-\vec{N}$ . It is feasible only if  $H_{-N} < 0$ , i.e. if the planes with negative normals get over the origin of coordinates. Therefore, the initial stress vector must be of such magnitude that the plane distances from the first formula of (4.1.40) at  $t = t_c$  are negative.

Special attention must be paid for the rate integral  $I_{-N}$  due to it stands for the regulation of time-dependent strain for the planes with normals  $-\vec{N}$ . To model the reverse creep, it is immediately clear that the requirement that  $I_{-N}$  be positive is needed.

The fact that the negative creep can be observed only if it is preceded by negative plastic deformation means that a material needs to obtain some compressive strain energy which then can be released in the form of time-dependent deformation (negative creep).

#### 4.1.4. Stress drop

**Portion 2-3.** Because of stress drop  $\Delta\vec{S}$ , the rate integral  $I_N$ , according to Eq. (3.8.4), yields the following form (Fig. 4.7)

$$I_N = B[S_1 \exp(-pt_c) - \Delta S]\Omega. \quad (4.1.41)$$

To meet the condition  $I_{-N} > 0$ , the magnitude of  $\Delta S$  must be greater than  $S_1 \exp(-pt_c)$  implying that  $I_N$  from (4.1.41) becomes negative. Then, according to Eq. (4.1.3), we obtain that

$$I_{-N} = -I_N = B[\Delta S - S_1 \exp(-pt_c)]\Omega > 0 \text{ and } I_N = 0. \quad (4.1.42)$$

As the stress vector shortens due to the stress drop, the planes with normals  $\vec{N}$  are no more at its endpoint and they stop producing inelastic deformation. This, in turn, means that there is no defect increment in positive direction, and Eq. (4.1.31) remains unchangeable until increments in defect intensity  $\psi_{-N}$  occur. This is possible if planes with normals  $-\vec{N}$  are shifted by vector  $\vec{S} + \Delta\vec{S}$ . For the rest planes Eq. (4.1.39) holds true.

Let us designate through  $S_5^-$  the length of stress vector when it reaches the first plane with negative normal. Since this plane is perpendicular to the stress vector,  $\Omega = 1$ , it is distanced from the origin as

$$H_{-N} = \vec{S} \cdot (-\vec{N}) = -S_5^-. \quad (4.1.43)$$

Therefore, to calculate the  $S_5^-$ , we use Eq. (4.1.5) where (i) the left-hand-side is  $-S_5^-$ ; (ii)  $\psi_{-N}$  is given by (4.1.31) at  $t = t_c$  and  $\Omega = 1$ ; (iii)  $I_{-N}$  is from Eq. (4.1.42) at  $\Delta S = S_1 - S_5^-$  and  $\Omega = 1$ . As a result,

$$-S_5^- = S_p + S_p - S_1[1 - B \exp(-pt_c)] + B[S_1 - S_5^- - S_1 \exp(-pt_c)], \quad (4.1.44)$$

$$S_5^- = S_1 - \frac{2S_p}{1 - B}. \quad (4.1.45)$$

Summarizing, the occurrence of negative plastic strain increment is possible if the magnitude of  $S_5^-$  is positive and the stress  $S_1 - \Delta S$  is less than  $S_5^-$ . These conditions, in the view of Eq. (4.1.45), can be met if

$$S_1 > \frac{2S_p}{1 - B} \text{ and } \Delta S > \frac{2S_p}{1 - B}. \quad (4.1.46)$$

If  $\Delta S \leq S_1$ , the fulfillment of the second inequality in (4.1.46) provides that of the first one.

According to Eq. (3.9.5), the increments in defect- and strain intensity are related to each other as

$$r\Delta\varphi_{-N} = \Delta\psi_{-N}. \quad (4.1.47)$$

It is worthwhile to remind once more that, in terms of the synthetic theory, the increase in defects and, consequently, in strain intensity is obtained only if the stress vector translates planes on its endpoint, i.e.  $H_{-N} = (\vec{S} + \Delta\vec{S}) \cdot (-\vec{N}) = -(S_1 - \Delta S)\Omega$ . Therefore, the defect intensity increment, relatively to the defects at point **2**, is determined as

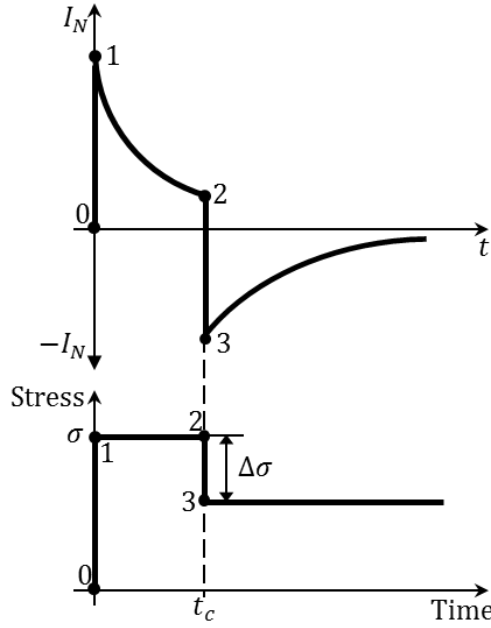


Fig. 4.7. Rate integral vs. time plot at  $\Omega = 1$ .

$$\Delta\psi_{-N} = H_{-N} - I_{-N} - \tilde{H}_{-N} = \Delta S(1 - B)\Omega - 2S_P, \quad (4.1.48)$$

where  $I_{-N}$  is given by (4.1.42) and  $\tilde{H}_{-N}$  stands for the plane distance at point **2** given by Eq. (4.1.40) at  $t = t_c$ . The domains of angles  $\alpha$ ,  $\beta$ , and  $\lambda$  where  $\Delta\psi_{-N} > 0$  are

$$\Omega_2: \quad \pi - \alpha_2 \leq |\alpha| \leq \pi, \quad \pi - \beta_2 \leq |\beta| \leq \pi, \quad 0 \leq \lambda \leq \lambda_2, \quad (4.1.49)$$

$$\cos \lambda_2 = \frac{2S_P}{\Delta S(1 - B) \cos \alpha \cos \beta}, \quad \cos \beta_2 = \frac{2S_P}{\Delta S(1 - B) \cos \alpha}, \quad (4.1.50)$$

$$\cos \alpha_2 = \frac{2S_P}{\Delta S(1 - B)}.$$

Beyond  $\Omega_2$  (we designate this range through  $\Omega_2^*$ ) the planes are not reached by the vector  $\vec{S} + \Delta\vec{S}$ , i.e.  $H_{-N} > (\vec{S} + \Delta\vec{S}) \cdot (-\vec{N})$ , and, consequently, do not take part in plastic deforming. Decompose  $\Omega_2^*$  into two parts,  $\Omega_2^* = \Omega_{2A}^* + \Omega_{2B}^*$ :

$$\Omega_{2A}^*: \quad \pi - \alpha_1 \leq |\alpha| \leq \pi - \alpha_2, \quad \pi - \beta_1 \leq |\beta| \leq \pi - \beta_2, \quad (4.1.51)$$

$$\Omega_{2B}^* = \tilde{\Omega}_1^*: \quad \pi/2 \leq |\alpha| \leq \pi - \alpha_1, \quad \pi/2 \leq |\beta| \leq \pi - \beta_1. \quad (4.1.52)$$

$\Omega_{2A}^*$  includes the planes which is not reached by  $\vec{S} + \Delta\vec{S}$ , but moved during the creep on **1-2** portion when  $\psi_N \neq 0$ .  $\Omega_{2B}^*$  includes the planes which did not move during the whole process ( $\psi_N = 0$ ), from point **0** to point **2**.

It is clear that there is no defect intensity increment within  $\Omega_2^*$ , i.e. Eq. (4.1.39) must be applied to calculate  $\psi_{-N}$  for the range (4.1.51-52).

The defect intensity distribution at point **3** is

$$\psi_{-N} = \begin{cases} \psi_{-N2} + \Delta\psi_{-N} = \Delta S(1 - B)\Omega - S_1[1 - B\exp(-pt_c)]\Omega - S_P & \text{for } \Omega_2 \\ \psi_{-N2} = S_P - S_1[1 - B\exp(-pt_c)]\Omega & \text{for } \Omega_{2A}^* \\ 0 & \text{for } \Omega_{2B}^* \end{cases} \quad (4.1.53)$$

where  $\psi_{-N2}$  denotes the defect intensity at point **2** given by Eq. (4.1.39) at  $t = t_c$ .

Now, the plane distance due to the stress drop is

$$H_{-N} = \begin{cases} (\vec{S} + \Delta\vec{S}) \cdot (-\vec{N}) & \text{for } \Omega_2 \\ S_P + \psi_{-N2} + I_{-N} & \text{for } \Omega_{2A}^* \\ S_P + I_{-N} & \text{for } \Omega_{2B}^* \end{cases} = \begin{cases} -(S_1 - \Delta S)\Omega & \text{for } \Omega_2 \\ 2S_P - (S_1 - B\Delta S)\Omega & \text{for } \Omega_{2A}^* \\ S_P + B[\Delta S - S_1\exp(-pt_c)]\Omega & \text{for } \Omega_{2B}^* \end{cases} \quad (4.1.54)$$

Fig. 4.5d shows the loading surface corresponding to point **3**. As seen, a corner point arises at loading point (the endpoint of  $\vec{S} + \Delta\vec{S}$ ), which is the sign of the arise of plastic deformation.

Eq. (3.8.3a) at  $I_N = 0$ , together with Eqs. (4.1.4) and (4.1.53), gives the distances to planes with positive normals.

The increment in the compressive plastic strain vector component ( $\Delta e$ ) is calculated by the integration of the strain intensity increment given by Eqs. (4.1.47) and (4.1.48) within boundaries (4.1.49):

$$\Delta e = \frac{1}{r} \int_{\pi-\alpha_2}^{\pi+\alpha_2} \cos \alpha \, d\alpha \int_{\pi-\beta_2}^{\pi+\beta_2} \cos^2 \beta \, d\beta \int_0^{\lambda_2} \Delta\varphi_{-N} \cos \lambda \, d\lambda = a_0 \Phi(a), \quad a = \frac{2\sigma_P}{\Delta\sigma(1-B)}, \quad (4.1.55)$$

where  $a_0$  and  $\Phi$  is from Eq. (4.1.21) and (4.1.23), respectively.

#### 4.1.5. Negative (reverse) creep

**Portion 3-4.** Rate integral  $I_{-N}$  for  $t > t_c$  behaves as (see Fig. 4.7)

$$I_{-N} = B[\Delta S - S_1\exp(-pt_c)]\exp[-p(t - t_c)]\Omega. \quad (4.1.56)$$

It is easy to see that  $I_N = 0$  for  $t > t_c$  due to  $I_{-N}$  vs. time curve constructed via Eq. (4.1.56) never cuts the time-axis.

Inspect the strain rate intensity for  $t > t_c$ . First of all, it is clear that the creep strain can develop only from the domain (4.1.49) or its sub-domain, where the planes are located on the endpoint of  $\vec{S} + \Delta\vec{S}$  at  $t = t_c$ , and  $H_{-N} = -(S_1 - \Delta S)\Omega$ . Therefore, the formulae for  $\psi_{-N}$  and  $\dot{\psi}_{-N}$ , according to Eqs. (4.1.5) and (4.1.56), take the form as follows

$$\begin{aligned} \psi_{-N} &= -(S_1 - \Delta S)\Omega - I_{-N} - S_P = \\ &\Delta S[1 - B\exp[-p(t - t_c)]]\Omega - S_1[1 - B\exp(-pt)]\Omega - S_P, \end{aligned} \quad (4.1.57)$$

$$\dot{\psi}_{-N} = -\dot{I}_{-N} = pI_{-N}.$$

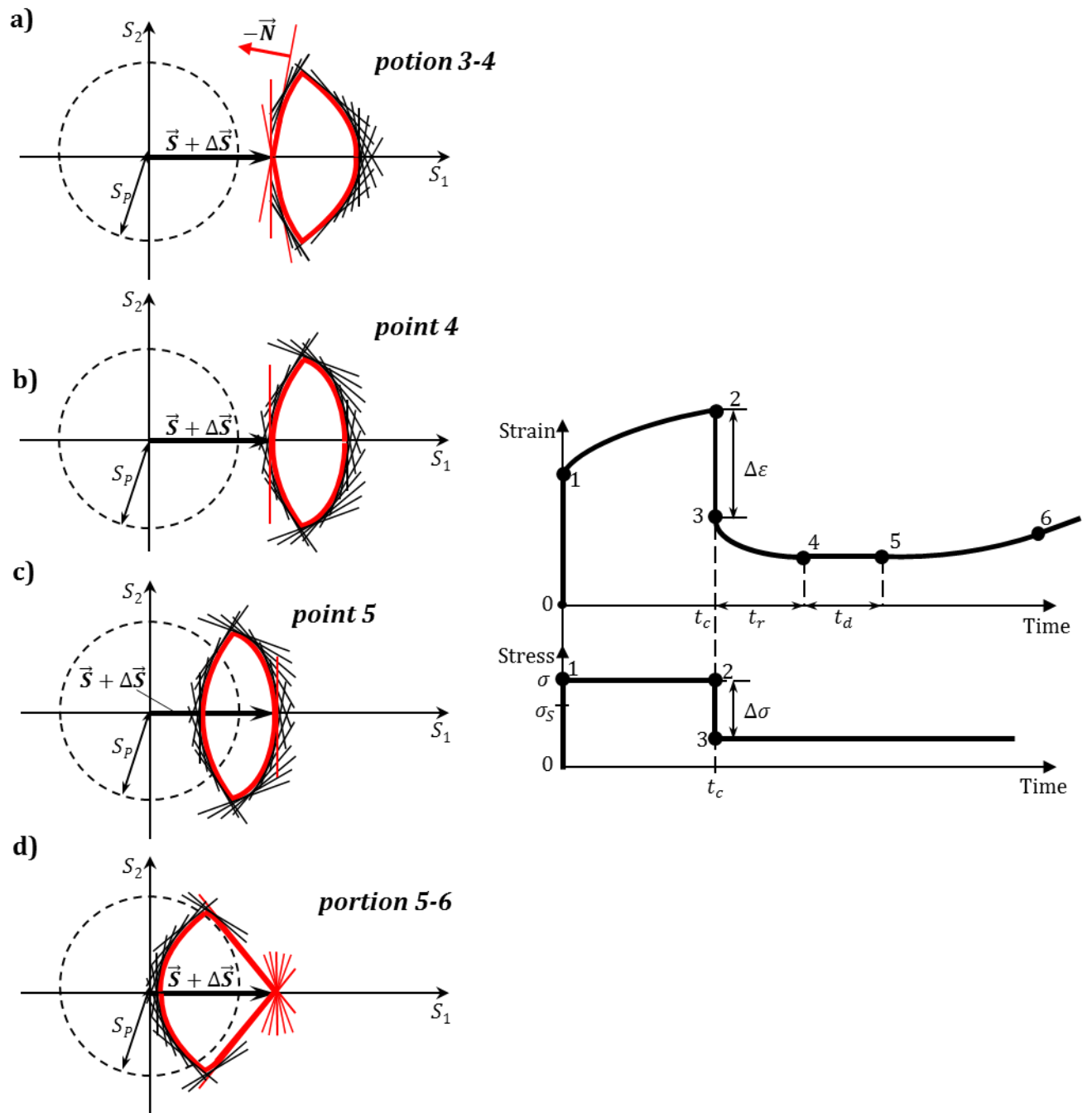


**Fig. 4.8.** Loading surfaces in  $S_1S_2$  coordinate plane corresponding to the portions 3-4-5-6. The planes with  $\lambda = 0$  are shown only

Further, Eqs. (3.8.7) and (4.1.57) give  $\dot{\varphi}_{-N}$  as

$$r\dot{\varphi}_{-N} = B(p - K)[\Delta S \exp(pt_c) - S_1] \exp(-pt) \Omega - K[(S_1 - \Delta S)\Omega + S_p]. \quad (4.1.58)$$

The domain of the positive values of  $\dot{\varphi}_{-N}$  is

$$\pi - \alpha_3 \leq |\alpha| \leq \pi, \quad \pi - \beta_3 \leq |\beta| \leq \pi, \quad 0 \leq \lambda \leq \lambda_3, \quad (4.1.59)$$

$$\cos \lambda_3 = \frac{KS_p}{[B(p - K)[\Delta S \exp(pt_c) - S_1] \exp(-pt) - K(S_1 - \Delta S)] \cos \alpha \cos \beta'}$$

$$\cos \beta_3 = \frac{KS_p}{[B(p - K)[\Delta S \exp(pt_c) - S_1] \exp(-pt) - K(S_1 - \Delta S)] \cos \alpha}, \quad (4.1.60)$$

$$\cos \alpha_3 = \frac{KS_p}{B(p - K)[\Delta S \exp(pt_c) - S_1] \exp(-pt) - K(S_1 - \Delta S)}.$$

Special attention must be paid to the relation between the domains of non-zero  $\dot{\varphi}_{-N}$  and  $\Delta\varphi_{-N}$ . In order to avoid a situation when the creep deformation develops on the planes which are not at the endpoint of the stress vector, we require that range (4.1.59) be not greater than that from (4.1.49) taken at  $t_c$ , i.e.  $\alpha_2 \geq \alpha_3(t = t_c)$ . To meet this condition, the following restriction must be imposed

$$\frac{B \left( 2 \frac{p}{K} - 1 \right) + 1}{B \exp(-pt_c) \left( \frac{p}{K} - 1 \right) + 1} \leq \frac{S_1}{\Delta S}. \quad (4.1.61)$$

If this inequality holds true, the planes from the domain

$$\pi - \alpha_2 \leq |\alpha| \leq \pi - \alpha_3, \quad \pi - \beta_2 \leq |\beta| \leq \pi - \beta_3 \quad (4.1.62)$$

do not take part in the development of reverse creep.

To calculate the negative creep strain rate vector component ( $\dot{e}^R$ ), Eq. (3.7.3), together with Eqs. (4.1.58) and (4.1.59), must be utilized. As a result, we have

$$\dot{e}^R = \int_{\pi - \alpha_3}^{\pi + \alpha_3} \cos \alpha \, d\alpha \int_{\pi - \beta_3}^{\pi + \beta_3} \cos^2 \beta \, d\beta \int_0^{\lambda_3} \dot{\varphi}_{-N} \cos \lambda \, d\lambda = a_0 K \Phi(a), \quad (4.1.63)$$

$$a = \frac{KS_p}{B(p - K)[\Delta S \exp(pt_c) - S_1] \exp(-pt) - K(S_1 - \Delta S)} \quad (t \geq t_c).$$

The analysis of (4.1.63) gives that the  $\dot{e}^R$  is a decreasing function of time and  $\dot{e}^R = 0$  at the instant of time ( $t = t_c + t_r$ ) when  $a = 1$ . This is in a full agreement with portion 3-4 in Fig. 4.8.

The duration of negative creep in a given direction,  $t_r^\Omega$ , is calculated by letting  $\dot{\varphi}_{-N} = 0$  in (4.1.58):

$$t_r^\Omega = \frac{1}{p} \ln \frac{B(p - K)[\Delta S - S_1 \exp(-pt_c)] \Omega}{K[(S_1 - \Delta S)\Omega + S_p]} \quad (4.1.64)$$

As follows from (4.1.64), the duration of negative creep is an increasing function of  $\Omega$ , and  $t_r^\Omega = 0$  on the boundary angles (4.1.60). For  $\Omega = 1$ , the formula above gets<sup>2</sup>

$$t_r = \frac{1}{p} \ln \frac{B(p-K)[\Delta S - S_1 \exp(-pt_c)]}{K(S_1 - \Delta S + S_p)}. \quad (4.1.65)$$

This means that the reverse creep strain lasts the longest for the slip system which is the most favorably oriented relatively to the vector  $\vec{S} + \Delta\vec{S}$ , i.e.  $\Omega = 1$ . As seen from (4.1.65),  $t_r > 0$  if the numerator is greater than the denominator:

$$[B(p-K) + K]\Delta S > [B(p-K)\exp(-pt_c) + K]S_1 + KS_p. \quad (4.1.66)$$

As follows from Eq. (4.1.65), the reverse creep time  $t_r$  grows with  $\Delta S$  if to hold  $S_1$  and  $t_c$  fixed; this is true for the whole range of  $\Delta S$ , from  $S_1 - S_5$  to  $S_1$  (complete unloading). Another result is the reverse creep time  $t_r$  grows with the initial creep duration  $t_c$  at fixed values of  $S_1$  and  $\Delta S$ . Furthermore, the function  $t_r(t_c)$  is bounded above by horizontal asymptote

$$\max t_r = \frac{1}{p} \ln \frac{B(p-K)\Delta S}{K(S_1 - \Delta S + S_p)} \text{ as } t_c \rightarrow \infty. \quad (4.1.67)$$

Once  $\dot{\varphi}_{-N} = 0$ , Eq. (3.8.7) degenerates into the following form

$$d\psi_{-N} = -K\psi_{-N}dt. \quad (4.1.68)$$

The solution of the differential equation above describes the process of defect relaxation,

$$\psi_{-N} = \psi_{-N0} \exp(-Kt), \quad (4.1.69)$$

where  $\psi_{-N0}$  is the value of defect intensity at the beginning of relaxation.

Beyond the domain (4.1.59), as there  $H_{-N} > (\vec{S} + \Delta\vec{S}) \cdot \vec{N}$ , the defect relaxation starts immediately at  $t = t_c$ , whereas within (4.1.59) the start of defects relaxation ( $t = t_c + t_r^\Omega$ ) depends upon the plane orientation due to  $t_r^\Omega = f(\Omega)$ .

Therefore, Eqs. (4.1.57), (4.1.53) and (4.1.69) give the defect intensity during reverse creep as

$$\psi_{-N} = \begin{cases} \Delta S[1 - B \exp(-p(t - t_c))] \Omega - S_1[1 - B \exp(-pt)] \Omega - S_p & (4.1.59) \text{ as } t \in [t_c, t_c + t_r^\Omega) \\ \frac{p}{p-K} [(\Delta S - S_1)\Omega - S_p] \exp[-K(t - (t_c + t_r^\Omega))] & (4.1.59) \text{ as } t \geq t_c + t_r^\Omega \\ \{\Delta S(1 - B)\Omega - S_1[1 - B \exp(-pt_c)]\Omega - S_p\} \exp[-K(t - t_c)] & (4.1.62) \text{ as } t \geq t_c \\ \{S_p - S_1[1 - B \exp(-pt_c)]\Omega\} \exp[-K(t - t_c)] & (4.1.51) \text{ as } t \geq t_c \\ 0 & (4.1.52) \end{cases} \quad (4.1.70)$$

The second row in the formula above is obtained if to insert  $t_r^\Omega$  into Eq. (4.1.57).

By adding  $\psi_{-N}$  from the formula above and  $S_p + I_{-N}$  ( $I_{-N}$  is from (4.1.56)), the distances to planes during reverse creep can be expressed as

<sup>2</sup> Eq. (4.1.65) can be also obtained from Eq. (4.1.63) by letting  $a = 1$ .

$$H_{-N} = \begin{cases} -(S_1 - \Delta S)\Omega, & \text{for the first row from (4.1.70)} \\ \psi_{-N0}\exp(-Kt) + I_{-N} + S_P \neq -(S_1 - \Delta S)\Omega, & \text{for the rest rows from (4.1.70)} \end{cases} \quad (4.1.71)$$

where  $\psi_{-N0}$  is determined as in the four last rows in Eq. (4.1.70).

The analysis of Eqs. (4.1.70) and (4.1.71) shows that, at different instants, planes start to move tending to their initial positions,  $\lim_{t \rightarrow \infty} H_{-N} = S_P$ , due to  $\lim_{t \rightarrow \infty} (\psi_{-N0}\exp(-Kt) + I_{-N}) = 0$ . At  $t = t_r$ , the domain (4.1.59) shrinks to a point symbolizing that the last plane has left the endpoint of the vector  $\vec{S} + \Delta\vec{S}$ . In other words, for  $t > t_r$ , the only relationship that governs the displacement of planes is the second relation from Eq. (4.1.71).

The plane distances  $H_N$  are governed by Eq. (3.8.3a) at  $I_N = 0$ , i.e. (4.1.70), and (4.1.4). The loading surfaces in the course of reverse creep ( $t_c < t < t_c + t_r$ ) and at the end of it ( $t = t_c + t_r$ ) are shown in Figs. 4.8a and 4.8b, respectively.

#### 4.1.6. Creep delay

**Portion 4-5.** As shown in the previous point, once a plane leaves the endpoint of vector  $\vec{S} + \Delta\vec{S}$ , the development of permanent deformation ceases on it, and the defect relaxation starts. Since, for  $t > t_c + t_r$ , the planes with neither positive nor negative normals are not located at the endpoint of  $\vec{S} + \Delta\vec{S}$ , the irrecoverable straining does not occur at all and the horizontal portion 4-5 (creep delay) is observed.

According to Eq. (4.1.4), Eq. (3.8.3a) written at  $I_N = 0$  as well as Eq. (4.1.71) for  $t > t_c + t_r^\Omega$ , the distance to planes with positive normals is

$$H_N = S_P + \psi_N = S_P + \frac{p}{p-K} [S_P - (\Delta S - S_1)\Omega - S_P] \exp \left[ -K \left( t - (t_c + t_r^\Omega) \right) \right], \quad (4.1.72)$$

which shows that the planes with positive normals move toward the origin of coordinate and these movements cease in each direction as the plane arrives at the endpoint of vector  $\vec{S} + \Delta\vec{S}$ .

The instant of time when a plane is on the endpoint of vector  $\vec{S} + \Delta\vec{S}$ ,  $t = t_c + t_r^\Omega + t_d^\Omega$ , can be found from Eq. (4.1.72) by letting on its left-hand side

$$H_N = (S_1 - \Delta S)\Omega. \quad (4.1.73)$$

As a result, the duration of the creep delay  $t_d^\Omega$  as a function of  $\Omega$  is

$$t_d^\Omega = \frac{1}{K} \ln \frac{p[S_P - (\Delta S - S_1)\Omega]}{(p-K)[(S_1 - \Delta S)\Omega - S_P]}. \quad (4.1.74)$$

The fact that the  $t_d^\Omega$  depends upon the orientation of plane ( $\Omega$ ) means that a slip system starts to produce a deformation only then, when its orientation becomes favorable relatively to the acting stress. The smallest value of  $t_d^\Omega$ , it is none other as the duration of the creep delay, is calculated by Eq. (4.1.74) at  $\Omega = 1$ :

$$t_d = \frac{1}{K} \ln \frac{p(S_P - \Delta S + S_1)}{(p-K)(S_1 - \Delta S - S_P)}. \quad (4.1.75)$$

For  $t > t_c + t_r + t_d$  the creep of positive sign starts developing and it is worthwhile to note that the formula for  $t_d$  holds true if

$$S_1 - \Delta S > S_p. \quad (4.1.76)$$

This inequality expresses an obvious condition for the occurring of the positive creep deformation: the acting stress  $S_1 - \Delta S$  must exceed the creep limit  $S_p$ . The loading surface at  $t = t_c + t_r + t_d$  is shown in Fig. 4.8c.

#### 4.1.7. Inverse creep

For  $t > t_c + t_r + t_d$ , the tensile (positive) strain is resumed. The defect intensity for the plane which have come back to the endpoint of  $\vec{S} + \Delta\vec{S}$ ,  $H_N = (S_1 - \Delta S)\Omega$ , is calculated by Eq. (3.8.3a) at  $I_N = 0$  as

$$\psi_N = (S_1 - \Delta S)\Omega - S_p, \quad d\psi_N = 0. \quad (4.1.77)$$

Since the defect intensity (4.1.77) does not depend on time, the time-dependent character of deformation is regulated by the fact that the number of planes at the endpoint of the stress vector increases with time. To capture this, one needs to write down Eq. (4.1.72) with  $H_N = (S_1 - \Delta S)\Omega$  on its left-hand side:

$$(S_1 - \Delta S)\Omega = S_p + \psi_N = S_p + \frac{p}{p-K} \left\{ [S_p - (\Delta S - S_1)\Omega] \exp \left[ -K \left( t - (t_c + t_r^\Omega) \right) \right] \right\}. \quad (4.1.78)$$

From this formula the boundary angles on which the creep strain is induced,  $\Omega^t$ , can be related to time as

$$\frac{(p-K) \left( \frac{S_1 - \Delta S}{S_p} \Omega^t - 1 \right)}{p \exp[K(t_c + t_r^\Omega)] \left( 1 + \frac{S_1 - \Delta S}{S_p} \Omega^t \right)} = \exp(-Kt). \quad (4.1.79)$$

The analysis of Eq. (4.1.79) shows that  $\Omega^t = 1$  at  $t = t_d$ , i.e. the plane perpendicular to the vector  $\vec{S} + \Delta\vec{S}$  is obtained. With the growth in time the domain  $\Omega^t$  expands and becomes steady as  $\exp(-Kt) \rightarrow 0$  (let us designate it through  $a$ ):

$$a = \frac{S_p}{S_1 - \Delta S}. \quad (4.1.80)$$

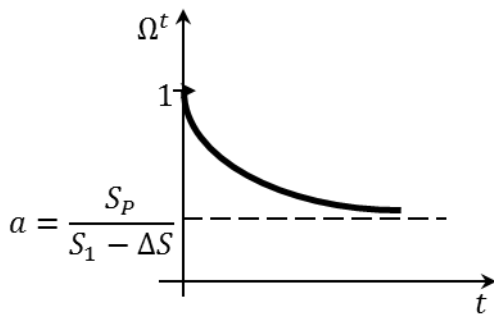


Fig. 4.9.  $\Omega^t(t)$  function.

The formula above corresponds to the case of steady-state creep, when the set of planes reached by stress vector does not change in time. The  $\Omega^t$ -against-time-plot is shown in Fig. 4.9.

Since  $d\psi_N = 0$  in Eq. (4.1.77), i.e. there is no increment in  $\psi_N$  for every slip system, Eq. (3.9.1) gives that:

$$r\dot{\phi}_N = K\psi_N = \text{const.} \quad (4.1.81)$$

Despite this fact, the time-dependent growth in macro-deformation-rate is modeled by the increasing number of planes (slip systems) getting involved in the development of the strain, which is governed by Eq. (4.1.79). The macro-deformation ( $\dot{\epsilon}^i$ ) is calculated by Eqs. (3.7.3), (4.1.81), (4.1.79) and (4.1.77) as

$$\dot{\epsilon}^i = \frac{K}{r} \iiint_{\Omega^t} \dot{\phi}_N \cos \alpha \cos^2 \beta \cos \lambda \, d\alpha d\beta d\lambda = Ka_0 \Psi(a, \Omega^t), \quad a = \frac{\sigma_p}{\sigma_1 - \Delta\sigma}, \quad (4.1.82)$$

$$\Psi(a, \Omega^t) = \frac{\arccos(\Omega^t)}{a} - \left(3 - \frac{\Omega^t}{a}\right) \sqrt{1 - (\Omega^t)^2} - \left(3 - \frac{2\Omega^t}{a}\right) (\Omega^t)^2 \ln \frac{1 + \sqrt{1 - (\Omega^t)^2}}{\Omega^t}.$$

As follows from Eq. (4.1.82)  $\dot{\epsilon}^i = 0$  at  $\Omega^t = 1$  ( $t = t_d$ ) and with the growth in time  $\Psi(a, \Omega^t) \rightarrow \Phi(a)$  as  $\Omega^t \rightarrow a$ . This means that  $\dot{\epsilon}^i$  is an increasing function of time which, in the course of time, tends to a constant value. Therefore, it can be inferred immediately that for  $t > t_c + t_r + t_d$  the strain-time curve is a concave one which transits into a straight portion. Therefore, Eq. (4.1.82) models the reverse creep shown by portion 5-6 in Fig. 4.8.

The loading surface corresponding to the reverse creep is shown in Fig. 4.8d. Again, the corner point arises at the loading point, which is typical for irrecoverable straining.

#### 4.1.8. Comparison of the model and experimental results

My goal here is:

- to calculate plastic contraction due to the stress drop,
- to plot negative creep diagram,
- to calculate the duration of negative creep ( $t_r$ ) and creep delay ( $t_d$ ).

The results obtained in terms of the synthetic model will be compared with experimental data obtained in uniaxial tension for  $\text{Ti}_3\text{SiC}_2$  alloy [Fig. 2.1b, Radovic et al. (2003)] and aluminum alloy PA4 (chemical composition 0.7-1.2% Mg, 0.6-1.0% Mn, 0.7-1.2% Si, 0.5% Fe, the rest Al) [Fig. 4.12, Osipiuk, (1993)].

To achieve the goal, the following series of parameters are needed: (i) experiment parameters, (ii) material constants, (iii) model constants. The first column in Table 4.1 contains the parameters of experiment on  $\text{Ti}_3\text{SiC}_2$  conducted by Radovic et al. (2003). The second column shows the constants of the synthetic theory via which the analytical diagrams are constructed (Figs. 4.10 and 4.11).

First of all, we read from Fig. 2.1.b the value of the specimen contraction due to the stress drop:  $\Delta\epsilon_{total} = 1.235 \times 10^{-4}$ . According to the Hooke law, an elastic contraction caused by the  $\Delta\sigma$  would be  $\Delta\epsilon_{el} = \Delta\sigma/E = 6.154 \times 10^{-5} < \Delta\epsilon_{total}$ . This fact implies the onset of plastic contraction due to the stress drop, which can be calculated as  $\Delta\epsilon = 1.235 \times 10^{-4} - 6.154 \times 10^{-5} = 6.196 \times 10^{-5}$ . By utilizing Eq. (4.1.55), I have obtained the plastic contraction  $\Delta\epsilon = 5.644 \times 10^{-5}$ , which deviates from the experiment only by 8.9%.

**Table 4.1.** Calculation parameters

<i>Material and experiment parameters</i>		<i>Model constants</i>	
Stress $\sigma$ , MPa	40	$B$	0.3163
Stress drop $\Delta\sigma$ , MPa	-20	$p, s^{-1}$	0.00453
Temperature, °C	1150	$r$ , MPa	38200
Young modulus $E$ , GPa; (Barsoum et al., 1999)	325	$c, \text{MPa}^{-k} \times \text{s}^{-1}$	502000
Creep limit $\sigma_p$ , MPa;	3.0	$k$	3.0
The creep activation energy $Q$ , J/mole; (Radovic et al., 2003)	$4.58 \times 10^5$		

To utilize the formulae derived for negative creep, we need to determine the value of the creep limit. We take creep limit at a given temperature as the value of tensile stress resulting in the strain rate of  $1.5 \cdot 10^{-5} \text{ h}^{-1}$ . Therefore,  $\sigma_p$  can be read from the experimental  $\dot{\epsilon} \sim \sigma$  line in Fig. 4.10 if to prolong it to the indicated value.

To calculate steady state creep rate, we use Eq.(4.1.36-37) as  $\exp(-pt) \rightarrow 0$ :

$$\dot{\epsilon} = a_0 K \Phi(a), \quad K = \exp\left(-\frac{Q}{RT}\right) \frac{9cr}{\pi^2} \tau_0^{k-1}, \quad \tau_0 = \sigma, \quad (4.1.83)$$

$$a_0 = \frac{\sqrt{2\pi}\sigma_p}{3\sqrt{3}r}, \quad \Phi(a) = \frac{\arccosa}{a} - 2\sqrt{1-a^2} + a^2 \ln \frac{1 + \sqrt{1-a^2}}{a}, \quad a = \frac{\sigma_p}{\sigma}. \quad (4.1.84)$$

The model line in Fig.4.10, which is obtained via the formulae above, shows good agreement with the experimental data.

Theoretical stress  $\sim$  time plot for the negative creep portion (Fig. 4.11) is constructed as

$$e^R = \int_{t_c}^t \dot{\epsilon}^R dt, \quad (4.1.85)$$

where  $\dot{\epsilon}^R$  is defined by Eq. (4.1.63). The value of the deformation at the beginning of negative creep ( $t = t_c$ ) we have read from the experimental curve ( $\approx 5.7 \cdot 10^{-4}$ ; Radovic et al., 2003))

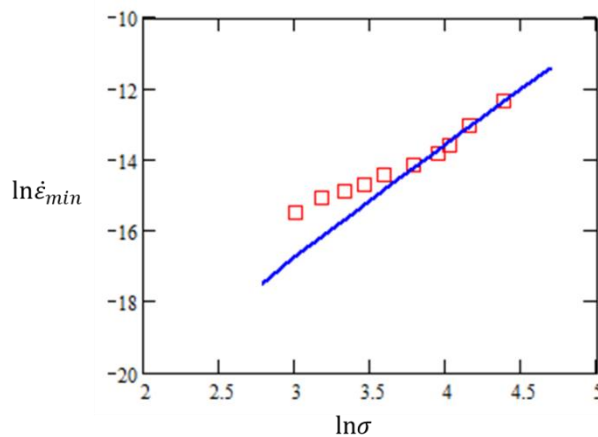


**Fig. 4.10.**  $\ln \dot{\epsilon}_{min}$  vs.  $\ln \sigma$  plot for  $\text{Ti}_3\text{SiC}_2$  alloy at 1150°C;  $\square$  – experiment (Radovic et al., 2003), line – model result. ( $\dot{\epsilon}_{min}$  is steady-state creep rate).

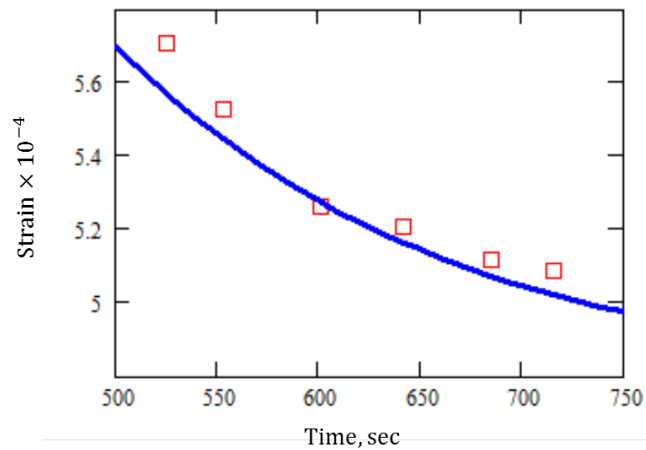


**Fig. 4.11.** Negative creep diagram of  $\text{Ti}_3\text{SiC}_2$  alloy at  $1150^\circ\text{C}$ ,  $\sigma = 20$  MPa;  $\square$  - experiment (Radovic et al., 2003), line - model result.

As follows from Figures 4.10 and 4.11, the synthetic theory gives a good agreement with the experimental data. It must be stressed that these diagrams as well as the value of  $\Delta\varepsilon$  are obtained with one and the same set of constants.

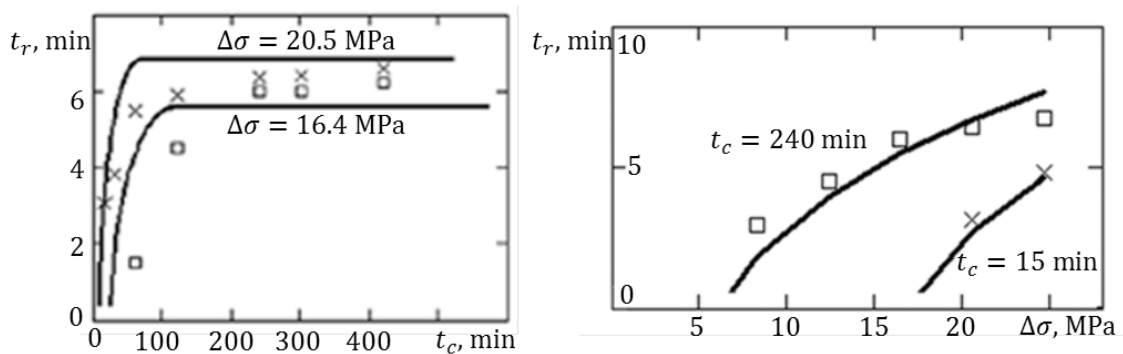


**Fig. 4.12.** Experimental and calculated  $t_r \sim t_c$  and  $t_r \sim \Delta\sigma$  curves.

Fig. 4.12 shows experimental results (symbols  $\square$  and  $\times$ ; Osipiuk, 1993) while calculated curves  $t_r \sim t_c$  and  $t_r \sim \Delta\sigma$  are constructed on the base of Eq. (4.1.65). The stress-drop tests were performed over the specimen of aluminum alloy PA4 at  $\sigma = 227$  MPa. The calculated curves are obtained for the following values of creep limit and model constants:  $\sigma_p = 10$  MPa,  $B = 0.05$ ,  $K = 2.5 \cdot 10^{-4} \text{ s}^{-1}$ ,  $p = 0.2 \text{ s}^{-1}$ . The comparison between the calculated results and experimental data shows satisfactory agreement.

## CONCLUSION (Thesis 1)

In terms of the synthetic theory, I have developed a model for phenomena accompanying stress-drop tests such as

- (i) stress-drop induced ***plastic contraction***, which is recorded in spite of the fact that the net stress remains positive;
- (ii) ***negative creep*** after which a pause in temporary strain (***creep delay***) is observed;
- (iii) ***invers creep*** whose diagram has a form of convex curve.

The results above have been achieved by introducing a relation between the deformation properties of materials for opposite directions, e.g. tension-compression.

Since all the phenomena modeled are observed in one experiment, they affect each other, the magnitudes of plastic contraction, negative (reverse) creep, creep delay, and inverse creep strongly depend upon the parameters of the portions preceding them. So, the task was not only to describe the phenomena mentioned in isolation from one another, but also to show the interplay between them. I have succeeded in establishing these interplays due to the basic features of the synthetic theory: a) the uniformed approach to the modeling of permanent deformation independently of instantaneous (plastic) or temporary (creep) deformation to be considered, and b) the intimate connection between the macro-deformation and the defect structure on the micro-level of material, which finds its manifestation in the evolution of loading surface.

The model results I have obtained – a) plastic contraction due to stress-drop, b) negative creep diagram, and c) negative creep duration as a function of stress drop and preceding creep duration – show good agreement with experimental data.

## 4.2 Influence of preliminary mechanical-thermal treatment (MTT) upon the secondary creep of metals

This chapter presents the generalization of the synthetic theory for modelling the secondary creep rate of metals as a function of preliminary mechanical-thermal treatment (see Figs. 2.14 and 2.15). If to denote the steady-state creep rate after MMT by  $\dot{\varepsilon}_M$ , the following relationships must be constructed:

$$\dot{\varepsilon}_M = \dot{\varepsilon}_M(\varepsilon_0, \gamma), \quad (4.2.1)$$

$$\dot{\varepsilon}_M = \dot{\varepsilon}_M(T_a), \quad (4.2.2)$$

$$\dot{\varepsilon}_M = \dot{\varepsilon}_M(t_a), \quad (4.2.3)$$

where  $\varepsilon_0$  is the level of plastic prestrain in the course of MTT,  $T_a$  is the anneal temperature,  $t_a$  is the anneal time;  $\gamma$  is the stacking fault energy of metal.

### 4.2.1 Preconditions

Since both plastic and creep deformation are involved in the issue, it is worthwhile to arrange into groups formulae derived in the previous Section needed for further considerations. The case of uniaxial tension is considered. The relationships below will be often used in the further derivations.

#### Plastic strain

For the case of plastic straining at home temperature and moderate loading rates, the rate-integral can be ignored. Then, according to Eq. (4.1.11) at  $I_N = 0$ , we have  $S_S = S_P$  and Eq. (3.8.3b) becomes

$$\psi_N = H_N^2 - S_S^2, \quad (4.2.4)$$

where  $S_S = \sqrt{2/3} \sigma_S$  is the radius of the Von-Mises yield sphere (3.8.2),  $\sigma_S$  is the yield strength of material at room temperature.

Since the first operation of MTT is plastic strain ( $e_0$ ), let us derive formulae defining it under the action of  $\sigma_0 > \sigma_S$  stress (index "0" here and throughout further stands for the characteristics of material in the plastic strain at room temperature). Acting in the same way as in Sec. 4.1.2, we obtain the plane distance and defect intensity as

$$H_{N0} = \frac{2}{3} \begin{cases} \sigma_0 \Omega, & \text{for } \Omega_0 \\ \sigma_S, & \text{for } \Omega_0^* \end{cases}, \quad \Omega = \cos \alpha \cos \beta \cos \lambda \quad (4.2.5)$$

$$\psi_{N0} = H_{N0}^2 - S_S^2 = \frac{2}{3} \begin{cases} (\sigma_0 \Omega)^2 - \sigma_S^2, & \text{for } \Omega_0 \\ 0, & \text{for } \Omega_0^* \end{cases} \quad (4.2.6)$$

$$\Omega_0: \quad -\alpha_0 \leq \alpha \leq \alpha_0, \quad -\beta_0 \leq \beta \leq \beta_0, \quad 0 \leq \lambda \leq \lambda_0,$$

$$\cos \lambda_0 = \frac{\sigma_S}{\sigma_0 \cos \alpha \cos \beta}, \quad \cos \beta_0 = \frac{\sigma_S}{\sigma_0 \cos \alpha}, \quad \cos \alpha_0 = \frac{\sigma_S}{\sigma_0}, \quad (4.2.7)$$

$$\Omega_0^*: \quad \alpha_0, \beta_0 \leq |\alpha|, |\beta| \leq \pi.$$

The formulae above are obtained from Eqs. (4.1.14-16) at  $B = 0$ , and  $\sigma_S$  is taken instead of  $\sigma_P$ . The only difference is that we use here the quadratic relationship between  $\psi_N$  and  $H_N$ . Formulae for the planes with normal vectors  $-\vec{N}$  are not considered here.

Loading surface constructed on the base of (4.2.5) is shown in Fig. 4.13a.

Now, Eq. (3.7.3) takes the following form

$$e_0 = \iiint_{\Omega_0} \varphi_N N_1 dV = \frac{1}{r_0} \iiint_{\Omega_0} \psi_N N_1 dV =$$

$$= \frac{2}{3r_0} \int_{-\alpha_0}^{\alpha_0} \int_{-\beta_0}^{\beta_0} \int_0^{\lambda_0} [(\sigma_0 \cos \alpha \cos \beta \cos \lambda)^2 - \sigma_S^2] \cos \alpha \cos^2 \beta \cos \lambda \, d\alpha d\beta d\lambda. \quad (4.2.8)$$

Integrating in the formula above gives

$$e_0 = a_0 \Phi(a), \quad (4.2.9)$$

$$\Phi(a) = \frac{1}{a^2} \left[ 2\sqrt{1-a^2} - 5a^2\sqrt{1-a^2} + 3a^4 \ln \frac{1+\sqrt{1-a^2}}{a} \right], \quad (4.2.10)$$

$$a_0 = \frac{\pi \sigma_S^2}{9r_0}, \quad (4.2.11)$$

$$a = \cos \alpha_0 = \frac{\sigma_S}{\sigma_0}, \quad 0 < a \leq 1. \quad (4.2.12)$$

Function  $\Phi$  behaves in a similar way as shown in Fig. 4.4.

#### Steady-state creep

Repeating the considerations from Sec. 4.1.2, we obtain formula for the defect intensity in creep for stress  $\sigma$  as

$$\psi_N = H_N^2 - S_P^2 = \frac{2}{3} \begin{cases} ((\sigma\Omega)^2 - \sigma_P^2, & \text{for } \Omega_1 \\ 0, & \text{for } \Omega_1^* \end{cases} \quad (4.2.13)$$

and formulae (3.9.1) and (3.7.3) give the steady-state creep rate:

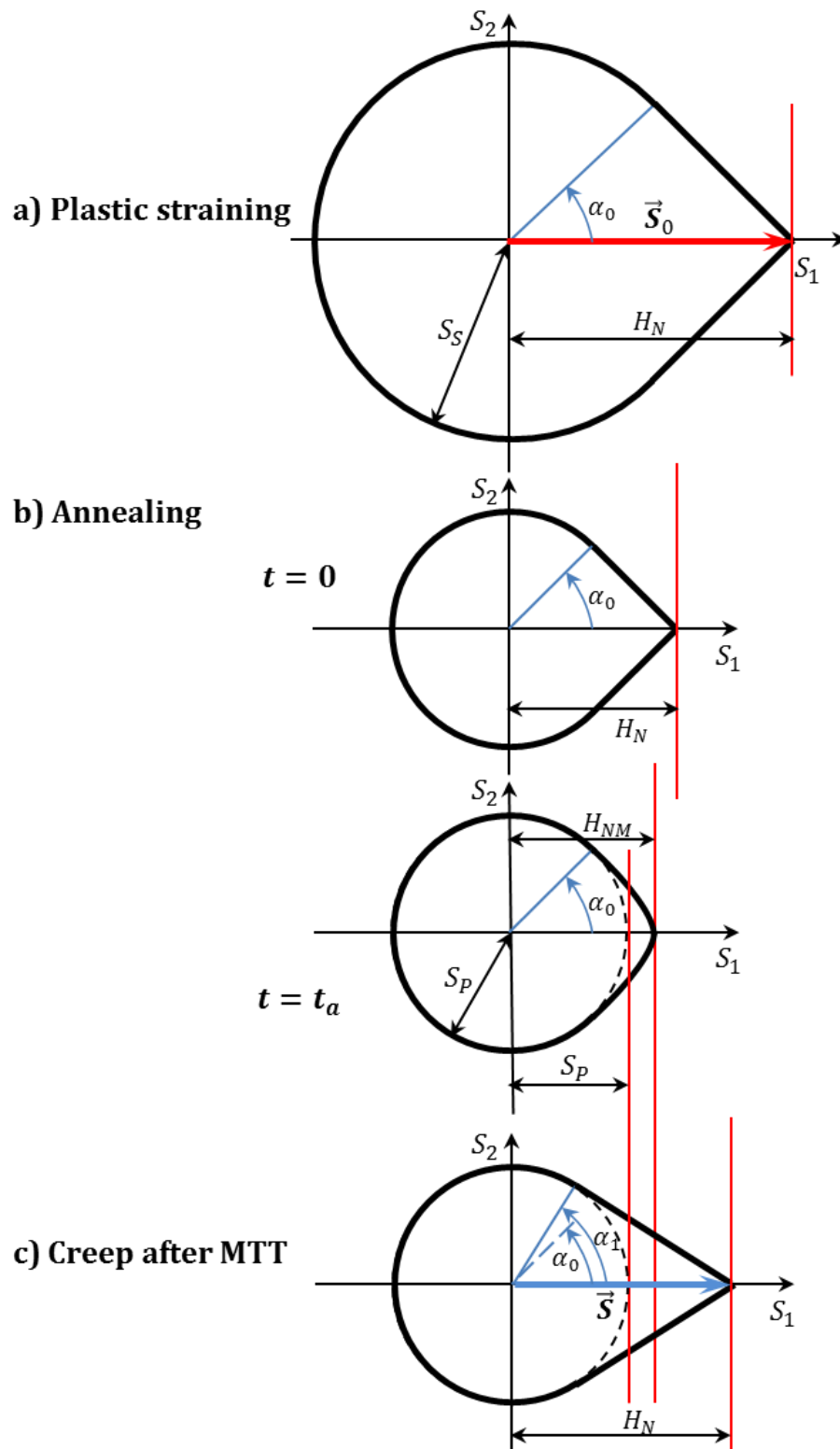


**Fig. 4.13** Loading surfaces in  $S_1S_2$  coordinate plane during MTT and subsequent creep (the planes with  $\alpha = 0$  only are shown in red) (Rusinko, 2010).

$$\dot{\epsilon} = \iiint_{\Omega_1} \dot{\phi}_N N_1 dV = \frac{K}{r} \iiint_{\Omega_1} \psi_N N_1 dV, \quad (4.2.14a)$$

$$\dot{\epsilon} = \frac{2K}{3r} \int_{-\alpha_1}^{\alpha_1} \int_{-\beta_1}^{\beta_1} \int_0^{\lambda_1} [(\sigma \cos \alpha \cos \beta \cos \lambda)^2 - \sigma_P^2] \cos \alpha \cos^2 \beta \cos \lambda d\alpha d\beta d\lambda, \quad (4.2.14b)$$

$$\Omega_1: \quad -\alpha_1 \leq \alpha \leq \alpha_1, \quad -\beta_1 \leq \beta \leq \beta_1, \quad 0 \leq \lambda \leq \lambda_1,$$

$$\cos \lambda_1 = \frac{\sigma_P}{\sigma \cos \alpha \cos \beta}, \quad \cos \beta_1 = \frac{\sigma_P}{\sigma \cos \alpha}, \quad \cos \alpha_1 = \frac{\sigma_P}{\sigma}, \quad (4.2.15)$$

$$\Omega_1^*: \quad \alpha_1, \beta_1 \leq |\alpha|, |\beta| \leq \pi.$$

In the formulae above,  $\sigma_P$  is the creep limit of material corresponding to the temperature of creep tests. Eqs. (4.2.13-15) are obtained from Eqs. (4.1.31-33) and (4.1.35-36) as  $\exp(-pt) \rightarrow 0$ .

Integrating in (4.2.14b) gives

$$\dot{\epsilon} = a_0 K \Phi(a), \quad a = \cos \alpha_1 = \frac{\sigma_P}{\sigma}, \quad a_0 = \frac{\pi \sigma_P^2}{9r}, \quad (4.2.16)$$

where  $\Phi$  is from (4.2.10).

#### 4.2.2 The generalization of the synthetic theory for the case of secondary creep as a function of the parameters of preliminary MTT

Relying upon the analysis regarding the influence of the substructure formed in the course of preliminary MTT on the rate of steady-state creep, we replace relation (4.2.13) with the following formula (Rusinko, 2002-2007, 2009, 2010):

$$\psi_N = H_N^2 - H_{NM}^2, \quad (4.2.17)$$

where  $H_{NM}$  is the plane distances after MTT, which reflects the resistance of the pretreated material to creep.

The quantity  $\psi_N$  is a decreasing function of  $H_{NM}$  and, hence, in view of relation (4.2.14a), the same is true for the rate of steady-state creep.

To find the quantity  $H_{NM}$ , we successively use relations

- a) (4.2.6) for the defect intensity developed in plastic prestrain, and
- b) (3.9.6) for annealing at stress-free-state.

However, the function  $K$  appearing in (3.9.3) cannot describe the evolution of defect structure for stress-free state because, according to (3.9.3),  $K(|\vec{S}| = 0) = 0$ . Moreover, to derive analytic expressions for the influence of the parameters of MTT on the thermomechanical resistance of defect structure, we replace the function  $K$  from (3.9.3) by the following functions:

$$K_M = K_M(H_{Nmax}, \gamma), \quad (4.2.18)$$

$$K_M = K_M(T_a), \quad (4.2.19)$$

$$K_M = K_M(t_a), \quad (4.2.20)$$

where  $H_{Nmax}$  is the maximum distance from the coordinate-origin to planes for the entire history of loading. We define the function  $K_M$  from (4.2.18) via the maximum distance since  $H_{Nmax}$  correlates with the level of plastic prestrain. Indeed, the greater stress vector acted during plastic deformation, the greater distance was travelled by the plane at its endpoint.

Let us consider separately cases (4.2.1-4.2.3) with the corresponding functions (4.2.18-4.2.20) for the case of uniaxial tension.

#### Case A

$$\dot{\boldsymbol{\varepsilon}}_M = \dot{\boldsymbol{\varepsilon}}_M(\boldsymbol{\varepsilon}_0, \gamma), \mathbf{T}_a = \mathbf{const}, t_a = \mathbf{const}$$

We propose the following form for  $K_M$ : (Rusinko, 2002, 2004)

$$K_M = K + \frac{H_{Nmax} - |\vec{S}|}{H_{Nmax}} \tilde{K}(\tilde{H}_{Nmax}, \gamma), \quad (4.2.21)$$

$$\tilde{K}(\tilde{H}_{Nmax}, \gamma) = Q_1 \left[ f_1(\tilde{H}_{Nmax}) + \frac{\gamma}{\Gamma} f_2(\tilde{H}_{Nmax}) \right],$$

$$\tilde{H}_{Nmax} = \frac{H_{Nmax} - \sigma_S}{\sigma_S},$$

$$f_1 = Q_2 \sqrt{\tilde{H}_{Nmax}}, \quad (4.2.22)$$

$$f_2 = \exp \left\{ - \left[ Q_3 (\tilde{H}_{Nmax} + Q_4)^2 \right] \right\}.$$

where  $Q_j$  ( $j = \overline{1,4}$ ) are model constants, the parameter  $\Gamma = 1 \text{ J/m}^2$  is used to guarantee the consistency of dimensions; besides,  $[\tilde{H}_{Nmax}] = 1, [Q_1] = \text{s}^{-1}, [Q_k] = 1$  ( $k = 2,3,4$ )  $\Rightarrow [K_M] = [K] = [\tilde{K}] = \text{s}^{-1}$ .

Under the conditions of uniaxial tension, the quantity  $H_{Nmax}$  can be obtained from Eq. (4.1.7) as:

$$H_{Nmax} = \max_{\alpha, \beta, \lambda} \vec{S}_0 \cdot \vec{N} = \max_{\alpha, \beta, \lambda} \sqrt{\frac{2}{3}} \sigma_0 \cos \alpha \cos \beta \cos \lambda \Rightarrow \quad (4.2.23)$$

$$\Rightarrow H_{Nmax} = H_N(\alpha = 0, \beta = 0, \lambda = 0) = \sqrt{\frac{2}{3}} \sigma_0 = |\vec{S}_0|.$$

Therefore, we are talking about the distance to the plane which is perpendicular to  $S_1$ -axis. Eq. (4.2.23) makes it clear how  $H_{Nmax}$  relates to the plastic prestrain, because the greater  $\sigma_0$ , the greater  $e_0$ . It is obvious that Eq. (4.2.23) holds true not only for a plastic strain but for any type of loading (proviso that loading path is a straight line).

Taking into account (4.2.23), it is easy to see that Eq. (4.2.21) gives different expressions for  $K_M$  depending on the presence/absence of loading:

$$K_M = \begin{cases} \tilde{K}, & \text{at } |\vec{S}| = 0 \\ K, & \text{during loading as } H_{Nmax} = |\vec{S}| \end{cases} \quad (4.2.24)$$

Now, having at hand formula (4.2.21), consider step by step the procedures involved in MTT and creep.

Plastic prestrain at room temperature ( $\varepsilon_0$ ), according to (3.2.2), is

$$\varepsilon_0 = \sqrt{\frac{2}{3}} e_0, \quad (4.2.25)$$

where  $e_0$  is determined via (4.2.9-12).

Annealing at temperature  $T_a$

Since the second procedure of MTT is an annealing at unloaded state ( $\vec{S} = 0$ ), there is no increment in plastic deformation,  $d\varphi_N = 0$ , and we arrive at differential equation (3.9.6) whose solution is

$$\psi_N = \psi_{N0} \exp(-K_M t). \quad (4.2.26)$$

To establish relationships for the degree of the hardening during annealing, the following must be done:

- since the transition from the cold hardening to the annealing ( $t = 0$ ) is accompanied with temperature increase from room temperature up to  $T_a$ , one has to replace in (4.2.4)  $\sigma_S$  by  $\sigma_P$  which corresponds to  $T_a$ ;
- insert the expression for  $\psi_N$  from (4.2.26) into (4.2.4) and obtain the following expression for  $H_N$ :

$$H_N^2 = \begin{cases} \psi_{N0} \exp(-K_M t) + S_P^2 & \text{for } \Omega_0 \\ S_P^2 & \text{for } \Omega_0^* \end{cases} \quad (4.2.27)$$

Eq.(4.2.27) at  $t = 0$ , together with (4.2.6), gives

$$H_N^2 = \frac{2}{3} \begin{cases} [(\sigma_0 \cos \alpha \cos \beta \cos \lambda)^2 - \sigma_S^2] + \sigma_P^2 & \text{for } \Omega_0 \\ \sigma_P^2 & \text{for } \Omega_0^* \end{cases} \quad (4.2.28)$$

where  $\Omega_0$  and  $\Omega_0^*$  are defined by (4.2.7). Comparing (4.2.28) to (4.2.5) shows that the transition from the cold hardening to the annealing results in a jump-like decrease of distances  $H_N$  in all directions. The loading surface constructed on the base of (4.2.28) is shown in Fig. 4.13b ( $t = 0$ ).

Let us study the distance to planes after the annealing ( $H_{NM}$ ), which is the key term in Eq. (4.2.17) governing the degree of the resistance of material after MTT. Formula (4.2.27) at ( $t = t_a$ ) gives that

$$H_{NM}^2 = \frac{2}{3} \begin{cases} [(\sigma_0 \cos \alpha \cos \beta \cos \lambda)^2 - \sigma_S^2] \exp[-\tilde{K}(\tilde{H}_{Nmax}, \gamma) t_a] + \sigma_P^2 & \text{for } \Omega_0 \\ \sigma_P^2 & \text{for } \Omega_0^* \end{cases} \quad (4.2.29)$$

As seen from this formula, planes moves toward the origin of coordinate, which is due to the defect relaxation observed during the anneal. Loading surface at  $t = t_a$  is shown in Fig. 4.13b.

According to (4.2.22),  $\tilde{H}_{Nmax} = (\sqrt{2/3} \sigma_0 - \sigma_S) / \sigma_S$ , which allows us to rewrite Eq. (4.2.29) as

$$H_{NM}^2 = F(\tilde{H}_{Nmax}) \exp[-\tilde{K}(\tilde{H}_{Nmax}, \gamma) t_a] + \sigma_P^2, \quad (4.2.30)$$

where  $F(\tilde{H}_{Nmax}) \equiv (\sigma_0 \cos \alpha \cos \beta \cos \lambda)^2 - \sigma_S^2$  is an increasing function of  $\tilde{H}_{Nmax}$ .

Summarizing, the value of  $H_{NM}$  depends on the concurrence between two functions,  $F$  and  $\exp(-\tilde{K})$ .

As follows from relation (4.2.21) the function  $\tilde{K}(\tilde{H}_{Nmax}, \gamma)$  behaves as an increasing function, due to  $f_1$ , which undergoes a perturbation ("wavelet") within  $[H_a, H_b]$  interval, which is caused by exponential function  $f_2$  (Fig. 4.14). The parameter  $\gamma$

- plays the role of a scaling factor: the larger  $\gamma$ , the smaller the value of  $\tilde{K}$ ,
- specifies the magnitude of the perturbation and its duration: the larger  $\gamma$ , the greater and more active the deviation of  $\tilde{K}$  from the power law (compare function  $\tilde{K}$  within  $[H_a^{(1)}, H_b^{(1)}]$  and  $[H_a^{(2)}, H_b^{(2)}]$ ).

For large values of  $\gamma$ , within the ranges  $\tilde{H}_{Nmax} \in [0, H_a^{(1)}]$  and  $\tilde{H}_{Nmax} > H_b^{(1)}$ , the function  $H_{NM}$  increases together with function  $F$ , because the influence of  $\exp(-\tilde{K})$  is insignificant. The increase in  $H_{NM}$  within these intervals illustrates the MTT-induced hardening of material, which corresponds to the descending branches in  $\dot{\epsilon} = f(\epsilon_0)$  plot (Fig. 2.16a). For  $\tilde{H}_{Nmax} \in [H_a^{(1)}, H_b^{(1)}]$ , function  $\tilde{K}$  increases swiftly. Therefore,  $\exp(-\tilde{K}) \rightarrow 0$  and the value of  $H_{NM}$  tends to  $\sqrt{2/3} \sigma_P$ . It is easy to see that relation (4.2.17) at  $H_{NM} = \sqrt{2/3} \sigma_P$  leads to the case of the creep rate in the absence of preliminary MTT, Eq. (4.2.13). The decrease in  $H_{NM}$  reflects the loss of the thermomechanical stability of the substructure formed in the course of MTT. Hence, the rate of steady-state creep approaches its initial value as a function of the degree of preliminary cold hardening.

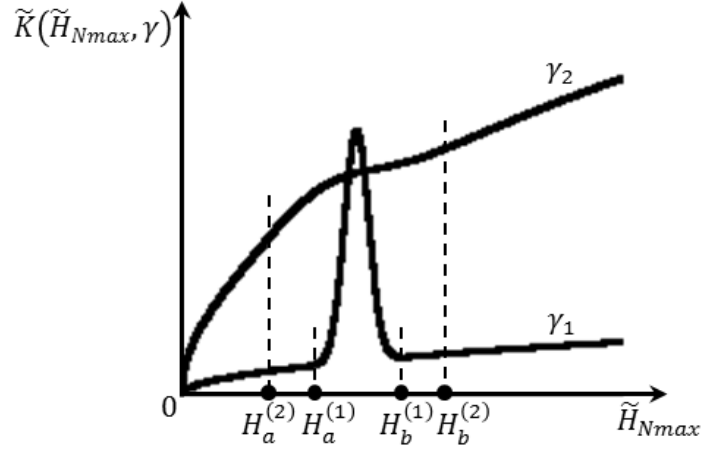


**Fig. 4.14** Qualitative appearance of function  $\tilde{K}(\tilde{H}_{Nmax}, \gamma)$  at two values of  $\gamma$ :  $\gamma_1 > \gamma_2$ .

For low values of  $\gamma$ , the perturbation of function  $\tilde{K}$  for  $\tilde{H}_{Nmax} \in [H_a^{(2)}, H_b^{(2)}]$  interval is insignificant. This is why the product  $F \exp(-\tilde{K})$  first increases but then, beginning from the large values of  $\tilde{H}_{Nmax}$ , decreases and tends to zero. This type of the behavior of  $H_{NM}$  reflects the MTT-induced hardening of the materials with low SFE.  $\dot{\epsilon} = f(\epsilon_0)$  function first decreases (descending branch in Fig. 2.16b), however, this effect disappears when the degree of cold hardening is high and the substructure loses its thermomechanical stability (ascending branch in Fig. 2.16b).

#### Steady-state creep after MMT

We now compute the rate of steady-state creep rate in the metal subjected to MTT (let us assume that  $T_a$  equals to the creep temperature). Here, we restrict ourselves to the case when the creep stress vector  $\vec{S}$  is such that the range of planes moved by it ( $\Omega_1$ ) is wider than that for vector  $\vec{S}_0$ , i.e.  $\Omega_1 \supset \Omega_0$ . Within  $\Omega_1 \setminus \Omega_0$  diapason, where tangent planes did not move during MTT ( $H_{NM} = \sqrt{2/3} \sigma_P$ ),  $\psi_N$  from Eq. (4.2.13) holds true. Consequently, the loading surface in creep after MTT (Fig. 4.13c) is formed by the same set of planes as for the case of ordinary creep. However, the planes from  $\Omega_0$  travel less distances at the endpoint of the  $\vec{S}$  than those for the material in a virgin state. It is this fact that governs the reaction of creep rate upon the preliminary treatment.

If to substitute  $H_{NM}$  given by (4.2.29) into relation (4.2.17), we obtain

$$\psi_N = \frac{2}{3} \begin{cases} (\sigma \cos \alpha \cos \beta \cos \lambda)^2 - [(\sigma_0 \cos \alpha \cos \beta \cos \lambda)^2 - \sigma_S^2] \exp(-\tilde{K} t_a) - \sigma_P^2 & \Omega_0 \\ (\sigma \cos \alpha \cos \beta \cos \lambda)^2 - \sigma_P^2 & \Omega_1 \setminus \Omega_0 \\ 0 & \Omega_1^* \end{cases} \quad (4.2.31)$$

Utilizing Eqs. (3.7.3) and (3.9.1) and integrating the function  $\psi_N$  over diapason  $\Omega_1$  lead us to the rate of steady-state creep ( $\dot{\epsilon}_M$ ) in the material subjected to preliminary MTT:

$$\begin{aligned}
\dot{\epsilon}_M &= \iiint_{\Omega_1} \dot{\varphi}_N N_1 dV = \frac{K}{r} \int_0^{\lambda_1} \int_{-\alpha_1}^{\alpha_1} \int_{-\beta_1}^{\beta_1} \psi_N \cos \alpha \cos^2 \beta \cos \lambda d\alpha d\beta d\lambda \\
&= \frac{2K}{3r} \left\{ \int_0^{\lambda_1} \int_{-\alpha_1}^{\alpha_1} \int_{-\beta_1}^{\beta_1} [(\sigma \cos \alpha \cos \beta \cos \lambda)^2 - \sigma_p^2] \cos \alpha \cos^2 \beta \cos \lambda d\alpha d\beta d\lambda \right. \\
&\quad \left. - \exp(-\tilde{K} t_a) \int_0^{\lambda_0} \int_{-\alpha_0}^{\alpha_0} \int_{-\beta_0}^{\beta_0} [(\sigma_0 \cos \alpha \cos \beta \cos \lambda)^2 - \sigma_s^2] \cos \alpha \cos^2 \beta \cos \lambda d\alpha d\beta d\lambda \right\}.
\end{aligned} \tag{4.2.32}$$

The first integral in the formula above coincides with relation (4.2.14b) and specifies the rate  $\dot{\epsilon}$  under normal conditions (without MTT). The second integral, according to (4.2.8), equals to  $r_0 e_0$ . Therefore,

$$\dot{\epsilon}_M = \dot{\epsilon} - K \frac{r_0}{r} \exp(-\tilde{K}(\tilde{H}_{Nmax}, \gamma) t_a) e_0, \tag{4.2.33}$$

$$K = \text{const}, \quad \tilde{K}(\tilde{H}_{Nmax}, \gamma) = \tilde{K}(e_0, \gamma) = \text{var}. \tag{4.2.34}$$

Let us analyze these formulas. In the absence of preliminary MTT, we have  $e_0 = 0$  and  $\dot{\epsilon}_M = \dot{\epsilon}$ . As the degree of plastic prestrain  $e_0$  increases, the product  $\exp(-\tilde{K}(e_0, \gamma) t_a) e_0$  behaves as the function  $F \exp(-\tilde{K})$  considered in details above. Thus, Eq. (4.2.33) qualitatively describes plots  $\dot{\epsilon} = f(\epsilon_0)$  from Fig. 2.16 for the different values of  $\gamma$ .

In order to obtain the dependence of the rate of steady-state creep on the degree of plastic prestrain, we use Eqs. (4.2.33) and (4.2.21), in which it is necessary to specify the following constants:  $\sigma_s$ ,  $\sigma_p$ ,  $r_0$ ,  $r$ ,  $K$ , and  $Q_j$ . Constant  $r_0$  in (4.2.9) is chosen for constructing stress-strain diagrams. Therefore, the magnitude of  $e_0$  in Eq. (4.2.33) is not used merely as a variable, but is calculated by (4.2.9). This is done to ensure that a value of stress  $\sigma_0$ , which is used in the definition of  $\tilde{K}$ , gives a correct value for  $e_0$ . Similar situation is observed relatively to constants  $r$  and  $K$ , which to be selected so that a correct value of  $\dot{\epsilon}$  in (4.2.33) is obtained (ordinary creep rate is calculated by (4.2.16)).

The constants  $Q_j$  remain free for variation and must be selected in constructing the calculated curves by using relations (4.2.33) and (4.2.21). Constants  $Q_1$  and  $Q_2$  governs the dynamic of the increase in  $\tilde{K}$ , while  $Q_3$  and  $Q_4$  determine the magnitude, shape and place of the "wavelet" on  $\tilde{K} \sim H_{Nmax}$  curve.

The calculated dependences of the rate of steady-state creep on the degree of plastic prestrain have been constructed for aluminum (Fig. 4.15) at

$$\sigma_s = 18.32 \text{ MPa}, \quad \sigma_p = 5.8 \text{ MPa} \quad (\text{Samsonov, 1965}), \quad r_0 = 7 \cdot 10^3 \text{ MPa}^2, \quad r = 3.5 \cdot 10^3 \text{ MPa}^2, \\ K = 1.075 \cdot 10^{-4} \text{ sec}^{-1}, \quad \gamma = 0.2 \text{ J/m}^2 \quad Q_1 = 15.05 \text{ s}^{-1}, \quad Q_2 = 0.22, \quad Q_3 = 15, \quad Q_4 = -0.6,$$

and for copper (Fig. 4.16) at

$$\sigma_s = 20 \text{ MPa}, \quad \sigma_p = 9 \text{ MPa} \quad (\text{Samsonov, 1965}), \quad r_0 = 5.8 \cdot 10^3 \text{ MPa}^2, \quad r = 1.0 \cdot 10^3 \text{ MPa}^2, \\ K = 4.17 \cdot 10^{-5} \text{ sec}^{-1}, \quad \gamma = 0.04 \text{ J/m}^2 \quad Q_1 = 42.18 \text{ s}^{-1}, \quad Q_2 = 4.5 \cdot 10^{-2}, \quad Q_3 = 1.765, \\ Q_4 = -1.5.$$

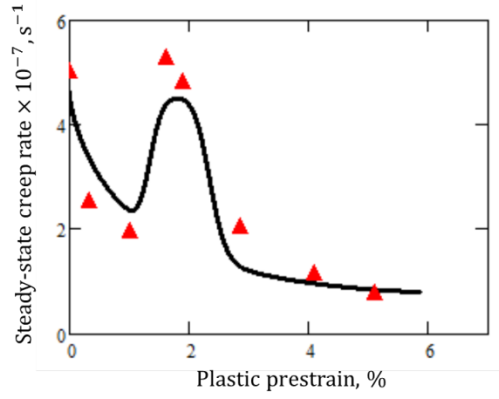


**Fig. 4.15.** Dependences of the rate of steady-state creep of aluminum in uniaxial tension ( $\sigma = 9.6$  MPa,  $T = 260^\circ\text{C}$ ) on the plastic prestrain in the course of MTT ( $T_a = 260^\circ\text{C}$ ,  $t_a = 1$  hour);  $\blacktriangle$  - test (Bazelyuk et al., 1971), line - model result.

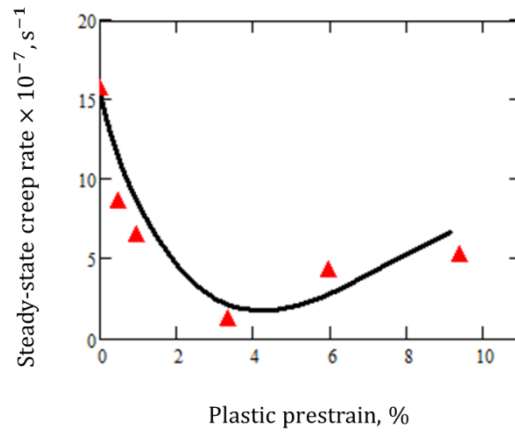


**Fig. 4.16.** Dependences of the rate of steady-state creep of copper in uniaxial tension ( $\sigma = 15$  MPa,  $T = 500^\circ\text{C}$ ) on the plastic prestrain in the course of MTT ( $T_a = 500^\circ\text{C}$ ,  $t_a = 1$  hour);  $\blacktriangle$  - test (Bazelyuk et al., 1970), line - model result.

### Case B

$$\dot{\varepsilon}_M = \dot{\varepsilon}_M(T_a), \varepsilon_0 = \text{const}, t_a = \text{const}$$

Let us define  $K_M$  as a function of anneal temperature in the following way (Rusinko, 2013):

$$K_M = K + \frac{H_{Nmax} - |\bar{S}|}{H_{Nmax}} kG(T_a),$$

$$G(T_a) = \frac{C_1}{(T_a - T_{min}) \exp[-C_2(T_a - T_{min})]}, \quad T_a > T_{min} \quad (4.2.35)$$

$$K_M = \begin{cases} K, & \text{during loading} \\ kG(T_a), & \text{in unloaded state} \end{cases}$$

where,  $T_{min}$  is the minimum temperature needed for dislocations to move and rearrange into stable substructure formation;  $C_1$ ,  $C_2$ , and  $k$  are model constants.

It is easy to see that all the formulae from **case A** remain unchangeable except the function  $K_M$ . Consequently we rewrite Eq. (4.2.29), the degree of the hardening of material due to MTT, as

$$H_{NM}^2 = \psi_{N0} \exp(-kG(T_a)t_a) + \frac{2}{3} \sigma_P^2 \quad (4.2.36)$$

$$= \frac{2}{3} \begin{cases} [(\sigma_0 \cos \alpha \cos \beta \cos \lambda)^2 - \sigma_S^2] \exp[-kG(T_a)t_a] + \sigma_P^2 & \text{for } \Omega_0 \\ \sigma_P^2 & \text{for } \Omega_0^* \end{cases}$$

As seen from (4.2.35) and (4.2.36), as  $T_a \rightarrow T_{min}$ , function  $G \rightarrow \infty$  implying that  $\exp[-kG(T_a)t_a]$  tends to zero, i.e.  $H_{NM} = \sqrt{2/3} \sigma_P$ . As  $T_a > T_{min}$ , function  $G$  first decreases and then, after a certain minimum is achieved, starts to increase. At large values of  $T_a$ , as  $G \rightarrow \infty$ , the distance  $H_{NM}$  again tends to  $\sqrt{2/3} \sigma_P$ . Qualitative plot of  $H_{NM}$  against  $T_a$  is shown in Fig. 4.16.

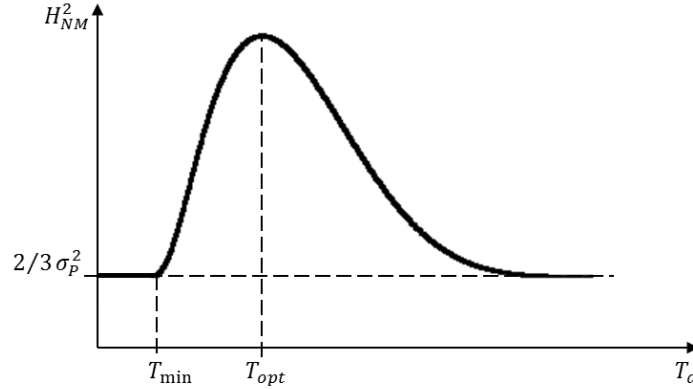


**Fig. 4.16**  $H_{NM}$  vs  $T_a$  plot constructed via Eq. (4.2.36).

Product  $\psi_{N0} \exp(-kG(T_a)t_a)$  from (4.2.36) characterizes the number of thermally stable defects after annealing, i.e. dislocations rearranged into polygonization walls. As  $T_a \leq T_{min}$ , polygonization does not occur and the plastic strain induced defects are abundant within the material matrix but they are not arranged in thermal stable configurations and incapable of offering resistance to high temperature creep. These defects are not effective barriers against the development of irrecoverable strain in the course of steady-state creep due to the high temperature contributes greatly to the disintegration of the pre-existing dislocation grid. As  $T_a > T_{min}$ , subgrain boundaries, similarly to creep, are being formed in the course of annealing, putting bounds upon the free path of dislocations during the creep, i.e. decreasing the rate of creep strain. The greater value of  $T_a$  (to some extent), the greater impetus for forming subgrain structures. Above a certain annealing-temperature, the dislocation structure, formed in plastic deformation, cease to be an effective restriction to the following creep strain due to the intensification of recrystallization during annealing. As a result, the resistance of the metal to irrecoverable deformation significantly decreases since the rapid migration of dislocation boundaries intensely “cleans” the deformed matrix, which facilitates the motion of dislocations under conditions of creep and increases the

rate of stationary creep as compared with its optimal value. Beginning from a certain value of temperature ( $T_1 = T_{max}$ ) the positive effect from MTT completely vanishes, i.e. the steady-state creep rate increases again and comes back to initial value according to the absence of preliminary MTT. Thus, the optimal degree of temperature,  $T_{opt}$ , should be chosen to avoid the possibility of intensive recrystallization. Experimental researchers (Fig. 2.19) give the same  $\dot{\epsilon} = f(T_a)$  tendency as discussed above, justifying the utilization of Eqs. (4.2.36).

Integral (4.2.32), rewritten with the  $K_M$  defined by (4.2.35), gives the dependence of steady-state creep on the value of the anneal temperature in the course of preliminary MTT:

$$\dot{\epsilon}_M = \dot{\epsilon} - K \frac{r_0}{r} \exp(-kG(T_a)t_a)e_0. \quad (4.2.37)$$

The analysis of this formula shows that the behavior of  $\dot{\epsilon}_M(T_a)$  is governed by the function  $G(T_a)$  as follows:

for  $T_{min} \leq T_a \leq T_{opt}$ ,  $G(T_a)$  decreases resulting in the decrease of  $\dot{\epsilon}_M(T_a)$ ;

for  $T_{opt} < T_a$ ,  $G(T_a)$  increases implying the growth in  $\dot{\epsilon}_M(T_a)$  to its initial value of  $\dot{\epsilon}$ .

The analytical  $\dot{\epsilon}_M(T_a)$  curve in Fig. 4.17b is plotted via Eqs. (4.2.37) and (4.2.35) for the following values of the material and model constants:  $\sigma_p = 7$  MPa (Tikhonov, 1986),  $r_0 = 4.8 \cdot 10^6$  MPa<sup>2</sup>,  $r = 0.65 \cdot 10^3$  MPa<sup>2</sup>,  $K = 2.2 \cdot 10^{-5}$  s<sup>-1</sup>,  $k = 2.53 \cdot 10^{-3}$ ,  $C_1 = 1.21$  °C/s,  $C_2 = 0.01$  °C<sup>-1</sup>,  $T_{min} = 400$ °C (Ivanova et al. 1967).

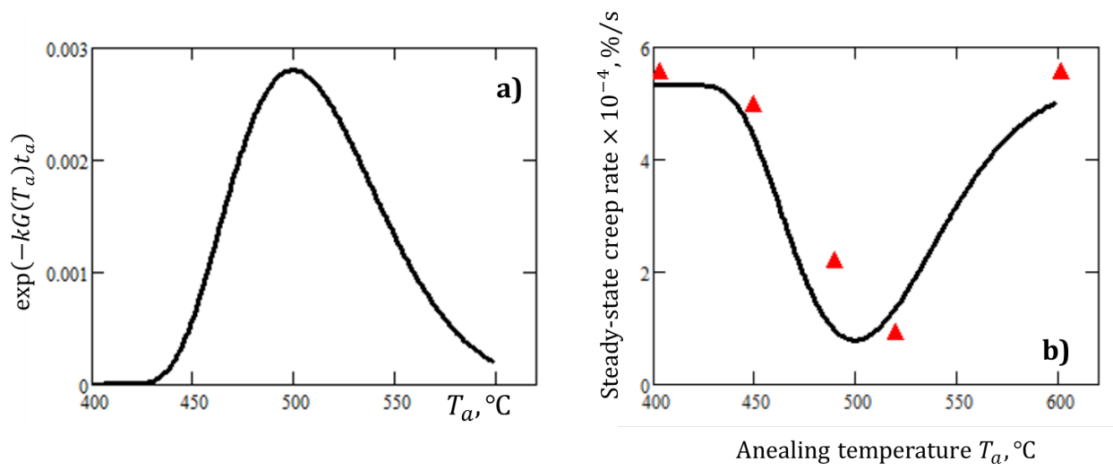


**Fig. 4.17 a)**  $\exp(-kG(T_a)t_a)$  vs  $T_a$  plot, **b)** Influence of annealing temperature  $T_a$  in the course of preliminary MTT upon the steady-state creep strain rate of Armco iron in uniaxial tension for the prestrain of 5% and the anneal time of 25 hours. Creep temperature and stress are  $T = 400$ °C and  $\sigma = 20$  MPa;  $\blacktriangle$  - test (Ivanova, V. et al. 1967), line - model result.

### Case C

$$\dot{\varepsilon}_M = \dot{\varepsilon}_M(t_a), \varepsilon_0 = \text{const}, T_a = \text{const}$$

In order to take into account the influence of the duration of annealing in the course of thermomechanical treatment on the rate of steady-state creep, we define the function  $K_M$  from relation (4.2.20) as (Rusinko, 2005)

$$K_M = K + \frac{H_{Nmax} - |\vec{S}|}{H_{Nmax}} \left[ A - \frac{B}{t} \right], \quad t > t_0 \quad (4.2.38)$$

$$K_M = \begin{cases} K, & \text{during loading} \\ A - \frac{B}{t}, & \text{in unloaded state} \end{cases}$$

where  $t_0$  is introduced to avoid singularity for  $K_M$ ;  $t_0$  can be chosen as small as we please.

If to substitute  $K_M$  from Eq. (4.2.38) in Eq. (3.9.6) and solve the differential equation, we get

$$\psi_N = \psi_{N0}(t - t_0)^B \exp[-A(t - t_0)]. \quad (4.2.39)$$

Now, formula (4.2.29) gets

$$\begin{aligned} H_{NM}^2 &= \psi_{N0}(t - t_0)^B \exp[-A(t - t_0)] + \frac{2}{3} \sigma_P^2 \\ &= \frac{2}{3} \begin{cases} [(\sigma_0 \cos \alpha \cos \beta \cos \lambda)^2 - \sigma_S^2](t - t_0)^B \exp[-A(t - t_0)] + \sigma_P^2 & \text{for } \Omega_0 \\ \sigma_P^2 & \text{for } \Omega_0^* \end{cases} \end{aligned} \quad (4.2.40)$$

It follows from relations (4.2.39) and (4.2.40) that there exists the optimal value of annealing duration ( $\tilde{t}$ ), for which the quantities  $H_{NM}(t)$  and  $\psi_N(t)$  are maximum (Fig. 4.18). The extremum of these functions characterizes the optimal combination of the number of defects after thermomechanical treatment with their thermal stability. It should be emphasized that the condition  $\psi_N(t \rightarrow t_0) \rightarrow 0$  does not mean that defects are absent in the body after cold hardening. In fact, this means that the defects of the crystal lattice do not form polygonal substructures without stabilizing annealing and, hence, do not resist creep. The condition  $\psi_N(t) \rightarrow 0$  for  $t \gg \tilde{t}$  means that the defects accumulated over the optimal number are thermally unstable and also do not affect the steady-state creep rate.

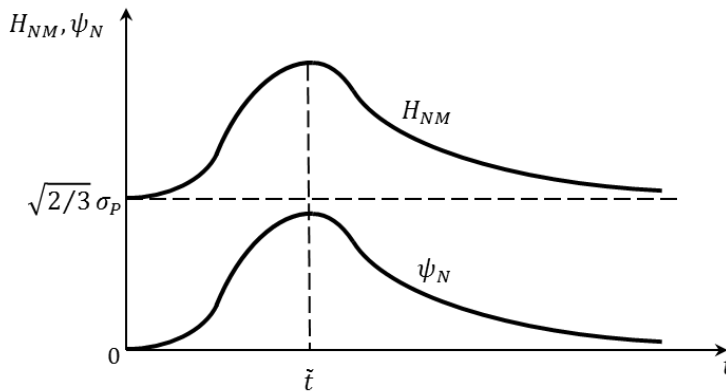


**Fig. 4.18.** The hardening of material ( $H_{NM}$ ) and the intensity of thermally stable defects ( $\psi_N$ ) after MTT as a function the duration of annealing; formulae (4.2.39) and (4.2.40).

Formula (4.2.32), rewritten with the  $K_M$  defined by (4.2.38), gives the dependence of steady-state creep on anneal duration in the course of preliminary MTT:

$$\dot{\epsilon}_M = \dot{\epsilon} - K \frac{r_0}{r} (t_a - t_0)^B \exp[-A(t_a - t_0)] e_0. \quad (4.2.41)$$

It follows from the relation above that, in the absence of stabilizing annealing, the steady-state creep rate remains constant:  $\dot{\epsilon}_M(t_a \rightarrow t_0) \rightarrow \dot{\epsilon}$ . If the duration of annealing is sufficiently large, then the exponential function in relation (4.2.41) tends to zero and the quantity  $\dot{\epsilon}_M$  returns to its initial value  $\dot{\epsilon}$ . Between these values, the dependence of the steady-state creep rate on the duration of annealing in the course of thermomechanical treatment possesses an extremum. Indeed, the function  $\dot{\epsilon}_M$  first decreases and then, after the attainment of the minimum value (corresponding to the optimal duration of annealing), returns to its initial value  $\dot{\epsilon}$ . This result agrees with the plot of the function  $\dot{\epsilon}_M$  in Fig. 2.20. Hence, relation (4.2.41) enables one to predict the rate of steady-state creep of materials as a function of the duration of stabilizing annealing in the course of thermomechanical treatment. Here, we consider only the qualitative description of the secondary creep rate as a function of anneal time.

## CONCLUSION (Thesis 2)

I have generalized the synthetic theory to the case of the steady state creep of materials preliminarily subjected to mechanical-thermal treatment. The influence of parameters of the treatment such as plastic pre-strain, anneal time, and anneal temperature have been modelled for materials with different stacking fault energies.

The primary importance of the results obtained is that the uniformed approach for modelling permanent strain, proposed in terms of the synthetic theory, makes it possible to describe three principally different states of body: a) plastic straining due to increasing stresses, b) defect relaxation in unloaded state, and c) creep deformation at constant stresses.

Calculated results show good agreement with experimental ones allowing us to predict and control the high-temperature strength of metals (creep rate) as a function of the parameters of preliminary mechanical-thermal treatment.

### 4.3 The generalization of the synthetic theory to the case of ultrasonic effects

This chapter presents the generalization of the synthetic theory for modeling the following phenomena accompanying the application of ultrasound:

- (i) ultrasonic hardening (Fig. 2.9),
- (ii) ultrasonic softening (Figs. 2.10 and 2.11),
- (iii) the influence of preliminary ultrasonic treatment upon the creep of metals (Figs. 2.17 and 2.18).

#### 4.3.1 Ultrasound defects

Following the analysis of the processes occurring in the crystalline structure of metal due to sonication (Sections 2.2.1 and 2.2.2), we introduce an average measure of defects within one slip system induced by ultrasound ( $\psi_{Nu}$ ) (Rusinko, 2011, 2012)

$$\psi_{Nu} = U^2 \vec{u} \cdot \vec{N}, \quad \vec{u} = \frac{\vec{S}_u}{|\vec{S}_u|}, \quad (4.3.1)$$

$$U = V_1 \left[ \frac{|\vec{S}_u| - |\vec{S}_{u0}|}{\sigma_s} \right]^{V_2} \left\{ 1 - \exp \left( - \frac{V_3 |\vec{S}_u| \Theta}{\sigma_s \tau} \right) \right\}. \quad (4.3.2)$$

$\vec{S}_u$  is an **ultrasonic stress vector** whose components ( $S_{u1}, S_{u2}, S_{u3}$ ) are calculated by Eq. (3.2.1) if to use the amplitudes of oscillating stress components. Vector  $\vec{u}$  is the unit vector giving the orientation of the line along which  $\vec{S}_u$  acts.  $|\vec{S}_{u0}|$  is a minimum oscillating stress (ultrasound power) needed to generate the ultrasonic defects; if  $|\vec{S}_u| < |\vec{S}_{u0}|$ , we set  $U = 0$ .  $\tau$  is the duration and  $\Theta$  is the homologous temperature of sonication, respectively;  $V_i$  ( $i = 1, 2, 3$ ) are model constants. The scalar product  $\vec{S}_u \cdot \vec{N}$  in (4.3.1) gives the tangent stress (resolved shear stress) acting within certain slip system thereby accounting for the orientation of the slip system relatively to the acting stress.

Eq. (4.3.2) describes the time dependent increase in the defects induced by ultrasound. By means of the term  $\exp \left( - \frac{V_3 |\vec{S}_u| \Theta}{\sigma_s \tau} \right)$ , the following experimental facts can be captured: (a) the number of ultrasonic defects is not a monotone function of sonication time, but, beginning from a certain moment ( $\tau^*$ ), the ultrasound defect intensity remains unchangeable; (b)  $\tau^*$  decreases with the temperature  $\Theta$  and ultrasound power that is expressed via  $|\vec{S}_u|$ ; (c) according to Kulemin (1978), the greater the yield limit of metal  $\sigma_s$ , the greater  $\tau^*$  (at a given  $|\vec{S}_u|$ , the ratio  $|\vec{S}_u|/\sigma_s$  decreases with the growth of  $\sigma_s$ , and the greater time is needed to reach the steady defect intensity).

Ultrasonic irradiation causes diametrically opposite effects dependently on the presence or absence of the simultaneous action of static (unidirectional) load. As such, we introduce the ultrasonic defect intensity into Eq. (3.8.1b)<sup>3</sup> in the following manner

$$H_N^2 = \psi_N + S_S^2 + F\psi_{Nu}, \quad (4.3.3)$$

where

$$F = 1 - 2h(|\vec{S}|). \quad (4.3.4)$$

In the formula above,  $h$  is the Heaviside step, besides we define that  $h(0) = 0$ . Consequently

$$F = \begin{cases} 1, & |\vec{S}| = 0 \\ -1, & |\vec{S}| \neq 0 \end{cases} \quad (4.3.5)$$

It is the function  $F$  that governs the manifestation of ultrasonic hardening or softening.

To avoid misunderstanding that the overall stress state is allegedly decoupled with the acoustic stress vector, the following reasoning is proposed. The static loading is expressed through the stress deviator vector ( $\vec{S}$ ), whereas the action of ultrasound is modeled by means of ultrasound defects intensity ( $\psi_{Nu}$ ), which is a function, among other things, of ultrasonic stress vector ( $\vec{S}_u$ ). In fact, the role of  $\vec{S}_u$ , as a vector, is reduced only to the unit vector  $\vec{u}$  specifying the direction of ultrasound vibrations (i.e. longitudinal, torsional etc.). The main accent is placed on the amplitude of oscillating stress,  $|\vec{S}_u|$ , which appears in the  $U$  from Eq. (4.3.2) and gives the magnitude of  $\psi_{Nu}$ . Therefore, there are (a) the static loading vector ( $\vec{S}$ ) and (b) ultrasound defects ( $\psi_{Nu}$ ); these quantities, through Eq. (4.3.3), governs the hardening state of material and its plastic straining.

#### 4.3.2 Acoustic irradiation without static loading: ultrasonic hardening.

$\psi_{Nu} \neq 0$  and  $\vec{S} = 0$ .

In the absence of static loading,  $\vec{S} = 0$ , we have  $\psi_N = 0$  and  $F = 1$ . Consequently, Eq. (4.3.3) gives that

$$H_N^2 = \frac{2}{3}\sigma_S^2 + \psi_{Nu}. \quad (4.3.6)$$

As follows from this formula, the distance to planes grows in the course of sonication that symbolizes the ultrasonic hardening of material. Repeating the reasoning relating to the analysis of Eq. (4.3.2), one can see that the progress in this process vanishes with the increase of  $\tau$ .

Consider the case of longitudinal ultrasonic waves when oscillating stretching-pressure stress acts,  $\sigma(\tau) = \sigma_m \sin(2\pi f\tau)$ , where  $f$  is the oscillation frequency. According to Eq. (3.2.1) or (4.1.6), the ultrasonic stress vector  $\vec{S}_u (\sqrt{2/3}\sigma_m, 0, 0)$  acts along the  $S_1$ -axis.

<sup>3</sup>  $I_N$  is taken to be zero in (3.8.1b).

Taking into account that for the case of uniaxial tension  $\vec{u} \cdot \vec{N} = N_1 = \cos \alpha \cos \beta \cos \lambda \equiv \Omega$ , Eqs. (4.3.2) and (4.3.6) become

$$U = V_1 \left[ \frac{\sqrt{2/3} (\sigma_m - \sigma_{m0})}{\sigma_s} \right]^{V_2} \left\{ 1 - \exp \left( - \frac{V_3 \sqrt{2/3} \sigma_m \Theta}{\sigma_s} \tau \right) \right\}, \quad (4.3.7)$$

$$H_N^2 = \frac{2}{3} \sigma_s^2 + (U\Omega)^2. \quad (4.3.8)$$

According to Kulemin (1978),  $\sigma_{m0}$  is about of  $(0.3 \div 0.85)\sigma_s$ .

If to draw the inner envelope of the planes whose distances are calculated by (4.3.8), we obtain the yield surface after ultrasonic irradiation as shown in Fig. 4.19.

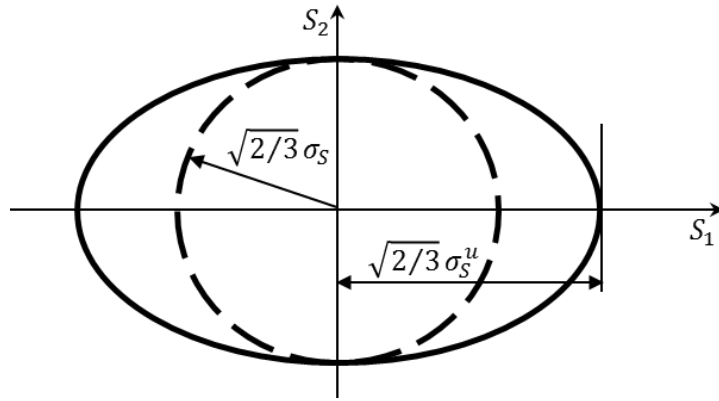


**Fig. 4.19.** Evolution of the yield surface due to sonication.

If to stretch the pre-sonicated specimen, its plastic deformation starts when the static stress vector reaches the first plane ( $\alpha = 0$ ,  $\beta = 0$ , and  $\lambda = 0$ ) distanced by  $H_N = \sqrt{2/3} \sigma_s^u$  from the origin of coordinates. Under these conditions, Eq. (4.3.8) gives that

$$(\sigma_s^u)^2 = \sigma_s^2 + \frac{3}{2} U^2, \quad (4.3.9)$$

where  $\sigma_s^u$  is the yield strength of metal that has incurred previous ultrasonic irradiation. This formula describes the effect of ultrasonic hardening (UH) as a function of ultrasonic vector-amplitude ( $\sigma_m$ ), sonication time ( $\tau$ ), and temperature ( $\Theta$ ). Therefore, the yield stress of material after ultrasonic irradiation, on the base of relations (4.3.9) and (4.3.7), is calculated as

$$\sigma_s^u = \sqrt{\sigma_s^2 + \frac{3}{2} \left\{ V_1 \left[ \frac{\sqrt{2/3} (\sigma_m - \sigma_{m0})}{\sigma_s} \right]^{V_2} \left\{ 1 - \exp \left( - \frac{V_3 \sqrt{2/3} \sigma_m \Theta}{\sigma_s} \tau \right) \right\} \right\}^2}. \quad (4.3.10)$$

### 4.3.3 Ultrasonic vibrations superimposed on plastic straining: ultrasonic softening.

$\vec{S} \neq 0$  and  $\psi_{Nu} \neq 0$ .

Let us determine the yield limit of material in uniaxial tension, i.e. the stress level inducing plastic deformation,  $\sigma_{Su}$ , for the case when a specimen is simultaneously exposed to the static and vibratory loading. In terms of the synthetic theory, this means that we must find the static stress vector  $(\sqrt{2/3} \sigma_{Su}, 0, 0)$  that reaches the first tangent plane ( $\Omega = 1$ ). For this plane, we have

$$\psi_N = 0, \quad H_N^2 = |\vec{S}|^2 = \frac{2}{3} \sigma_{Su}^2, \quad \psi_{Nu} = U^2. \quad (4.3.11)$$

By inserting the relations above into Eq. (4.3.3) at  $F = -1$ , we obtain that the stress level needed for the onset of plastic deformation under the simultaneous action of static and ultrasonic loading ( $\sigma_{Su}^2$ ) is related to the  $\sigma_S^2$  in a static loading as

$$\sigma_{Su}^2 = \sigma_S^2 - \frac{3}{2} U^2. \quad (4.3.12)$$

Eq. (4.3.12) describes the phenomenon of the decrease in the stress required to induce plastic deformation, which is due to the ultrasound ( $U$ ) is superimposed on the static loading. The  $U$  is determined by (4.3.7),

$$U = V_1 \left[ \frac{\sqrt{2/3} (\sigma_m - \sigma_{m0})}{\sigma_S} \right]^{V_2} \left\{ 1 - \exp \left( - \frac{V_3 \sqrt{2/3} \sigma_m \Theta}{\sigma_S} \tilde{\tau} \right) \right\}, \quad (4.3.13)$$

where the instant  $\tilde{\tau}$  is calculated as a ratio  $\sigma_{Su}/\sigma'$  ( $\sigma'$  is the static loading rate). The generalization of synthetic theory similar to (4.3.12) has been done in author's work (Rusynko, 2001), however it is applicable only to the modeling of ultrasonic softening.

To calculate a plastic shift within one slip system, i.e. the strain intensity, use relations (3.9.5) and (4.3.3) at  $F = -1$ , which results in the following relationship:

$$r \varphi_N = \left( \sqrt{2/3} \sigma \cos \alpha \cos \beta \cos \lambda \right)^2 - 2/3 \sigma_S^2 + (U \cos \alpha \cos \beta \cos \lambda)^2. \quad (4.3.14)$$

The ranges of angles for non-zero  $\varphi_N$  are determined from the relation above by letting successively  $\varphi_N = 0$ ,  $\lambda = 0$ , and  $\beta = 0$  as

$$-\alpha_u \leq \alpha \leq \alpha_u, \quad -\beta_u \leq \beta \leq \beta_u, \quad 0 \leq \lambda \leq \lambda_u,$$

$$\cos \lambda_u = \frac{\sigma_S}{\cos \alpha \cos \beta \sqrt{\sigma^2 + \frac{3}{2} U^2}}, \quad \cos \beta_u = \frac{\sigma_S}{\cos \alpha \sqrt{\sigma^2 + \frac{3}{2} U^2}}, \quad (4.3.15)$$

$$\cos \alpha_u = \frac{\sigma_S}{\sqrt{\sigma^2 + \frac{3}{2} U^2}}.$$

By inserting the  $\varphi_N$  from (4.3.14) into Eq. (3.7.3), we obtain plastic strain vector component ( $e_u$ ) for the simultaneous action of unidirectional and vibrating loading:

$$e_u = \int_{-\alpha_u}^{\alpha_u} \int_{-\beta_u}^{\beta_u} \int_0^{\lambda_u} \varphi_N \cos \alpha \cos^2 \beta \cos \lambda \, d\alpha d\beta d\lambda = \quad (4.3.16)$$

$$= \frac{2}{3r} \int_{-\alpha_u}^{\alpha_u} \int_{-\beta_u}^{\beta_u} \int_0^{\lambda_{1u}} \left[ \left( \sigma^2 + \frac{3}{2} U^2 \right) (\cos \alpha \cos \beta \cos \lambda)^2 - \sigma_s^2 \right] \cos \alpha \cos^2 \beta \cos \lambda \, d\alpha d\beta d\lambda.$$

It is easy to see that this integral is identical to that from (4.2.8) if to replace  $\sigma^2 + \frac{3}{2} U^2$  by  $\sigma_0^2$ . Therefore, now, formula (4.2.9) takes the following form:

$$e_u = \frac{\pi \sigma_s^2}{9r} \Phi(\cos \alpha_u) = \frac{\pi \sigma_s^2}{9r} \Phi \left( \frac{\sigma_s}{\sqrt{\sigma^2 + \frac{3}{2} U^2}} \right). \quad (4.3.17)$$

If to let  $U = 0$  in (4.3.17), we obtain Eq. (4.2.9).

Recall that  $\Phi(\xi)$  is a decreasing function of its argument  $\xi$ , and  $\Phi(1) = 0$  (see Fig. 4.4). It is easy to conclude from Eqs. (4.3.17) and (4.2.12) that for a given static stress  $\cos \alpha_u < \cos \alpha_0$  and, consequently,  $\Phi(\cos \alpha_u) > \Phi(\cos \alpha_0)$ , i.e.  $e_u > e_0$  (see Figs. 2.10 and 2.11). It must be noted that the difference between  $e_0$  and  $e_u$  progressively increases due to the presence of  $U$  in the denominator of Eq. (4.3.17). This fact ensures that the stress-strain diagram under the superimposed ultrasound is of flatter form than that for the case of pure static loading. Besides, due to the presence of  $U$  in (4.3.17), the onset of plastic flow takes place at the stress less than  $\sigma_s$ .

#### 4.3.4 Influence of preliminary ultrasound treatment upon the steady-state creep of metals of different stacking fault energies

To model the influence of the duration of preliminary ultrasound treatment upon the steady-state creep rate of metals (see Figs. 2.17 and 2.18), similarly to Sec. 4.2, we modify Eq. (4.2.13) by introducing a measure of the hardening of material obtained in the course of the ultrasound treatment. Since the hardening of material is characterized by the distances to planes, we propose to replace the creep limit of material in (4.2.13) (an initial strength of material at its virgin state,  $H_N = S_P = \sqrt{2/3} \sigma_P$ ) by the distances to planes ( $H_{Nu}$ ) after UT (Rusinko, 2014):

$$\psi_N = H_N^2 - H_{Nu}^2. \quad (4.3.18)$$

It is easy to see that an increase in  $H_{Nu}$  leads to the decrease in  $\psi_N$  and via Eq. (4.2.14a) to the smaller values of  $\dot{\epsilon}$ . In the case  $H_{Nu} = \sqrt{2/3} \sigma_P$  we return to Eq. (4.2.13), and the integral (4.2.14b) will give the rate of ordinary creep, i.e. without preliminary UT.

In what follows, we deal with the  $H_{Nu}$ . After the sonication of specimen (the first procedure in UT), the distance to planes is calculated via (4.3.6). To model the behavior of the ultrasound defects during annealing (the second procedure in UT), we use Eq. (3.9.6),

$$d\psi_{Nu} = -K_U\psi_{Nu}dt, \quad (4.3.19)$$

where, instead of the function  $K$  defined by (3.9.3), we introduce a new function,  $K_U$ ,

$$K_U = K_U[U(\tau)], \quad (4.3.20)$$

where  $U$  is defined by (4.3.2), which ensures that  $K_U$  is a function of the duration of preliminary sonication  $\tau$ . There are two reasons to use Eq. (4.3.20) with function  $K_U$

- 1) Formula (3.9.6) gives  $d\psi_N = 0$  for a load-free state because of  $K = 0$  as  $|\vec{S}| = 0$ . In contrast to  $K$ ,  $K_U \neq 0$  in the course of annealing due to the defects cumulated during sonication.
- 2) Since we are studying the influence of ultrasound treatment upon the following steady creep, we define function  $K_U$  so that it governs the number of **thermally stable defects** ( $\tilde{\psi}_{Nu}$ ) capable impeding processes during the creep following the UT. This requirement is in line with the fact that UT-defects whose number exceeds an optimal value do not offer resistance to the creep. Therefore, only the intensity of thermally stable defects must be taken into account. For example, a long-duration sonication results in the great total number of defects after UT, but the stable fraction of these defects tends to zero ( $\tilde{\psi}_{Nu} \rightarrow 0$ ), which is manifested in the increasing portions of  $\dot{\epsilon} \sim \tau$  curves in Figs. 2.17 and 2.18.

If to insert the solution of Eq. (4.3.19),

$$\tilde{\psi}_{Nu} = \psi_{Nu}\exp(-K_U t_a), \quad (4.3.21)$$

into formula (4.3.6), we obtain the distances to planes upon completion of UT:

$$\begin{aligned} [H_{Nu}]^2 &= \frac{2}{3}\sigma_p^2 + \tilde{\psi}_{Nu} = \frac{2}{3}\sigma_p^2 + \psi_{Nu}\exp(-K_U t_a) = \\ &= \frac{2}{3}\sigma_p^2 + U(\tau)^2\exp(-K_U(\tau)t_a)\Omega, \end{aligned} \quad (4.3.22)$$

where  $t_a$  is the duration of annealing ( $t_a = \text{const}$ ), and  $\sigma_s$  is replaced by  $\sigma_p$  which corresponds to  $T_a$ .

According to the basic postulate of the synthetic theory stating that the distance to plane expresses the hardening of material,  $H_{Nu}(\tau)$  from the formula above gives the degree of the UT-hardening of material with respect to creep.

To model the thermal stability of UT-substructure, i.e. its capability of impeding high-temperature creep, we define the function  $K_U$  from (4.3.20) in the following way (Rusinko, 2014)

$$K_U = K + [1 - h(|\vec{S}|)]\{A_1 \cdot f_1 + A_2 \cdot \exp[-(f_2)^{A_3}]\}, \quad (4.3.23)$$

where  $h$  is the Heaviside function defined at zero as  $h(0) = 0$ . It is easy to see that

$$K_U = A_1 f_1 + A_2 \cdot \exp[-(f_2)^{A_3}] \quad \text{in the course of annealing,} \quad (4.3.24)$$

$$K_U = K \quad \text{for creep.} \quad (4.3.25)$$

In Eq. (4.3.23), we define  $f_1$  and  $f_2$  as

$$f_1 = \left(\frac{dU}{d\tau}\right)^{-1}, \quad f_2 = A_4 \frac{\sqrt{(A_5 U)^2 + \sigma_S^2} - \sigma_S}{\sigma_S} + A_6, \quad (4.3.26)$$

where  $A_j$  ( $j = 1 \dots 6$ ) are the model constants. We set  $A_2 = 0$  and  $A_2 > 0$  for the materials with low and high stacking fault energy (SFE), respectively.

Consider the case  $A_2 = 0$ :

$$K_U = A_1 \left(\frac{dU}{d\tau}\right)^{-1}. \quad (4.3.27)$$

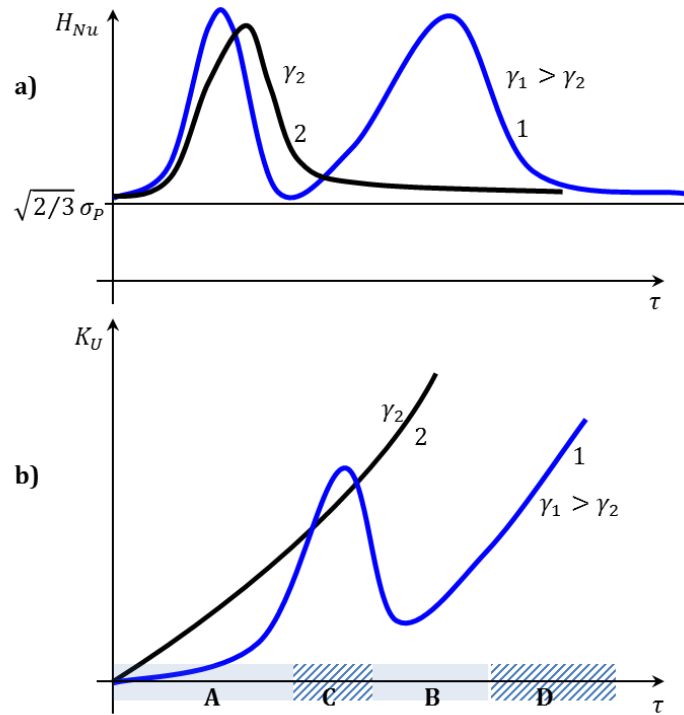


**Fig. 4.20.**  $H_{Nu} \sim \tau$  and  $K_U \sim \tau$  plots for different stacking fault energies.

As seen from Eq. (4.3.2), function  $U(\tau)$  has a decreasing time derivative thereby ensuring the increasing behavior of  $K_U$  as a function of  $\tau$  (curve 2 in Fig. 4.20b). So, the product  $\psi_{Nu}(\tau) \exp[-K_U(\tau)t_a]$  from Eq. (4.3.22) implies that function  $H_{Nu}$  has a single maximum (curve 2 in Fig. 4.20a). The maximum in  $H_{Nu}$ , via Eqs. (4.3.18) and (4.2.14a), corresponds to the minimum in the creep rate (optimal pre-sonication time in Fig. 2.18), and when  $H_{Nu} \rightarrow \sqrt{2/3} \sigma_P$  the creep rate tends to its initial value (UT-substructure loses its thermal stability). Therefore, function  $A_1(dU/d\tau)^{-1}$  from (4.3.27) governs the dynamics of the hardening of presonicated material and the position of  $\tau_{opt}$  instant.

If  $A_2 > 0$ , function  $K_U$  constructed on the basis of Eqs. (4.3.23) and (4.3.26) (curve 1 in Fig. 4.20b), gives  $H_{Nu}$  two maximum peaks (curve 1 in Fig. 4.20a). Such a situation is typical

for the metals with great values of  $\gamma$ : the first maximum of  $H_{Nu}$  symbolizes an optimal ratio between the defects generated during ultrasonic irradiation and their high-temperature stability (the first minimum on  $\dot{\varepsilon} = \dot{\varepsilon}(\tau)$  curve in Fig. 2.17), while the second one reflects the hardening effect originated from point defects whose pinning give a considerable hardening which manifests itself beginning only from a certain pre-sonication time (the second minimum on  $\dot{\varepsilon} = \dot{\varepsilon}(\tau)$  curve in Fig. 2.17).

It is the “wavelet” on  $K_U(\tau)$  curve that makes it possible to obtain two maximums in  $H_{Nu}$ . Indeed, small values of  $K_U$  before and after the wavelet (zones A and B in Fig. 4.20b) give the increases in  $H_{Nu}$  (hardening) while the high values of  $K_U$  in zones C and D lead to the decrease  $H_{Nu}$  (the loss of thermal stability (C) and the appearance of microcracks (D)).

It must be stressed once more that quantities  $H_{Nu}$  (the UT-induced material hardening with respect to the subsequent creep) and  $\psi_{Nu}$  (the number of the defects developed during sonication) behaves in different ways as functions of sonication time  $\tau$ . The latter is an increasing function of  $\tau$  for  $\tau \in [0, \tau^*]$ , while the former varies with  $\tau$  in a non-monotonous way depending on the number of UT-induced defects and their capability of restricting the high-temperature creep.

Now, for the case of uniaxial tension under stress  $\sigma$ , we calculate the steady state creep rate of metal ( $\dot{\varepsilon}_U$ ) subjected to preliminary UT. For this purpose, we insert  $H_{Nu}$  from (4.3.22), where  $K_U$  is defined by (4.3.23), into Eq. (4.2.14):

$$\begin{aligned} \dot{\varepsilon}_U &= \frac{K}{r} \iiint_{\Omega_U} \psi_N N_1 dV = \\ &= \frac{2K}{3r} \int_{-\alpha_{1U}}^{\alpha_{1U}} \cos \alpha d\alpha \int_{-\beta_{1U}}^{\beta_{1U}} \cos^2 \beta d\beta \int_0^{\lambda_{1U}} \left\{ \left[ \sigma^2 - \frac{3}{2} U^2 \exp(-K_U t_a) \right] \cos^2 \alpha \cos^2 \beta \cos^2 \lambda - \sigma_p^2 \right\} \cos \lambda d\lambda. \end{aligned} \quad (4.3.28)$$

The integration is carried out only in those directions where  $\psi_N > 0$  (the expression in square brackets). The integration limits ( $\Omega_U$ ) are obtained from conditions  $\psi_N = 0$ ,  $\lambda = 0$ , and  $\beta = 0$ :

$$\cos \lambda_U = \frac{\sigma_p}{\cos \alpha \cos \beta \sqrt{\sigma^2 - \frac{3}{2} U^2 \exp(-K_U t_a)}}, \quad (4.3.29)$$

$$\cos \beta_U = \frac{\sigma_p}{\cos \alpha \sqrt{\sigma^2 - \frac{3}{2} U^2 \exp(-K_U t_a)}}, \quad (4.3.30)$$

$$\cos \alpha_U \equiv a_U = \frac{\sigma_p}{\sqrt{\sigma^2 - \frac{3}{2} U^2 \exp(-K_U t_a)}}. \quad (4.3.31)$$

Integrating in (4.3.28) over the limits (4.3.29-31) gives

$$\dot{\varepsilon}_U = a_0 \Phi(a_U), \quad a_0 = \frac{\pi K \sigma_p^2}{9r}, \quad (4.3.32)$$

where  $\Phi$  is from Eq. (4.2.10).

The ordinary creep rate in uniaxial tension, i.e. without preliminary UT, is calculated by Eq. (4.2.16), and it is easy to see that the only difference between (4.3.32) and (4.2.16) is the expression for the arguments of  $\Phi$ , i.e. between  $a_U$  and  $a$ . Comparing them, one can infer that  $\dot{\epsilon}_U \leq \dot{\epsilon}$  due to  $a_U \geq a$ . This difference is due to the term  $\frac{3}{2}U^2 \exp(-K_U t_a)$  in  $a_U$ , which, according to Eq. (4.3.22), governs the value of  $H_{Nu}$ , i.e. the degree of UT-hardening.

Let us give a geometric interpretation of the results obtained for different sonication times ( $\tau_{(a)} = 0, \tau_{(c)} > \tau_{(b)}$ ) in preliminary UT. For simplicity, without losing generality, we study the evolution of loading surface during sonication and annealing in  $S_1 S_2$  coordinate plane. The first column in Fig. 4.21 illustrates the loading surfaces after ultrasonic irradiation constructed as the inner envelope of planes whose distances  $H_N$  are determined by Eqs. (4.3.7) and (4.3.8). Let us evaluate the degree of material hardening via the distance to the tangent plane calculated by Eq. (4.3.8) at  $\Omega = 1, H_{Nmax}$ . It is easy to see that

$$H_{Nmax(c)} > H_{Nmax(b)} > H_{Nmax(a)}, \quad H_{Nmax(a)} = \sqrt{2/3} \sigma_S, \quad (4.3.33)$$

which gives an increase in the yield limit of sonicated material with the growth of sonication time ( $\tau$ ).

Loading surfaces from the second column in Fig. 4.21 illustrate the degree of the hardening of material with respect to creep after the stabilizing annealing. They are constructed as the inner envelopes to the planes whose distances  $H_{Nu}$  are defined by Eq. (4.3.22). If to compare these distances at  $\Omega = 1$  (let us designate them through  $H_U$ ), we observe the following relation between them (in contrast to Eq. (4.3.33))

$$H_{U(b)} > H_{U(c)} > H_{U(a)}, \quad H_{U(a)} = \sqrt{2/3} \sigma_p. \quad (4.3.34)$$

In other words, we observe the situation when the sonication time  $\tau_{(c)}$  exceeding an optimal value (for example, let it be  $\tau_{(b)}$ ) leads to a loss of the thermal stability of UT-substructure, which is manifested in a decrease in the resistance to creep deformation. The further increase in  $\tau_{(c)}$  implies that  $H_{U(c)} \rightarrow \sqrt{2/3} \sigma_p$ , i.e. the loading surface regains a form of the initial sphere of radius  $\sqrt{2/3} \sigma_p$ .

Together with the loading surface after UT, the second column in Fig. 4.21 shows the boundary planes reached by stress vector  $\vec{S}$  during creep; their orientation is given by boundary angles  $\alpha_U$ . It is easy to see that

$$\alpha_{U(b)} < \alpha_{U(c)} < \alpha_1. \quad (4.3.35)$$

Conclusions:

- a) the greater  $H_{U(b)}$ , the smaller  $\alpha_{1U(b)}$  – the increase in the hardening of material due to UT decreases the number of slip systems involved in creep deformation, i.e. reached by the stress vector  $\vec{S}$ ;
- b) the greater  $H_{U(b)}$ , the smaller distances are covered by planes at the endpoint of the  $\vec{S}$  from their initial positions.

Both these facts lead to the decrease in the steady state creep rate of the material subjected to preliminary ultrasonic treatment.

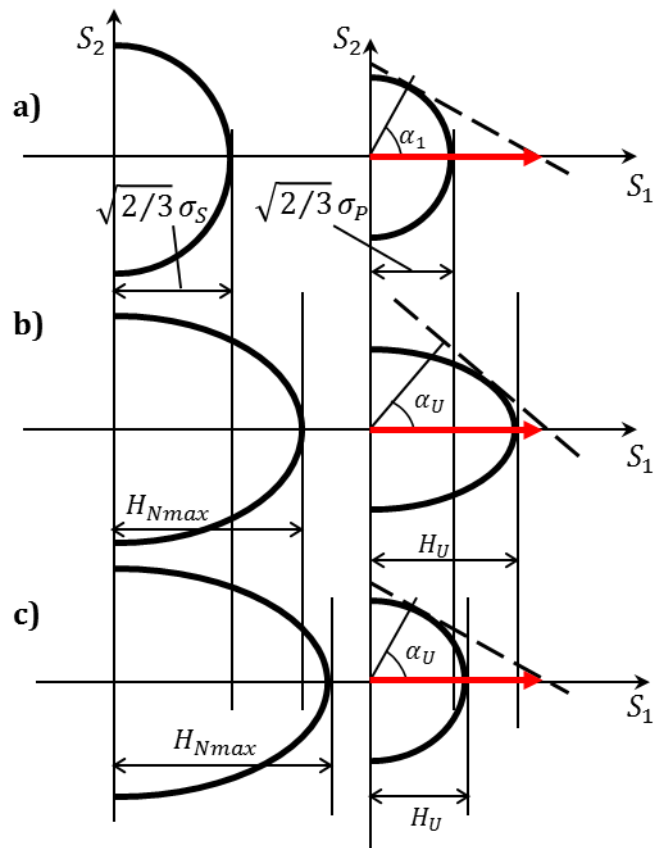


**Fig. 4.21.** Yield surface (a) and loading surfaces (b and c) in  $S_1 - S_2$  coordinate-plane after ultrasound irradiations of different times (first column). The orientation of the boundary plane (angles  $\alpha_U$ ) under the condition of steady state creep that follows the UT (second column) (b and c) and without UT (a):  $\alpha_1 > \alpha_{U(c)} > \alpha_{U(b)}$ ,  $\alpha_{U(c)} \rightarrow \alpha_1$ .

### 4.3.5 Results, discussion.

This section presents theoretical results of ultrasound effects upon the strength properties of copper and aluminum (Table 4.2 contains physical properties of the materials involved in our calculations). Here we deal with the construction of the following plots:

- 1) Yield strength vs sonication time ( $\sigma_s^u \sim \tau$ ) for Cu and Al (ultrasonic hardening).
- 2) Yield strength vs ultrasound stress amplitude ( $\sigma_s^u \sim \sigma_m$ ) for Cu and Al (ultrasonic hardening).
- 3) Stress vs strain ( $\sigma \sim \varepsilon$ ) for Cu with simultaneous action of ultrasound (ultrasonic softening).
- 4) Secondary creep rate vs sonication time ( $\dot{\varepsilon} \sim \tau$ ) for Cu and Al (influence of UT upon the creep rate).

**Table 4.2 Physical properties of Cu and Al.**

	Copper	Aluminum
Young modulus $E$ , GPa	117	69
Speed of sound $c$ , m/s	4600	6420
Melting point $T_m$ , °C	1085	660

To obtain the diagrams listed above, it is necessary to specify the model constants entering the relationships of the synthetic theory.

#### A: $\sigma_s^u \sim \tau$ and $\sigma_s^u \sim \sigma_m$ diagrams.

Constants  $V_i$  ( $i = 1, 2, 3$ ) enter Eq. (4.3.10) which is used for constructing diagrams for the yield limit of material under the action of ultrasound alone as a function of

- (a) the duration of ultrasound irradiation ( $\tau$ ) at  $\sigma_m = \text{const}$ , and
- (b) the ultrasound stress amplitude ( $\sigma_m$ ) at  $\tau = \text{const}$ .

The constant  $V_3$  is responsible for the change in  $\sigma_s^u$  as a function of  $\tau$  at  $\sigma_m = \text{const}$ , while the constants  $V_1$  and  $V_2$  govern  $\sigma_s^u \sim \sigma_m$  diagrams at  $\tau = \text{const}$ . The experimental and analytical diagrams  $\sigma_s^u \sim \tau$  and  $\sigma_s^u \sim \sigma_m$  are shown in Figs. 4.22 and 4.23, respectively.

In experiments for ultrasonic hardening, they form a standing wave along the specimen with its stress-antinode at  $x = l/2$ , where  $l$  is half the length of acoustic wave ( $\lambda$ ) in the medium:

$$\lambda = c/f, \quad (4.3.36)$$

where  $f$  is the oscillating stress frequency. As such, at  $x = l/2$ , they reduce the specimen diameter so that the plastic deformation in a static tensile of pre-sonicated material concentrates in the section of maximum ultrasonic hardening. This means that the sinusoidal distribution of vibrating stress during the sonication can be neglected, and Eq. (4.3.10) is readily applicable to the modeling of ultrasonic hardening effect.

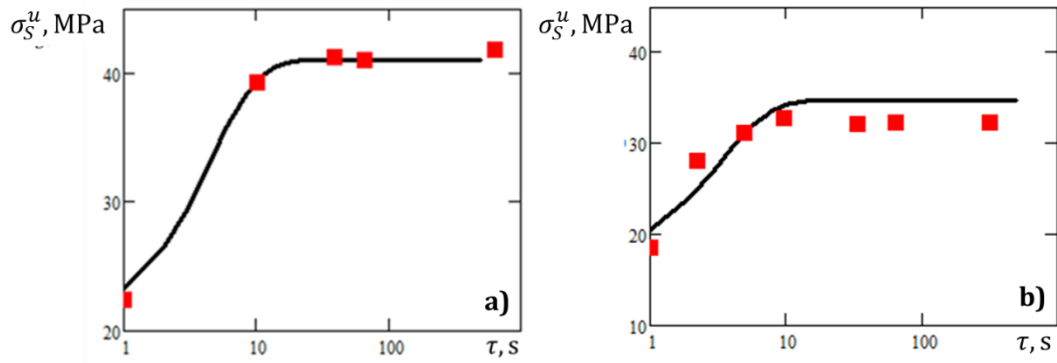


**Fig. 4.22.** Increase in the yield strength of a) copper and b) aluminum as a function of sonication time at a)  $\sigma_m = 67$  MPa and b)  $\sigma_m = 164$  MPa;  $t = 20^\circ\text{C}$ : ■ - experiment (Kulemin, 1978), line - model result.

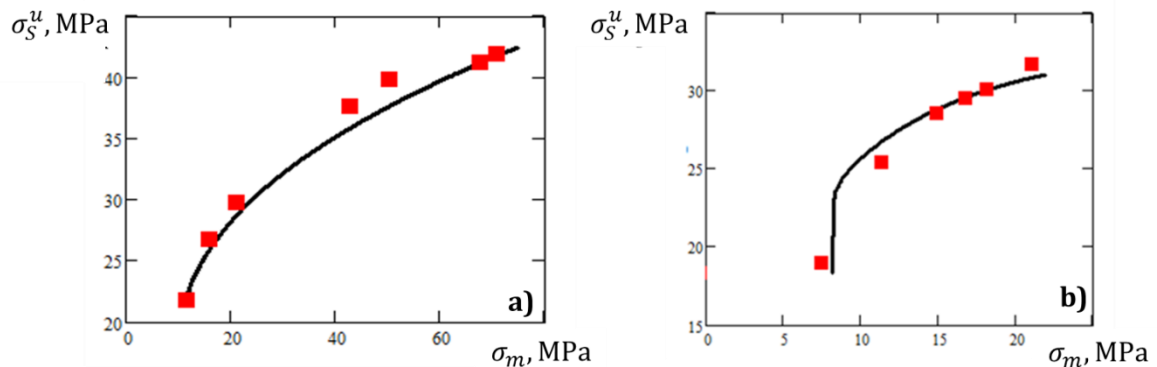


**Fig. 4.23.** Increase in the yield strength of a) copper and b) aluminum as a function of ultrasound stress amplitude at  $\tau = 60$  s;  $t = 20^\circ\text{C}$ : ■ - experiment (Kulemin, 1978), line - model result.

The analytical results for the figures above are obtained via Eq. (4.3.10) at the following data

*Copper:*  $\sigma_S = 21.7$  MPa,  $\sigma_{m0} = 0.45\sigma_S = 11.7$  MPa,  $\sigma_m = 67$  MPa,  $V_1 = 22$  MPa,  $V_2 = 0.35$ ,  $V_3 = 6.0 \text{ s}^{-1}$ .

*Aluminum:*  $\sigma_S = 18.3$  MPa,  $\sigma_{m0} = 0.45\sigma_S = 8.24$  MPa,  $\sigma_m = 164$  MPa,  $V_1 = 22$  MPa,  $V_2 = 0.047$ ,  $V_3 = 1.7 \text{ s}^{-1}$ .

### **B: $\sigma \sim \varepsilon$ diagram with acoustic energy.**

To plot  $\sigma \sim \varepsilon$  diagrams for static and combined loading, we use Eqs. (4.3.17) and (4.3.13), where four constants,  $r$  and  $V_i$  ( $i = 1, 2, 3$ ), have to be specified.

(i) To find the constant  $r$ , we use the data of tensile testing of copper specimens at room temperature (Fig. 4.24, curve 1). The theoretical tensile stress-strain diagram is plotted according to relations (4.3.17) at  $U = 0$ , and the constant  $r$  is chosen to make the theoretical curve as close to the experimental data as possible. The constant  $r$  characterizes the hardening of material in the course of plastic deformation.

(ii) When constructing stress-strain diagrams accompanied by ultrasound (Fig. 4.24, curve 2) for the specimen with a constant diameter along its gage length, the sinusoidal distribution of ultrasonic stress must be taken into account. In other words, every cross

section of specimen is subjected to the constant tensile stress ( $\sigma(x) = \text{const} \equiv \sigma, \forall x \in [0, l]$ ) and oscillating stress whose amplitude is distributed as

$$\sigma_m(x) = \sigma_m \sin kx, \quad (4.3.37)$$

where  $k = 2\pi f/c$ ,  $l = \lambda/2$ ,  $\lambda$  is calculated by (4.3.36). Therefore, the plastic (permanent) deformation of the specimen is calculated as

$$\varepsilon_u = \frac{\int_0^l e_u(x) dx}{l}. \quad (4.3.38)$$

For every  $x$ , the plastic strain  $e_u(x)$  is obtained from Eqs. (4.3.17), where the function  $U(x)$  is calculated by Eqs. (4.3.13) and (4.3.37) (Fig. 4.25). Model constants  $V_i$  standing in  $U$  must be chosen so that the analytical  $\sigma \sim \varepsilon_u$  diagram fits the experimental result. The values of  $r$  and  $V_i$ , together with other quantities used in the calculation, are presented below:

$r = 3.3 \times 10^4 \text{ MPa}^2$ ,  $V_1 = 20.0 \text{ MPa}$ ,  $V_2 = 3.0$ ,  $V_3 = 1.59 \times 10^{-1}$ ,  $\sigma_m = 130 \text{ MPa}$ ,  $\sigma_{m0} = 10.5 \text{ MPa}$ ,  $\sigma_s = 35 \text{ MPa}$  (Severdenko et al. 1967),  $\theta = 0.018$ , experiment duration  $\tau = 120 \text{ s}$ ,  $f = 20 \text{ kHz}$ ,  $\lambda = c/f = 0.115 \text{ m}$ .

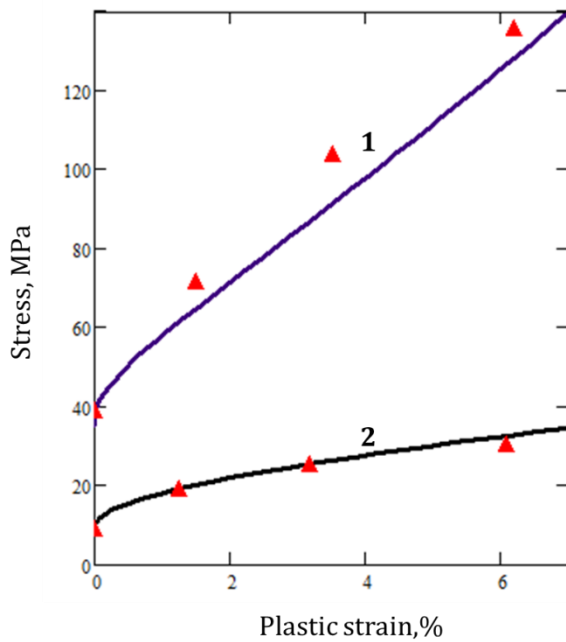


**Fig. 4.24.** Stress vs strain diagrams of copper at room temperature: **1** – static loading, **2** – with superimposed ultrasound,  $\sigma_m = 130 \text{ MPa}$ ;  $\blacktriangle$  – experiment (Severdenko et al. 1967), line – model result.

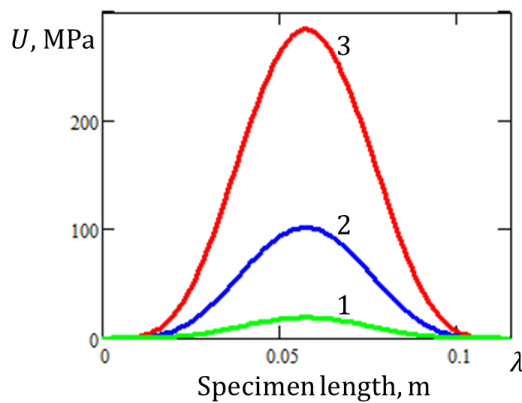


**Fig. 4.25** The distribution of  $U$  function along the specimen for different instants: **1** –  $\tau = 5 \text{ s}$ , **2** –  $\tau = 30 \text{ s}$ , **3** –  $\tau = 120 \text{ s}$ .

### C: $\dot{\epsilon} \sim \tau$ diagrams after UT.

The procedure of sonication is the same as discussed at point A. The experiments to be modeled give the values of oscillation displacement amplitude ( $A$ ) which can be converted into ultrasonic stress amplitude, to be used in Eq. (4.3.2), as (Rusinko, 2012)

$$\sigma_m = \frac{4\pi f}{c} EA. \quad (4.3.39)$$

To plot the  $\dot{\epsilon} \sim \tau$  diagrams, we use Eqs. (4.3.32), (4.3.31), and (4.3.24-26), that requires to specify model constants such as  $K$ ,  $r$ ,  $V_i$  ( $i = 1, 2, 3$ ), and  $A_j$  ( $j = \overline{1, 6}$ ).

Constants  $r$  and  $V_i$  have been analyzed earlier. Constant  $K$ , together with  $r$ , governs the steady-state creep of material for conventional creep (without UT). Constants  $A_j$  govern the behavior of  $K_U$  in Eqs. (4.3.24-26), they determine the magnitude, shape, and place of the “wavelet” on  $K_U \sim \tau$  curve. Compare function  $K_U$  for copper ( $A_2 = 0$ ) and aluminum ( $A_2 \neq 0$ ) in Fig. 4.26. The presence of “wavelet” on  $K_U \sim \tau$  curve for aluminum ensures two maximum in  $H_{Nu} \sim \tau$  plot, in contrast to the case of copper.

Below, we present experimental and theoretical  $\dot{\epsilon} \sim \tau$  plots accompanied by the values of data used for their construction

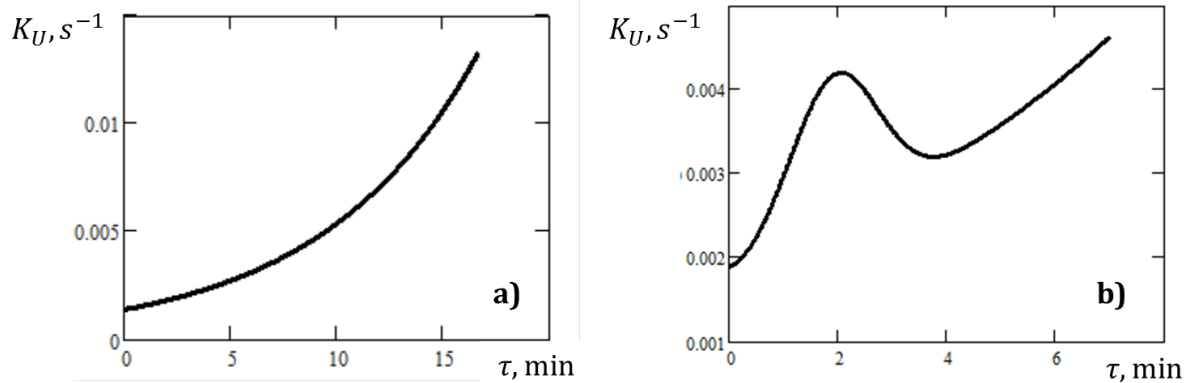


**Fig. 4.26.**  $K_U \sim \tau$  function for a) copper, b) aluminum.

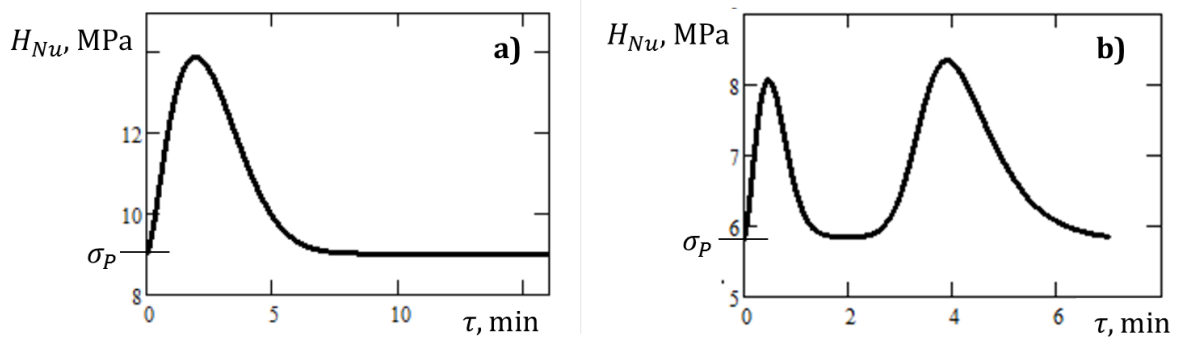


**Fig. 4.27.** Evolution of the resistance of material against creep for a) copper and b) aluminum as a function of sonication duration in the course of UT: Eq. (4.3.22) at  $\Omega = 1$ .

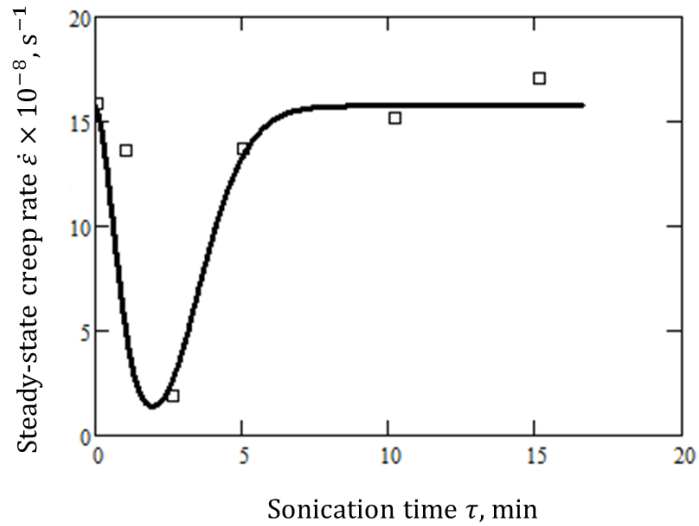


**Fig. 4.28.** Steady-state creep rate of copper in uniaxial tension ( $\sigma = 15$  MPa,  $T = 500^\circ\text{C}$ ) as a function of sonication time in the course of ultrasound treatment ( $T_a = 500^\circ\text{C}$ ,  $t_a = 1$  hour);  $\square$  -experiment (Bazelyuk et al., 1970), line - theoretical result.

$$\sigma_S = 20 \text{ MPa}, \sigma_P = 15 \text{ MPa},$$

$$A = 25 \text{ } \mu\text{m}, f = 20 \text{ kHz}, \sigma_m = 159.8 \text{ MPa}, \sigma_{m0} = 0.3\sigma_S = 6 \text{ MPa}, \Theta = 0.018,$$

$$r = 3.3 \times 10^4 \text{ MPa}^2, K = 2.293 \times 10^{-4} \text{ s}^{-1},$$

$$V_1 = 1.01 \text{ MPa}, V_2 = 3.7, V_3 = 1.53 \times 10^{-2} \text{ s}^{-1}, A_1 = 2.3 \times 10^{-3} \text{ MPa/s}.$$

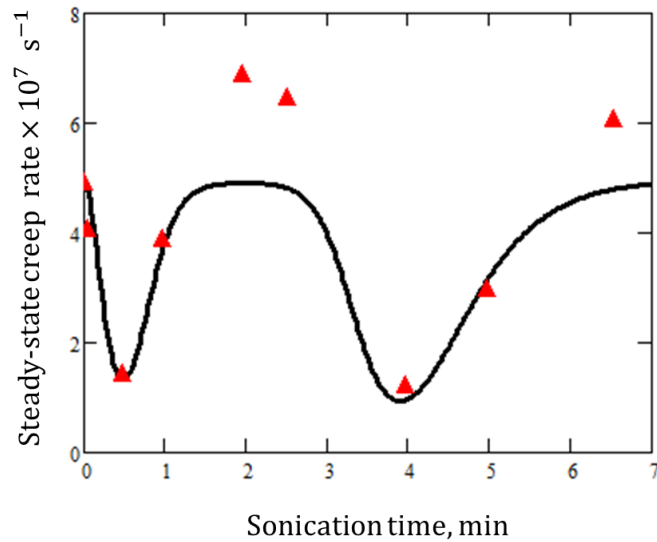


**Fig. 4.29.** Steady-state creep rate of aluminum in uniaxial tension ( $\sigma = 9.6$  MPa,  $T = 260^\circ\text{C}$ ) as a function of sonication time in the course of ultrasound treatment ( $T_a = 260^\circ\text{C}$ ,  $t_a = 1$  hour);  $\blacktriangle$  -experiment (Bazelyuk et al., 1971), line - model result.

$$\sigma_S = 18.3 \text{ MPa}, \sigma_P = 5.8 \text{ MPa},$$

$$A = 15 \text{ } \mu\text{m}, f = 20 \text{ kHz}, \sigma_m = 40.5 \text{ MPa}, \sigma_{m0} = 0.45\sigma_S = 8.2 \text{ MPa}, \Theta = 0.03,$$

$$K/r = 3.27 \times 10^{-8} \text{ (MPa}^2 \cdot \text{s)}^{-1},$$

$$V_1 = 3.65 \times 10^3 \text{ MPa}, V_2 = 2.37 \times 10^{-1}, V_3 = 3.92 \times 10^{-2} \text{ s}^{-1},$$

$$A_1 = 1.6 \times 10^{-2} \text{ MPa/s}, \quad A_2 = 2.4 \times 10^{-2} \text{ s}^{-1}, \quad A_3 = 2, \quad A_4 = 6.91, \quad A_5 = 1.0 \times 10^{-2},$$

$$A_6 = 1.25 \times 10^{-1}.$$

Comparing the model results with the tests shows that the synthetic theory gives good agreement with experiments. Some discrepancy is observed only for thermally unstable UT-structures, e.g. for  $\tau > 15$  min from Fig. 4.28, and for  $2 < \tau < 3$ , and  $\tau > 6$  min from Fig. 4.29. This is accounted for by the approach to model  $\dot{\varepsilon} \sim \tau$  diagrams. When material loses its possibility to resist creep deformation,  $H_{Nu}$  tends to  $\sigma_p$ , and Eq. (4.3.18) leads to the case of ordinary creep ( $\dot{\varepsilon}$ ).

Summarizing, the results obtained give answer for the most valuable question: what sonication duration results in the improving of strength properties of material.

### CONCLUSION (Thesis 3)

On the base of the synthetic theory, I have developed a mathematical model for the analytical description of the phenomena as follows:

- (i) **ultrasonic hardening** – an increase in the yield strength of material recorded after its sonication; the dependence of the yield strength upon the sonication time and the alternating stress amplitude has been considered;
- (ii) **ultrasonic softening** observed during plastic straining under the simultaneous action of static and ultrasonic loading; effects – a) decrease in the stress needed to induce plastic flow, b) more intensive development of the deformation comparatively to the action of unidirectional loading alone;
- (iii) the influence of preliminary **ultrasonic treatment** (sonication + stabilizing anneal) upon the steady-state creep rate of materials with different stacking fault energies.

The problems above have been solved by introducing a new function, ultrasound defect intensity. This function expresses an average measure of the crystalline grid defects induced by acoustic energy within one slip system.

It is worthwhile to stress again that all the relations considered here have been derived via the single system of constitutive equations (3.8.7).

Good agreement between analytical results and experimental data testifies not only to qualitative, but also to quantitative reliability of the model presented.

## Conclusions and suggestions for further work

This thesis gives the results of investigations of a number of problems in Solids Mechanics. There were three main themes addressed in this study. The first theme is a string of phenomena accompanying the creep after the stepwise decrease of acting stress such as negative creep, creep delay, and inverse creep. The most surprising result is the stress-drop causes plastic and creep deformation in the direction opposite to that of net stress. Creep deformation at the decreased stress tends to its steady-state stage unlike conventional creep, but shows increasing rate (inverse creep). The transition between the negative and inverse creep lays across the portion of zero strain increment called as creep delay, which is an incubation period needed for the material structure to get prepared for resuming deformation in the direction of the net stress after the stress drop. It is absolutely clear that the modelling of the phenomena above cannot be accomplished in terms of phenomenological concepts, where creep rate is related to the actual value of acting stress without taking into account the loading prehistory. Another doubtless conclusion is that a theory whose results originate from the analysis of the evolution of the processes occurring at the micro level of material is strongly needed. Such a theory is the synthetic theory of permanent deformation, where deformation is calculated on two levels of material structure, i.e. macro deformation strongly depends on the processes occurring at the micro level of material during plastic or creep deformation. To catch the phenomena discussed above I have proposed a relationship which defines the hardening features in material for forward and reversal directions of straining. This modification of the synthetic theory makes it possible to model all the phenomena faced in stress-drop test. What is equally important is that the formulae obtained allows us to conclude about the interplay between negative creep, creep delay, and inverse creep, which appear one after another.

The second theme of the thesis is the influence of preliminary mechanical-thermal treatment, which consists of plastic strain and subsequent anneal at unloaded state, upon steady-state creep. According to experiments, the creep rate of pretreated specimens is a non-monotone function of such variables as plastic prestrain, anneal temperature, and anneal time. Again dilemma arises when attempts are made to model the creep as a function of the acting stresses alone, i.e. to ignore loading prehistory. This problem has been solved in terms of the synthetic theory by inspecting the thermal stability of the material defect structure that is formed during the treatment. Thermally stable defects are determined by their ability to impede the processes occurring in the course of creep rather than their quantity. By utilizing this approach, I have developed a model for predicting the steady state creep rate of metals with different values of stacking fault energies that imply different mechanism governing the creep. Again, we take full advantage of the main feature of the synthetic theory to model permanent deformation by means of the study and analysis of real physical processes governing the phenomenon of our interest. Suggestions for further work: so far, formulae for creep rate contain separately the parameters of preliminary mechanical-thermal treatment. Relationships including all them should be developed.

The third theme is an investigation into the ultrasound effects upon plastic and creep deformation of metals. They are: (i) ultrasonic softening, when ultrasound is superimposed on unidirectional loading and intensifies the progress in inelastic straining; (ii) ultrasonic hardening which is observed as ultrasound acts alone and increases the strength parameter of sonicated material; besides, we study (iii) ultrasonic treatment (sonication + stabilizing anneal) as an effective instrument to improve the strength of material, namely, to decrease its creep rate. To model the points listed above, I have introduced into consideration an average measure of the defects of crystalline grid nucleated due to acoustic energy, ultrasound defect intensity. The law of their development in time and as a function of alternating stress amplitude is dictated by numerous experimental results investigating the influence of acoustic energy upon the crystalline structure of metals. By inserting the ultrasound defect intensity into the basic equations of the synthetic theory I have realized the possibility to model all the three cases on ultrasound effects mentioned above. With further investigations, I would like to continue developing the synthetic theory in order to model so-called residual hardening or softening which are observed in combined, ultrasonic and static, loading after the ultrasound is switched off.

To conclude, I summarize the main contributions of this work: I have generalized the synthetic theory so that it has become possible to model: (i) peculiarities of plastic and strain deformation due to the step-wise decrease in the acting stress, (ii) steady-state creep rate as a function of preliminary mechanical treatment, and (iii) deformation properties of material subjected to ultrasound. All model results give good agreement with experimental data (numerical calculations have been carried out by using the MathCad13-Professional software package), which testifies not only to qualitative, but also to quantitative reliability of the synthetic theory.

## References

- Abramov, O. V. (1994). *Ultrasound in liquid and solid metals*. CRC press.
- Ádány, S. (2013). Decomposition of in-plane shear in thin-walled members. *Thin-Walled Structures*, **73**: 27-38.
- Asaro, R. J. (1983). Micromechanics of crystals and polycrystals, *Advances in Applied Mechanics*, **23**: 1-115.
- Asaro, R. J. (1983). Crystal plasticity, *Journal of Applied Mechanics*, **501**: 921-934.
- Asaro, R., & Lubarda, V. (2006). *Mechanics of solids and materials*. Cambridge University Press.
- Asaro, R., & Rice, J. (1977). Strain localization in ductile single crystals, *Journal of the Mechanics and Physics of Solids*, **25**: 309-338.
- Astashev, V. K., & Babitsky, V. I. (2007). *Ultrasonic processes and machines: dynamics, control and applications*. Springer Science & Business Media.
- Balázs, L. Gy. (szerk.) (2015). Vasbeton: cikkgyűjtemény és köszöntések Dr. Tassi Géza egyetemi tanár, a műszaki tudományok doktora (MTA) születésének 90. évfordulója alkalmára. Budapest: Art Atelier Kft., 402 p.
- Barsoum, M. W., El-Raghy, T., Rawn, C. J., Porter, W. D., Wang, H., Payzant, E. A., & Hubbard, C. R. (1999). Thermal properties of Ti<sub>3</sub>SiC<sub>2</sub>. *Journal of Physics and Chemistry of Solids*, **60**: 429-439.
- Batdorf, S. and Budiansky, B. (1949) A mathematical theory of plasticity based on the concept of slip, *NACA, Technical note*, 871.
- Bayley, C. J., Brekelmans, W. A. M., & Geers, M. G. D. (2006). A comparison of dislocation induced back stress formulations in strain gradient crystal plasticity. *International Journal of Solids and Structures*, **43**: 7268-7286.
- Bazelyuk, G. Y., Gontareva, R. G., Kozyrskii, O. I., Tarasenko, L. V., Tikhonov, L. V., & Matsievskaya, S. Y. (1980). Combined action of cyclic heat treatment and ultrasonic emission on the structural condition and mechanical properties of X16N11M3 steel. *Strength of Materials*, **12**: 1139-1145 (In Russian).
- Bazelyuk, G. Y., Kozyrsky, G., Polotsky, Y. I. & Petrunin, G. A. (1970). Effect of previous ultrasonic irradiation on the high-temperature creep and microhardness of copper. *Fizika Metallov i Metallovedenie*, **29**: 508-511 (In Russian).
- Bazelyuk, G. Y., Kozyrsky, G., Petrunin, G. A., & Polotsky, Y. I. (1971). Effect of preliminary ultrasonic irradiation and thermomechanical treatment on the creep-resistance of Al. *Fizika Metallov i Metallovedenie*, **32**: 145-151 (In Russian).
- Béda Gy. and Kozák I. (1987) *Rugalmas testek mechanikája*, Műszaki Könyvkiadó, Budapest.
- Béda Gy., Kozák I. and Verhás J. (1995). *Continuum Mechanics*. Academic Publisher, Budapest, 1995.
- Belozerova, E. (1992) Change in the dislocation structure of alkali-halide crystals in ultrasound and electric fields. DSc dissertation, Kostroma (in Russian)
- Bertóti, E. (2016). On divergence-free stress fields and zero-energy stress functions in elasticity. *Mechanics Research Communications*, **71**: 20-24.
- Betten, J. (2005). *Creep Mechanics*, Springer, Berlin.
- Biront, V. S. (1979). Kinetics of ultrasonic hardening. *Metal Science and Heat Treatment*, **21**: 195-198.
- Blagoveshchenskii, V. V., & Panin, I. G. (2007). An increase in the rate of plastic deformation under the effect of ultrasound. *The Physics of Metals and Metallography*, **103**: 424-426.
- Blaħa, F., & Langenecker, B. (1955). Dehnung von Zink-kristallen unter Ultraschalleinwirkung. *Naturwissenschaften*, **42**: 556-556.
- Bojtár, I., & Vörös, G. (1986). *A végeselem-módszer alkalmazása lemez és héjszerkezetekre*. Budapest: Műszaki Könyvkiadó, 163 p.
- Bokor, J., & Gáspár, P. (2008). *Irányítástechnika járműdinamikai alkalmazásokkal*. Typotex Kiadó, Budapest.
- Borbély, A., Blum, W., & Ungar, T. (2000). On the relaxation of the long-range internal stresses of deformed copper upon unloading. *Materials Science and Engineering: A*, **276**: 186-194.
- Borbély, A., Hoffmann, G., Aernoudt, E., & Ungar, T. (1997). Dislocation arrangement and residual long-range internal stresses in copper single crystals at large deformations. *Acta Materialia*, **45**: 89-98.
- Buerger M. J. (1979). *Crystal-Structure Analysis*. Krieger Pub Co.

- Cadek, J. (1987). The back stress concept in power law creep of metals: a review. *Materials Science and Engineering*, **94**: 79-92.
- Cadek, J. (1988). *Creep in Metallic Materials*. Amsterdam: Elsevier Science publishers, **1**: 205-234.
- Carroll, M. C., Serin, K., & Eggeler, G. (2004). Anisotropic strain hardening following load reversal during high-temperature creep testing of superalloy single crystals. *Materials Science and Engineering: A*, **387**: 590-594.
- Carry, C., & Strudel, J. L. (1978). Apparent and effective creep parameters in single crystals of a nickel base superalloy—II. Secondary creep. *Acta Metallurgica*, **26**: 859-870.
- Chaboche, J. L. (1996) Unified Cyclic Viscoplastic Constitutive Equations: Development, Capabilities, and Thermodynamic Frame Work, In: Krausz, Alexander S., and K. Krausz, eds. *Unified constitutive laws of plastic deformation*. Elsevier.
- Chaboche, J. L. (1997). Thermodynamic formulation of constitutive equations and application to the viscoplasticity and viscoelasticity of metals and polymers. *International Journal of Solids and Structures*, **34**: 2239-2254.
- Chakrabarty, J. (2000). *Applied plasticity* (Vol. 88). New York: Springer.
- Chen, W. F., & Han, D. J. (2007). *Plasticity for structural engineers*. J. Ross Publishing.
- Cravotto, G., & Cintas, P. (2012). Harnessing mechanochemical effects with ultrasound-induced reactions. *Chemical Science*, **3**: 295-307.
- Daud, Y., Lucas, M., & Huang, Z. (2007). Modelling the effects of superimposed ultrasonic vibrations on tension and compression tests of aluminium. *Journal of Materials Processing Technology*, **186**: 179-190.
- Davies, P. W., & Wilshire, B. (1971). On internal stress measurement and the mechanism of high temperature creep. *Scripta Metallurgica*, **5**: 475-478.
- Demchenko, L. V., Kozyrskii, G., Kononenko, V. A., & Mordiyuk, N. (1976). The nature of high-temperature creep of solid solutions submitted to ultrasound treatment (Ni-Al alloys). *Metallofizika*, **63**: 51-54.
- Demchenko, L., Kononenko, V., & Mordiyuk, N. (1973). Changes in the disorientation of the substructure of a nickel-aluminum alloy under ultrasonic treatment and creep. *Fizika Metallov i Metallovedenie*, **35**: 1309-1312.
- Domokos G. (1988). Axiálisan terhelt vasbeton keresztmetszet semleges tengelyének számítása konvergens iterációval a II. feszültségi állapotban. *Építés- és Építészettudomány*, **19**: 395-405.
- Dulácska, E. et al. (2001). In Gyulai J, Kiss J. (szerk.). *Építési műszaki ellenőrök kézikönyve*. Budapest: TERC Kereskedelmi és Szolgáltató Kft, 640 p.
- Égert, J., & Keppler, I. (2007). *A végeelem módszer mechanikai alapjai*. Győr: Universitas-Győr Nonprofit Kft., 205 p.
- Eskin, G. I., & Eskin, D. G. (2014). *Ultrasonic treatment of light alloy melts*. CRC Press.
- Evans, R. W., Roach, W. J. F., & Wilshire, B. (1985). A re-interpretation of r and h measurements during creep. *Materials Science and Engineering*, **73**: L5-L8.
- Farkas, J., & Jármay, K. (2015). *Fémszerkezetek innovatív tervezése*. Miskolc: Gazdász Elasztik Kft.
- Feigen, M. (1954). Inelastic behavior under combined tension and torsion, *2nd USNCAM*, pp. 469-476.
- Fernezelyi, S., Matuscsák, T., Farkas, J. (2003). *Épületek teherhordó szerkezetei*. Budapest: Verlag Dashöfer Szakkiadó Kft.
- Fisher, J. W., Statnikov, E. S., & Tehini, L. (2001, October). Fatigue strength enhancement by means of weld design change and the application of ultrasonic impact treatment. In *Proc. of Intl. Symp. On Steel Bridges, Chicago*.
- Friedel, J. (1964). *Dislocations*. Pergamon, New York.
- Gaspar, Z. (1993). *Tartók statikája III. Rúdszerkezetek*. Műegyetemi Kiadó, Budapest.
- Gáspár, Zs, & Németh, R. (2002). Equilibrium paths of twisted and bended bars. In: *Proc. of the International Symposium Anniversary of Pollack Mihály Engineering Faculty. Konferencia helye, ideje: Pécs, Magyarország, 2002.05.31-2002.06.01*. Pécs: pp. 139-149.
- Gindin, I. A., Malik, G. N., Neklyudov, I. M., & Rozumnyi, O. T. (1972). Effect of ultrasonic vibrations on the parameters of the hardening curve for copper single crystals. *Soviet Physics Journal*, **15**: 192-196.
- Ginsztler J., Hidasi B., Dévényi L. (2000). *Alkalmazott anyagtudomány*. Műegyetemi Kiadó.

- Ginsztler, J. & Verő, B. (2001) *Hőkezelés*. In: A technológia helyzete és jövője. Budapest: MTA Társadalomkutató Központ, pp. 143-155.
- Ginsztler, J., Nam, S. W., & Szabó, P. J. (2004). Factors affecting the change of subgrain size of 15Mo3 steel during creep. *Materials at High Temperatures*, **21**: 187-192.
- Ginsztler, J., Gaál, Z., Szabó, P. J., & Dévényi, L. (2010). Grain boundary investigation of AISI 304 type steel using EBSD. In *Materials Science Forum* (**659**: 307-311). Trans Tech Publications.
- Guyot, P. (1966). Thermal activation of the reactions between attractive dislocations. *Acta Met*, **14**: 955-959.
- Hegedűs, I., Farkas, Gy., Dunai, L., Kovács, T. (szerk.) (2016) *A BME Hidak és Szerkezetek Tanszék Tudományos Közleményei*: Budapest: BME Hidak és Szerkezetek Tanszéke, 406 p.
- Hill, R (1950). *The Mathematical Theory of Plasticity*. Oxford University Press, New York.
- Honeycombe, R.W.K (1984). *The Plastic Deformation of Metals*. Edward Arnold.
- Huang, H., Pequegnat, A., Chang, B. H., Mayer, M., Du, D., & Zhou, Y. (2009). Influence of superimposed ultrasound on deformability of Cu. *Journal of Applied Physics*, **106**: 113514.
- Hutchinson, J. W. (2000). Plasticity at the micron scale. *International Journal of Solids and Structures*, **37**: 225-238.
- Ilyushin, A. A. (1963). *Plasticity: Fundamentals of general mathematical theory*. Akademiai Nauk, SSSR. (in Russian).
- Ivanova, V. S., & Gordienko, L. K. (1964). *New Ways of Increasing the Strength of Metals*. Iron and Steel Institute, Moscow.
- Ivanova, V. S., Gordienko, L. K., Fritsman, Z. G., & Zubarev, P. V. (1967). Mechanico-thermal treatment as an effective method of increasing the high-temperature strength of metals and alloys. *Materials Science*, **2**: 88-93.
- Jonas, J. J. (1970). The dissipation stress in obstacle- and drag-controlled glide. *Materials Science and Engineering*, **6**: 377-383.
- Joshimure, J. (1958). Comment on the slip theory of Batdorf and Budiansky. *Bull. ISME*, **1**: 109-113.
- Kalishky, S. (1989). *Plasticity: theory and engineering applications* (Vol. 21). North-Holland.
- Kalishky, S., Kurutz, M., Szilárdi Gy. (1990) *Mechanika II. Szilárdságtan*. Tankönyvkiadó.
- Kalishky, S., Kurutz, M., Nédli, P., (1974). Képlékenységtani feladatok közelítő és numerikus megoldásai. In: *Az MTA Műszaki Mechanikai Tanszéki Munkaközösség II, Budapest, Hungary*, 10/1974, p. 1.
- Kalishky, S., & Logo, J. (2006). Optimal design of elasto-plastic structures subjected to normal and extreme loads. *Computers&Structures*, **84**: 1770-1779.
- Kassner, M. E. (2015). *Fundamentals of creep in metals and alloys*. Butterworth-Heinemann.
- Kassner, M. E., Geantil, P., Levine, L. E., & Larson, B. C. (2009). Backstress, the Bauschinger effect and cyclic deformation. In *Materials Science Forum*, **604**: 39-51. Trans Tech Publications.
- Keith, R. E., & Gilman, J. J. (1959, January). Progress report on dislocation behavior in lithium fluoride crystals during cyclic loading. In *Symposium on Basic Mechanisms of Fatigue. ASTM International*.
- Kenedy, A. (1962), *Processes of Creep and Fatigue in Metals*. Oliver and Boyd, Edinburg.
- Kirchner, H. O. K., Kromp, W. K., Prinz, F. B., & Trimmel, P. (1985). Plastic deformation under simultaneous cyclic and unidirectional loading at low and ultrasonic frequencies. *Materials science and engineering*, **68**: 197-206.
- Kocsis, L., Kiss, R., & Illyés, Á. (szerk.) (2007). *Mozgászervek biomechanikája*. Budapest: TERC Kereskedelmi és Szolgáltató Kft.
- Koiter, W. T. (1953). Stress-strain relations, uniqueness and variational theorems for elastic-plastic materials with a singular yield surface. *Quarterly of applied mathematics*, **11**: 350-354.
- Kollár, L. (1995). *Vasbeton-szilárdságtan*. Műegyetemi Kiadó, Budapest.
- Kollár, L. P., & Springer, G. S. (2003). *Mechanics of composite structures*. Cambridge university press.
- Konovalov, E., & Remizovskij, E. (1964). *The application of ultrasound in mechanical engineering industry*, Minsk (in Russian).
- Kovács, Á., & Kovács, A. (2013). Determination of elastic properties of a square-form porous nanofilter. In: *E Carrera, F Miglioretti, M Petrolo (szerk.) Proceedings of the 6th Thematic ECCOMAS Conference: SMART 2013. Konferencia helye, ideje: Torino, Olaszország, 2013.06.24-2013.06.26*. Torino: pp. 1-6.

- Kovács, F., & Tarnai, T. (2009). Two-dimensional analysis of bar-and-joint assemblies on a sphere: Equilibrium, compatibility and stiffness. *International Journal of Solids and Structures*, **46**: 1317-1325.
- Kozlov, A., Mordyuk, N. (1986). The influence of preliminary ultrasound treatment on the strength of metals, *In: Ultrasonic vibrations and their impact upon the mechanical characteristics of metals*, Kiev, pp. 31-34 (in Russian).
- Kozák, I., & Szeidl, Gy. (2013). *Tenzorszámítás indexes jelölésmódban*. Második, bővített kiadás. Miskolc-Egyetemváros: Miskolci Egyetem.
- Kralik, G., Weiss, B. (1967) Für die Ultraschallverfestigung von Kurdisch Flächen- senirlsenen Metalen und Legirungen. *Zs Metallkunde*, **58**: 471-475.
- Kromp, W., & Weiss, B. (1971). Electrical resistivity of copper after high frequency fatigue (ultrasonic fatigue at 20 kHz). *Scripta Metallurgica*, **5**: 499-504.
- Kuksa, L., Lebedev, A., & Koval'chuk, B. (1986). Laws of distribution of microscopic strains in two-phase polycrystalline alloys under simple and complex loading. *Strength of Materials*, **18**: 1-5.
- Kulemin, A. V. (1978). Ultrasound and diffusion in metals. *Metallurgiya, Moscow* (in Russian).
- Kurutz-Kovacs, M. (1981). State change analysis of structures with generalized conditional joints. *Periodica Polytechnica. Civil Engineering*, **25**: 169.
- Langenecker, B. (1966). Effects of ultrasound on deformation characteristics of metals. *IEEE transactions on sonics and ultrasonics*, **13**: 1-8.
- Lichatchev, V., & Malinin, V. (1993). *Structural-analytic theory of strength*. St. Petersburg.
- Lloyd, G. J., & McElroy, R. J. (1974). On the anelastic contribution to creep. *Acta Metallurgica*, **22**: 339-348.
- Louchet, F. (1995). A model of negative creep in nickel-based superalloys. *Scripta metallurgica et materialia*, **33**: 913-918.
- Lum, I., Huang, H., Chang, B. H., Mayer, M., Du, D., & Zhou, Y. (2009). Effects of superimposed ultrasound on deformation of gold. *Journal of Applied Physics*, **105**: 024905.
- McLean, D. (1957). *Grain Boundaries in Metals*. Oxford, Clarendon Press.
- McLean, D. (1962). *Mechanical Properties of Metals*. John Wiley and Sons, New York-London.
- Meskó, D., & Csébfalvi, A. (2013). Modeling method in the architectural planning of reliable complex health-care systems. *Pollack Periodica*, **8**: 35-46.
- Mitra, S. K., & McLean, D. (1966, December). Work hardening and recovery in creep. In *Proceedings of the Royal Society of London A: Mathematical, Physical and Engineering Sciences* (**295**: 288-299). The Royal Society.
- Moraru, L. (2007). Ultrasound action on strength properties of polycrystalline metals. *The Annals of University Dunarea de Jos Galati, Fascicle VIII Tribology*, 74-77.
- Mordyuk, B. N., Prokopenko, G. I., Milman, Y. V., Iefimov, M. O., & Sameljuk, A. V. (2013). Enhanced fatigue durability of Al-6Mg alloy by applying ultrasonic impact peening: Effects of surface hardening and reinforcement with AlCuFe quasicrystalline particles. *Materials Science and Engineering: A*, **563**: 138-146.
- Mordyuk, N. S. (1970). Effect of ultrasonic vibrations on the physical properties of metals and alloys: Review. *Metallofizika*, **31**: 83-107.
- Mordyuk, N. S., & Demchenko, L. V. (1978). Structural Changes and Creep in Molybdenum Single-Crystals Given Preliminary Ultrasonic Treatment. *Akad. Nauk Ukr. SSR, Metallofiz.*, **72**: 50-53.
- Mughrabi, H. (1983). Dislocation wall and cell structures and long-range internal stresses in deformed metal crystals. *Acta metallurgica*, **31**: 1367-1379.
- Murty, K. L., & Yoon, K. K. (1979). Creep transients in zircaloy cladding. *Scripta Metallurgica*, **13**: 299-302.
- Nádai, A. (1950). *Theory of flow and fracture of solids* (Vol. 1). McGraw-Hill.
- Nadai, A., & Hodge, P. G. (1963). Theory of Flow and Fracture of Solids, vol. II. *Journal of Applied Mechanics*, **30**: 640.
- Nédli, P. (1989). Plastic limit analysis of spatial large panel structures. *Periodica Polytechnica. Civil Engineering*, **33**: 171-182.
- Nemat-Nasser, S., & Okinaka, T. (1996). A new computational approach to crystal plasticity: fcc single crystal. *Mechanics of materials*, **24**: 43-57.
- Novikov, I. I. (1974). *Heat Treatment Theory for Metals*. Metallurgiya, Moscow.

- Ohashi, Y., Kawai, M., & Momose, T. (1986). Effects of prior plasticity on subsequent creep of type 316 stainless steel at elevated temperature. *Journal of Engineering Materials and Technology*, **108**: 68-74.
- Osipiuk, W. (1990). Zastosowanie teorii poślizgów do opisu pełzania wstępnego (The description of reverse creep in terms of slip concept), *Rozprawy Inżynierskie*, **30**: 259-271. (in Polish)
- Osipiuk, V. (1991) Explanation and analytical description of delayed creep, *International Applied Mechanics*, **27**: 374-378.
- Osipiuk, W. (1993) Development of slip concept for describing rate-effects and creep of materials. *DSc dissertation, Polytechnic University of Bialystok and Lvov, 211p.* (in Russian)
- Osipiuk, W. and Rusinko, K. (1996). Description of the stress relaxation process under plane stress conditions, *Int. J. of Pressure Vessels and Piping*, **65**: 97-100.
- Ostrovskii, I. V., Steblenko, L. P., & Nadochii, A. B. (2000). Ultrasound-induced surface hardening of dislocation-free silicon. *Semiconductors*, **34**: 251-254.
- Páczelt, I. (1999) *Végeselem-módszer a mérnöki gyakorlatban*, I. kötet. Miskolci Egyetemi Kiadó.
- Páczelt, I., Szabo, B., & Szabó, T. (1999). Solution of contact problem using the hp-version of the finite element method. *Computers & Mathematics with Applications*, **38**: 49-69.
- Páczelt, I., & Mróz, Z. (2009). On the analysis of steady-state sliding wear processes. *Tribology international*, **42**: 275-283.
- Pálossy, L. Scharle, P., & Szalatkay, I. (1993). Earth Walls. New York: Ellis Horwood (Ellis Horwood series in civil engineering).
- Pasierb, A., & Wojnar, A. (1992). An experimental investigation of deep drawing and drawing processes of thin-walled products with utilization of ultrasonic vibrations. *Journal of Materials Processing Technology*, **34**: 489-494.
- Peirce, D., Asaro, R. J., & Needleman, A. (1983). Material rate dependence and localized deformation in crystalline solids. *Acta metallurgica*, **31**: 1951-1976.
- Peslo, A. (1984). Ultrasonic hardening of aluminium alloys. *Ultrasonics*, **22**: 37-41.
- Pines, B., & Omeljanenko, J. (1969). Dislocation multiplications in metals and ionic crystals under ultrasound. *Fiz. metallov i metallovedeniye*, **28**: 110-114 (In Russian).
- Poirier, J. P. (1977). Microscopic creep models and the interpretation of stress-drop tests during creep. *Acta Metallurgica*, **25**: 913-917.
- Poirier, J. P. (1985). *Creep of crystals: high-temperature deformation processes in metals, ceramics and minerals*. Cambridge University Press.
- Polockij, I., Belostockij, V., Nikitova, G. (1980). Mechanical properties of NiCr previously deformed with ultrasound frequency, in: *The strength of Materials and Structural Members under Sonic and Ultrasonic Load Frequencies*, Kiev, pp. 146-150 (in Russian).
- Popov, L.G. (1987). Generalization of Rabotnov model of plasticity for five-dimensional stress-deviator space. *J. Izv. Nauk USSR (USSR Acad. Sci.), Mech. Tverdogo Tela*, **5**: 126-134.
- Price, C. W. (1990). Use of Kolmogorov-Johnson-Mehl-Avrami kinetics in recrystallization of metals and crystallization of metallic glasses. *Acta Metallurgica et Materialia*, **38**: 727-738.
- Puga, H., Carneiro, V., Barbosa, J., & Vieira, V. (2015). Effect of Ultrasonic Treatment in the Static and Dynamic Mechanical Behavior of AZ91D Mg Alloy. *Metals*, **5**: 2210-2221.
- Rabotnov, Ju. N. (1969). *Creep problems in structural members* (Vol. 7). North-Holland Pub. Co.
- Radovic, M., Barsoum, M.W., El-Raghy, T. and Wiederhorn, S.M. (2003). Tensile creep of coarse-grained Ti<sub>3</sub>SiC<sub>2</sub> in the 1000-1200°C temperature range. *Journal of Alloys and Compounds*, **361**: 299-312.
- Rusinko, K. N. (1981). *Theory of Plasticity and Nonsteady Creep*. Vyscha Shkola, Lviv.
- Rusinko, K. N. (1986). *Specific Features of Inelastic Deformation of Solid Bodies*. Vyscha Shkola, Lviv.
- Rusinko, K. N., & Andrusik, Y. F. (1993). Plastic deformation of a strain-hardening material under loading in the three-dimensional subspace of the five-dimensional space of plastic deviators. *Izv. Ross. Akad. Nauk, Mekh. Tverd. Tela*, **2**: 92-101.
- Rusinko, A. (1999). Mathematical Description of Metal Plastic Strain under Ultrasonic Irradiation. *Mashinoznavstvo (Mechanical Engineering)*, No 12, pp. 16-18. (in Ukrainian)
- Rusynko, A. (2001). Mathematical description of ultrasonic softening of metals within the framework of the synthetic theory of plasticity. *Materials Science*, **37**: 671-676.

- Rusinko, A. (2002). Analytic dependence of the rate of stationary creep of metals on the level of plastic prestraining. *Strength of Materials*, **34**: 381-389.
- Rusynko, A. (2002). Effect of preliminary mechanical and thermal treatment on the unsteady creep of metals. *Materials Science*, **38**: 824-832.
- Rusinko, A. (2002). Kinetics of loading surface under mechanical-thermal treatment and unsteady-state creep of metals. *Mashinostroyeniye (Mechanical Engineering)*, No 8, pp. 42-48. (in Ukrainian)
- Rusinko, A. (2003). Influence of ultrasound on plastic deformation of metals. *Bulletin of National University of Kyiv, Series: Physics and Mathematics*, **10**: 157-162. (in Ukrainian)
- Rusynko, A. (2004). Influence of preliminary mechanical and thermal treatment on the steady-state creep of metals. *Materials Science*, **40**: 223-231.
- Rusinko, A. (2004). Creep deformation and mechanic-thermal processing, *Mashinostroyeniye (Mechanical Engineering)*, No. 3, pp. 24-29. (in Ukrainian)
- Rusinko, A. (2004). Influence of ultrasound on steady-state creep deformation. *Tekhnicheskaya Mekhanika*, **1**: 124-130. (in Russian)
- Rusinko, A. (2004). Ultrasound hardening of metals. *Mathematical Methods and Physicomechanical Fields*, **47**: 129-133. (in Ukrainian)
- Rusinko, A. (2005). Kinetics of loading surface at ultrasound irradiation. *Bulletin of Donyetsk National University*, **1**: 144-148. (in Russian)
- Rusynko, A. (2005). Analytic description of the effect of duration of the procedure of annealing performed after deformation on the steady-state creep of metals. *Materials Science*, **41**: 280-283.
- Rusinko, A. (2006). Analytical description of unsteady-state creep of metals after mechanics-thermal treatment. *Mathematical Methods and Physics-Chemical Fields*, **49**: 163-170. (in Ukrainian)
- Ruszinkó, E. (2007). Az előzetes mechanikai-termikus és ultrahangos megmunkálások hatása a képlékeny és kúszás alakváltozásra. In *Nemzetközi Gépész és Biztonságtechnikai Szimpózium, Budapesti Műszaki Főiskola, Bánki Donát Gépész és Biztonságtechnikai Mérnöki Kar, 2007. November 14., 7 ó.*
- Rusinko, A., Ginsztler, J., & Dévényi, L. (2007). Analytic description of the formation of pores under conditions of steady-state creep of metals. *Strength of Materials*, **39**: 74-79.
- Rusinko, A. (2008). Bases and advances of the synthetic theory of irreversible deformation, *XXII International Congress of Theoretical and Applied Mechanics (ICTAM) 25-29 August 2008, Adelaide, Australia*.
- Rusinko, A. (2009). Plastic-creep deformation interrelation. *7<sup>th</sup> EUROMECH Solid Mechanics Conference 7-11 September 2009, Lisbon, Portugal*, pp. 49-50.
- Rusinko, A., & Rusinko, K. (2009). Synthetic theory of irreversible deformation in the context of fundamental bases of plasticity. *Mechanics of Materials*, **41**: 106-120.
- Ruszinkó, E. (2009). The Influence of Preliminary Mechanical-thermal Treatment on the Plastic and Creep Deformation of Turbine Disks. *J. Meccanica*. **44**: 13-25.
- Ruszinkó, E. (2010). Képlékeny és kúszás alakváltozás kölcsönhatása. In *Gépész, Mechatronikai és Biztonságtechnikai Szimpózium, Bánki Donát Gépész és Biztonságtechnikai Mérnöki Kar Óbudai Egyetem, 2010 November 11., 2010, Budapest, Hungary*.
- Rusinko, A. (2010). Creep deformation in terms of synthetic theory. *Advances and Applications in Mechanical Engineering and Technology*, **1**: 69-108.
- Rusinko, A. (2010). Non-Classical Problems of Irreversible Deformation in Terms of the Synthetic Theory, *Acta Polytechnica Hungarica*, **7**: 25-62.
- Rusinko, A. (2011). The modeling of Haazen-Kelly's effect in terms of the synthetic theory of irreversible deformation. In *9<sup>th</sup> International Congress on Thermal Stresses, June 5-9, 2011, Budapest, Hungary, paper TS2011\_1295597075*.
- Rusinko, A. (2011). Phase transformation strain in terms of the synthetic theory. In *2011 World Congress on Engineering and Technology (CET2011), 2011 International Conference on Material Sciences and Technology (MST2011), Oct. 28. - Nov. 2, 2011, Shanghai, China*, pp. 161-164.
- Rusinko, A., & Rusinko, K. (2011). *Plasticity and Creep of Metals*. Springer Science & Business Media.
- Rusinko, A. (2011). Analytical description of ultrasonic hardening and softening. *Ultrasonics*, **51**: 709-714.
- Ruszinkó, E. (2012): Ultrasound treatment and steady-state creep of metals, In *Proceedings of Inter-Academia 11<sup>th</sup> International Conference on Global Research and Education, 27-30 August, Budapest, Hungary*, pp. 141-150.

- Rusinko, A. (2012). Effects of Ultrasound on Plastic and Creep Deformation of Metals. *ASME 2012 International Mechanical Engineering Congress, November 9-15, 2012, Houston, USA*.
- Rusinko, A. (2012). Peculiarities of irreversible straining in step-wise loading, reverse and inverse creep. *Acta Mechanica Solida Sinica*, **25**: 152-167.
- Rusinko, A. (2012). *Ultrasound and Irrecoverable Deformation in Metals Modeling of Plastic and Creep Deformation*. LAP Lambert Academic Publishing.
- Rusinko, A. (2013). Influence of Annealing Temperature in the Course of Mechanical-Thermal Treatment upon the Steady-State Creep Rate of Metals. *Journal of Mechanics*, **29**: 535-538.
- Rusinkó, E. (2013). Loading Surface in the Course of Mechanical-Thermal Treatment and Steady-State Creep of Metals. *Acta Polytechnica Hungarica*, **10**: 153-164.
- Rusinkó, E. (2013). Képlékeny alakváltozás nem arányos terhelés alatt. *A Miskolci Egyetem közleményei. Multidiszciplináris tudományok*, 3. kötet. 1. sz. pp. 9-20.
- Rusinko, A., & Fenyvesi, D. (2014). On the Advantages of the Theories of Plasticity with Singular Loading Surface. *Journal of Materials Science and Chemical Engineering*, **2**: 14.
- Rusinko, A. (2014). Feigen's Phenomenon in Terms of the Synthetic Theory. *International Journal of Engineering Research and Applications*, **4**: 172-180.
- Rusinko, A. (2014). Influence of preliminary ultrasonic treatment upon the steady-state creep of metals of different stacking fault energies. *Ultrasonics*, **54**: 90-98.
- Rusinko, A. (2015). Irrecoverable deformation of tin in terms of the synthetic theory. *Materials Science and Engineering: A*, **631**: 97-103.
- Rusinko, A. (2015). Peculiarities of permanent deformation of tin: ordinary loading conditions and effect of DC. *9<sup>th</sup> European Solid Mechanics Conference, July 6-10, 2015, Madrid, Spain*.
- Rusinko, A. (2016). Modeling the effect of DC on the creep of metals in terms of the synthetic theory of irrecoverable deformation. *Mechanics of Materials*, **93**: 163-167.
- Sági, G., Szilas, Á., Fekete, G. Csizmadia, B. (szerk.) (2016). *Solved problems in Statics*, Gödöllő: Szent István Egyetemi Kiadó, 92 p.
- Samsonov, G. V. (1965). *Physicochemical Properties of Elements*. Naukova Dumka, Kiev (in Russian).
- Sanders Jr., J.L. (1954) Plastic Stress-Strain Relations Based on Linear Loading Functions. *Proceedings of the Second USA National Congress of Applied Mechanics*, Ann Arbor, 14-18 June 1954, 455-460.
- Sastry, D. H., Luton, M. J., & Jonas, J. J. (1974). Stacking fault energy and its influence on high-temperature plastic flow in Zr-Sn alloys. *Philosophical Magazine*, **30**: 115-127.
- Schneibel, J. H., & Horton, J. A. (1988). Evolution of dislocation structure during inverse creep of a nickel aluminide: Ni-23.5 Al-0.5 Hf-0.2 B (at.%). *Journal of Materials Research*, **3**: 651-655.
- Severdenko, V.P., Klubovich, V.V., & Jelin, V.I. (1967). Research into the elongation of copper at high temperatures in an ultrasonic field, in: *The Application of Ultrasound in the Industry, Minsk*, pp. 242-246 (in Russian).
- Severdenko, V., Skripnichenko, A., Tjalovskij, M. (1979). *Ultrasound and Strength*, Minsk (in Russian).
- Sarhosis, V., Bagi, K., Lemos, J. V., & Milani, G. (Eds.). (2016). *Computational Modeling of Masonry Structures Using the Discrete Element Method*. IGI Global.
- Siddiq, A., & El Sayed, T. (2011). Acoustic softening in metals during ultrasonic assisted deformation via CP-FEM. *Materials Letters*, **65**: 356-359.
- Siddiq, A., & Ghassemieh, E. (2008). Thermomechanical analyses of ultrasonic welding process using thermal and acoustic softening effects. *Mechanics of Materials*, **40**: 982-1000.
- Singh, R., & Khamba, J. S. (2007). Investigation for ultrasonic machining of titanium and its alloys. *Journal of Materials Processing Technology*, **183**: 363-367.
- Siu, K. W., & Ngan, A. H. W. (2011). Understanding acoustoplasticity through dislocation dynamics simulations. *Philosophical Magazine*, **91**: 4367-4387.
- Sleeswyk, A. W., James, M. R., Plantinga, D. H., & Maathuis, W. S. T. (1978). Reversible strain in cyclic plastic deformation. *Acta Metallurgica*, **26**: 1265-1271.
- Smallman, R. E., Rong, T. S., Lee, S. C. D., & Jones, I. P. (2002). Inverse creep of intermetallics. *Materials Science and Engineering: A*, **329**: 852-855.
- Statnikov, E. (2004). Physics and mechanism of ultrasonic impact treatment. *IIV Document*, **13**, 2004-04.

- Stépán, G. (1989). *Retarded dynamical systems: stability and characteristic functions*. Longman Scientific & Technical.
- Tarnai, T. (2003). Zero stiffness elastic structures. *International Journal of Mechanical Sciences*, **45**: 425-431.
- Terentjev, V. F., Kogan, I. S., & Orlov, L. G. (1975). Molybdenum dislocations structure change during fatigue. *Fizika Metallov i Metallovedenie*, **40**: 199-202.
- Thiel, M., Kurths, J., Romano, M., Károlyi, Gy., A de Moura (szerk.) (2010). *Nonlinear dynamics and chaos: Advances and perspectives*. Berlin; Heidelberg: Springer.
- Tikhonov, L. (1986). *Structure and Properties of Metals and Alloys. Reference Book*. Naukova Dumka, Kiev (in Russian).
- Tong Wen, Li Wei, Xia Chen, Chun-lei Pei (2011). Effects of ultrasonic vibration on plastic deformation of AZ31 during the tensile process. *International Journal of Minerals, Metallurgy, and Materials*, **18**: 70-76.
- Várkonyi, P. L. (2016). Dynamics of mechanical systems with two sliding contacts: new facets of Painlevé's paradox. *Archive of Applied Mechanics*, pp. 1-15.
- Westmacott, K. H., & Langenecker, B. (1965). Dislocation structure in ultrasonically irradiated aluminum. *Physical Review Letters*, **14**: 221.
- Witthauer, A. T., Kim, G. Y., Faidley, L. E., Zou, Q. Z., & Wang, Z. (2014). Effects of acoustic softening and hardening in high-frequency vibration-assisted punching of aluminum. *Materials and Manufacturing Processes*, **29**: 1184-1189.
- Zalka, K. A. (2002). *Global structural analysis of buildings*. CRC Press.